NASA CR-
147424

(NASA-CR-147424) SELECTED ASPECTS OF LUNAR MARE GEOLOGY FROM APOLLO ORBITAL PHOTOGRAPHY Final Report (State Univ. of New York, Geneseo.) 177 p HC $7.50 CSCL 03B
N76-17002
Unclas
G3/91 09976

SELECTED ASPECTS OF LUNAR MARE GEOLOGY FROM APOLLO ORBITAL PHOTOGRAPHY

FINAL REPORT
NASA CONTRACT NAS9-12770
JANUARY 1976

Prepared
by

PRINCIPAL INVESTIGATOR
RICHARD A. YOUNG

CO-INVESTIGATOR
WILLIAM J. BRENNAN

Department of Geological Sciences
State University College of Arts and Science
Geneseo, New York, 14454

FORWARD

This report summarizes the results of NASA Contract NAS9-12770 (Eastern Maria Data Analysis Experiment) begun June 1972, amended August 1973, and modified March 1975.

Initial work on the project during its early phases was performed with the aid of Drs. Robert W. Wolfe and Douglas J. Nichols, former co-investigators who obtained full-time employment outside the State University of New York during the contract period. Although the main thrust of the final report reflects few concrete results directly related to tasks accomplished by these two individuals, we wish to acknowledge the significant contributions of both Drs. Wolfe and Nichols regarding the overall initial organization and subsequent modifications of this project. Contributions by these two individuals are included in the section on References and Bibliography indicated as resulting directly from support provided by this contract.

We also gratefully acknowledge the excellent support provided by NASA Technical Monitor S. N. Hardee and his staff at the Johnson Space Center.

The report is organized in sections dealing with categories of features which have long been of interest in understanding the geological evolution of the moon. Relative ages of individual maria are first established from crater size-frequency distributions. A thorough understanding of the effects of prolonged impact gardening is essential to any discussion of the characteristics of features formed within the maria. Sections II through VI deal with features and processes related to the evolution of the mare surfaces, whereas Sections VII and VIII summarize the regional implications of mare basin formation and structure, including some results from other Apollo surface and orbital experiments.

The Appendix and Tables include pertinent data which support our findings, but which are best presented in tabular form.

Figures have been grouped in 4 sections to facilitate reading of the text. The figures, text, and figure captions have been separated for reasons of economy and to maximize the detail and information which each enlarged photograph contains. An attempt was made to select representative examples of geological features rather than to include too many expensive plates, all illustrating the same kinds of features.

Lunar Topographic Orthophotomaps (LTO) have been referenced wherever pertinent, as well as Apollo orbital photography frames. The tremendous number of orbital photographs used in this study is necessarily abbreviated by the choice of illustrations for a report of this scope.

Publications supported directly by this contract are indicated by asterisks in the Reference and Bibliography Section.

Some suggestions for further studies based on findings in this report are summarized in the final section, General Conclusions and Recommendations.

ABSTRACT

Crater size-frequency distributions (100-500 m) are shown to provide significant integrated information concerning mare surface ages, subsurface stratigraphy, and surficial geology. Equilibrium cratering gradually reduces the relative numbers of craters smaller than 300-400 m in diameter as surfaces age and regolith thickens. On young mare surfaces it is possible to compare regions flooded at intervals closely spaced in time to obtain some approximate measure of relative flux distributions through time. The independent results for surface ages in this report are in good agreement with other published crater ages, and can provide further, unique information concerning subsurface geology.

Mare ridges and sinuous rilles are shown to be closely related to volcanic and tectonic processes with ridges often representing the prolonged interplay of volcanism, plutonism and tectonism along reactivated basement fractures. Thrust faulting along mare ridges and their highland extensions is inadequate to explain the compound morphologies observed along these widespread features.

Slope erosion debris along mare highland contacts in the form of talus aprons provides independent verification of relative mare surface ages, and slope morphologies could be utilized to compare the relative ages of young highland scarps and highland craters, as well as to qualitatively study the relative change in erosion rates as extrapolated to the impact flux. Lunar slope erosion does not produce parallel retreat of scarps as is common on the earth.

Old craters in the lunar maria have been modified by tectonic and volcanic processes that can be readily shown to have been common throughout the maria. No unequivocal evidence was found to suggest that some large lunar craters or ring structures might be analogous to terrestrial volcanic calderas or ring dikes, although intrusion along circular impact fractures is associated with regeneration of buried crater rims.

The existing correlations of large ring structures among various circular mare basins is shown to be based on criteria that are inconsistent and nonstandardized. A means of comparing equivalent ring structures in the different maria is proposed which takes into account the important characteristics of young unflooded basins (Orientale) as well as the progressive development of tectonic and volcanic features within the older flooded maria.

Whereas some specific geologic aspects of several of the lunar maria are discussed throughout all sections of this report, Mare Smythii is examined in some detail because of its great age and significantly different surface morphology.

TABLE OF CONTENTS

I. CRATER SIZE-FREQUENCY DISTRIBUTIONS AND RELATIVE AGES OF MARE SURFACES

A. Introduction

High resolution panoramic camera photographic coverage by the Apollo missions across portions of several lunar maria permits a more uniform, systematic, and accurate investigation of the detailed morphology of mare surfaces. Most previous attempts to verify or quantify relative ages of mare surfaces have been based upon demonstrable stratigraphic relationships, theoretical models of crater size-frequency distributions, and crater degradation models. Many of these models seem to imply that the response of the lunar surface materials to the impact flux within the equilibrium cratering range (Gault, 1970) is relatively constant from one mare region to another. Recent studies (Young et al., 1974) have suggested that surface or subsurface stratigraphic variations might be significant when studying the apparent crater size-frequency distributions in the different maria. The present study was undertaken to attempt an evaluation of the possible effect of differences in mare stratigraphy on mare crater size-frequency distributions. The results have documented the existence of anomalous crater distributions at diameters below the equilibrium limit and unexplained crater distributions near the upper limit of the equilibrium range (200-300 m).

Earlier work on crater size-frequency distributions (Gault, 1970; Soderblom, 1970) suggested that the most promising crater size range for study should be above the so-called saturation and equilibrium diameters, below which it has often been assumed the appearance of the different maria would be very similar. The decision to study the crater diameter interval from 100 to 500 m was an attempt to completely overlap the assumed saturation diameter interval in order to obtain statistically meaningful results in the smallest feasible area.

A parameter that has not been adequately evaluated in past studies is the actual effect of sun elevation on crater size-frequency distributions. Cursory examination of a variety of lunar photographs leads to the general conclusion that many more craters can be seen on lower sun elevation photographs. This is an oversimplified assumption which is largely an illusion related to the distinctness of craters on low sun elevation photographs.

Ignoring the effect of variable sun elevations for the present, the standard measurement area in this study was taken as the smallest square (350 km^2) which would fit within the width of a single panoramic camera frame at its center and which would not be affected significantly by lack of photographic rectification. When such an area is chosen, the total number of craters with apparent diameters between 100

and 500 m varies generally from 500 to 3000, depending on the relative age of the surface and the sun elevation of the photographs.

B. Crater Diameter Measurements

Obviously it would be desirable to measure all craters stereoscopically to obtain more precise results. However, the practical problems associated with such precise measurements, including the variable overlap of the panoramic frames, eliminated this approach. In addition, most photography of the terrestrial planets has been and is likely to be largely nonstereographic. Thus a practical method of comparison should be based on the most commonly available photographic products.

Measurements performed on two-dimensional photographs indicate only the apparent diameter of craters as interpreted from shadows, which bear a complex relationship to rim crest shape. In general, the apparent measured diameter will vary as a function of the sun elevation, the amount of crater degradation, and individual operator perception.

It is assumed that apparent crater diameters measured at very low sun elevations closely approach the actual crater diameters because the shadows more clearly define the entire crater rim and the sun's rays become more nearly tangent to the true rim crest. However, at sun angles below 3 degrees the shadow lengths increase sufficiently so that they begin to obscure small craters adjacent to larger ones, and a significant number of additional craters having interior slopes of 1 to 3 degrees gradually become visible, drastically altering the nature of the apparent size-frequency distributions (Soderblom, 1972). Alternatively, these very low sun elevation photographs are one of the few pieces of direct evidence indicating that impact saturation, as defined by Gault (1970), is a real phenomenon on the lunar surface. The photographs discussed by Soderblom (1972) illustrate that equilibrium and saturation cratering has occurred up to the diameter range of 100 to 300 m. This is supported by the work of McGill (1974).

Other problems related to accurate diameter measurements include variable film contrast resulting from differences in film exposure and processing, as well as real surface albedo differences, which appear to reflect both age differences, chemical differences, and thin surficial mantling deposits or rays. Even under ideal conditions, individual perception of crater rims may result in each person obtaining slightly different measurements (see Table 2). Results vary the most for greatly degraded (subdued) craters. In addition each person seems to have a different "threshold" below which subtle depressions are not recognized as craters. We have attempted to minimize these differences by averaging the results of three individuals. This averages both the number of craters in each category as well as the apparent diameter for each crater. I

have used the same three individuals for all the data in this study except where noted, and I assume that it would be valid to compare their results with those of a similar group using the same technique. The differences between individual results are similar to those described in detail by Greeley and Gault (1970), except that during our studies the differences between individuals tended to become less marked as the individuals gained experience.

C. Data Collection Method

A Zeiss particle size analyzer was used, as described by Greelye and Gault (1970). Craters are measured by a superimposed circular spot of light, and no attempt was made to distinguish between individual primary and secondary craters. However, areas containing obvious secondary rays and unusual irregularities were avoided. Because it was desirable to study minor deviations from expected crater size-frequency distributions, a small linear increment for size categories was chosen. The resulting crater size intervals varied from 16 to 20 m between photographs according to available standard 2X photographic products supplied by NASA and the constraints of the Zeiss instrument. The instrument was operated continuously in the linear mode, reduced range to avoid discontinuities related to scale changes (Greeley and Gault, 1970).

No attempt was made to precisely equalize the scales of the available photography because of a desire to develop a method which could be applied by other investigators with a minimum of time and expense. It was also determined that accurate computation of photoscales without laser altimetry or precise orbital data can be extremely difficult. Despite our careful attempts to consider all possible factors affecting photographic scales, we experienced errors of up to 10% in calculating linear scales when later compared with the published lunar topographic maps compiled from the metric camera photography. All of our results have been corrected by assuming that the topographic map scales are more correct than our calculations or assumptions regarding spacecraft altitudes where lasar altimetry was not available. This problem leads us to suspect that comparisons of data from earlier studies of crater distributions might contain minor discrepancies which are merely scale errors due to inaccurate information concerning orbital parameters or the exact shape of the moon's surface. The magnitude of some of our scale errors could have been simply the result of incorrect assumptions but might be a factor when the results of several individuals are compared.

D. Reliability and Reproducibility

Differences among individuals: The three individuals who collected most of the data for this study each possessed a distinctive way of counting craters in that each tended to produce results which were consistently above, near, or below the

group average (see Table 2). Occasionally, with specific photographs two of the individuals would produce results which were uncharacteristic of their normal performance. An example of individual differences in the raw data is shown in Table 2. If individual results appeared to be inconsistent with regard to the group average or in comparison with the individual's usual performance, the individual or the group was asked to go over the photograph to see whether additional craters had been overlooked. On these few occasions the individuals were not told how their performance related to the other individuals.

No attempt was made to have individuals look at each other's photographs to find uncounted craters, since we believe that the recognition of degraded craters is a somewhat subjective process. In view of individual differences in detecting and measuring individual craters, it is believed to be more accurate to average individual results from different photographs than to have several individuals measure different numbers of craters on a single photograph, if each person has a different degree of personal bias. The project director did survey each photograph and data set individually during the work in an attempt to detect extraordinary discrepancies. Individuals were usually not required to count craters for more than 2 hours per day, generally for 1 hour in the morning and a second hour during the afternoon.

Accuracy of crater measurements: An attempt was made to determine whether individuals were obtaining consistent and reproducible results throughout the study. One test consisted of measuring a known number of inked circles on white paper. This verified that even when the objects counted have rather well-defined characteristics, individuals will measure them differently, but each individual tends to deviate from the norm in a consistent fashion. Although the circles were of a specific predetermined size, the results of the group produced a mode for each size over two interval categories (an actual mean range of 0.18 mm), which would represent approximately 18 m for craters actually counted on the photographs we used. The implications of these results are that any crater measured by an individual has about a 50% chance of being placed in either of two size categories, whose mean diameters differ by approximately 18 m and whose absolute range is 36 m (0.36 mm). These figures will vary slightly for each region because scales of the photos ranged from approximately 16.5 m/mm to 19.5 m/mm.

When a similar test was performed using a specific group of craters marked and numbered on an actual photograph, each individual tended to perceive and measure craters as being close to, greater than, or less than the mean in a consistent way. One individual consistently placed most craters in the interval above the group mean, the second person placed them consistently in the next interval below the group mean, and the third person consistently placed the craters very near the group mean.

These results substantiate our conclusions that crater size-frequency measurements on two dimensional photographs should be collected by at least two and preferably three individuals. This conclusion applies regardless of the sun elevation of the photographs in the range of our tests from 24 to 43 degrees and probably at all sun elevations.

Changes over the period of the study: There appeared to be a gradual improvement in the ability of the three individuals to measure craters diameters correctly over the period of this study (11 months). This was most evident in the craters measured on relatively high sun elevation photographs (34 to 52 degrees). The sun elevation corrections reported by one of us (Young, 1975) were somewhat modified by the end of the study so that very little difference was detectable on photographs of the same regions measured at these sun elevations. The distinct difference in the range of sun elevations from 4 to 34 degrees still remained. We attribute this change to the improvement in the ability of persons to recognize the position of the true rim crest of a crater after substantial experience in viewing individual craters on many different photographs. Subtle albedo differences on high sun elevation photography may become more important to an individual as he or she gains experience in measuring craters. This observation further complicates the reliability of using data obtained by different groups at different times. However, most of the significant differences between mare regions which we shall discuss cannot be due to the kinds of errors we have discussed here. Errors in measurement produced by minor differences in individual perception all tend to displace our curves parallel to themselves. The more marked changes in crater size-frequency curve slopes as plotted in this report record more significant differences in the total number of craters throughout broader ranges of the diameter interval from 100 to 600 m.

E. Size-Frequency Distributions

Figure 1 illustrates the general shape and characteristics of the curves for most of the areas examined in this study. The choice of a semi-log plot of equal diameter intervals (not cumulative) for our data was dictated by the observation that a least-squares fit of the data for this type of plot generally gave the highest correlation coefficient for the two straight line segments indicated by the broken curve. Not only are the data divided into two sets which closely approximate straight lines, but, in addition, there are one or two crater intervals between the curve segments that do not generally lie on either line and consistently indicate an abrupt flattening of the curve toward larger diameters. In other words, there is an abrupt increase in the number of craters near the break in slope (B) above the number that would have been predicted by extension of either portion of the curve. This flattening is typically accompanied by a conspicuous relative decrease in craters at the top of the lower curve segment (C). This

discontinuity can be seen in all of the different types of plots shown in Figure 1 for comparison but is best defined by the semi-log plot.

Soderblom and Lebofsky (1972) have discussed the significance of a steepening in the gneralized size-frequency distribution curve for craters between 100 m and 1 km and attributed the steeper, presumably straight, slope to the population of secondaries from larger craters. However, all our detailed results and those of many other investigators (Greeley and Gault, 1970, 1973; Shoemaker et al., 1969) indicate a variety of slope changes and irregularities in the actual size-frequency curves for individual areas. Although Soderblom and Lebofsky's analysis of the general significance of secondaries over large mare regions may be valid, the actual characteristics of curves for small individual areas should be carefully examined to determine whether additional complicating factors could be significant in the interval between 100 m and 1 km.

We processed our earlier data (Young, 1975) with a program to compute correlation coefficients for least squares best fits of the data to straight lines. It is clear from the comparisons in Figure 1 that a cumulative log-log plot for this restricted range departs significantly from a straight line. For the other two plots on Figure 1 the data were divided into two sets for each curve on either side of the diameter at which the "excess" craters occur (flattening of curve at B, Figure 1). We have concluded that precise computer-generated slopes for our curves are unwarranted. The variations in individual and group results indicate that duplication of the same measurements could produce slightly different curve slopes. For any two regions which differ significantly, the individual curves need only be contrasted in a qualitative way. The curves comparisons are also somewhat dependent upon the photographic scales in cases where the scales differ by 20% or more, although this effect tends to be similar to that of sun elevation and shift curves parallel to themselves.

At the present time we have completed detailed analyses of 34 different mare areas throughout 8 different maria (Table 1). In most of the cases that we tested, the correlation coefficient for the semi-log plots we have used are equal to or higher than the values for the log-log plots. The correlation coefficients for the small diameter portions of the curves ranged between 0.960 and 0.999 in the areas tested, but are somewhat lower and less consistent for the large diameter portions of the curves due to the scatter in the nonequilibrium part of the curve (C, Figure 1). The differences between the semi-log and log-log correlation coefficients are generally $\pm$ 0.005 or less, which is probably not very significant in view of the nature of the variations associated with individual crater counts.

Because the results presented here indicate a slightly better fit of the data for a semi-log plot over this restricted

size range, we have departed from the usual method of presenting similar data to emphasize the existence and position of the discontinuities in our curves. The relatively abrupt increase in relative numbers of craters at the break in the curve (Figure 1, B) can be seen in all of our raw data, whether averaged or individual results are considered. Additional reasons for choosing this type of semi-log plot are related to a method of correcting for changing sun elevations, discussed in a following section, as well as locating more easily the diameters where some of the curves intersect. All of these factors can be most conveniently and readily portrayed only on the semi-log plot used here. On cumulative frequency plots it is impossible to separate the numbers of craters in individual size increments without having the original numerical data in tabular form. This method of presenting the data is viewed as a convenient empirical means of contrasting important curve characteristics which are difficult to illustrate on the other types of frequency plots.

To compare the crater frequencies within two or more regions there are several factors to consider which, taken together, are of quantitative significance. The important characteristics are: 1) the approximate slope of the small diameter range (above B, Figure 1), 2) the total number of craters in the interval below B, or in equal intervals for two regions in this part of the curve, and 3) the actual diameter (projected intersection of curves) where the break in the slope occurs. There is little purpose in trying to categorize the lower curve segment by means of a computer-fitted curve, whereas the total number of craters over the broader interval is significant.

Although obvious secondary crater clusters and rays were usually avoided, an attempt was made to assess the contribution and significance of secondary craters to our results. Test areas near the Crater Brayley in Mare Imbrium and near the Crater Peirce in Mare Crisium were chosen so that areas located on and off obvious rays were counted.

The possible physical significance of the general shape of the compound frequency curve will be examined before the added complications of rays, stratigraphy, and changing sun elevations are considered. If a physical explanation can be attached to the nature of the curve, it can be used to establish a common reference point for more exact comparisons of several curves in the same area at different sun elevations, and for evaluating other significant factors.

F. Definition of Saturation and Equilibrium Cratering

Saturation cratering for a specified diameter (Gault, 1970) is defined as the condition where the surface has been covered by enough craters of that diameter to produce a hexagonal-closest-packing arrangment. Due to random overlapping of impacts

during this process, true saturation will not occur for a particular diameter until the number of craters is actually 2.6 times the minimum number of craters needed to exactly cover the surface. When considering a continuum of crater sizes, Gault (1970) has shown by calculation and experiment that an equilibrium condition should occur when the number of visible craters of a given size is between 1% and 10% of the saturation value. At equilibrium for a specific crater population (size range), the nature of the general appearance of the surface remains constant as new craters form and old ones are destroyed. The relative proportions of craters of different sizes remain constant. It is this process that is interpreted as most important in the production and reworking of the regolith (Gault, 1970). Photographs taken at low sun angles indicate that equilibrium and saturation cratering must have occurred up to crater diameters of at least 100 to 300 m (Soderblom, 1972) in someaareas.

G. Relation of Equilibrium Cratering to Observed Frequency Distribution Curves

The equilibrium condition should result in a relatively uniform size-frequency distribution for craters below the maximum equilibrium diameter, since a steady state condition is implied. We assume that the upper (smaller diameter) portion of our curve reflects the achievement of equilibrium (as discussed by Gault, 1970), although the very large number of extensively degraded craters actually present is not visible at a sun elevation of 19 degrees. This condition must be indirectly related to regolith thickness on the assumption that the depth-to-diameter ratio for small craters which have completely saturated the surface is approximately one fifth. Gault (1970) has shown that the saturation diameter is less than the maximum equilibrium diameter.

It also appears likely that craters formed in regolith should have different sizes, relative to the impacting objects, than similar impacts into solid rock. This can be inferred from studies of terrestrial explosion cratering, even though the process is different in significant respects (Murphy and Vortman, 1961; Oberbeck, 1971). Thus one would expect a change in the size-frequency distribution for impact craters across the regolith/bedrock transition zone even if the flux of impacting objects formed a smooth geometric progression. One would expect a measurable effect to occur as impacts penetrated the regolith/bedrock transition zone due to reflection and refraction of shock waves and seismic energy within the different materials. Such a transition effect should be most distinct where regolith is moderately thin and uniform and should gradually disappear as the regolith thickens and the transition zone becomes more gradational.

The curve in Figure 1 appears to account for the characteristics defined above. The distribution of craters less than

250 m in diameter is continuous and regular (equilibrium condition of Gault, 1970), whereas the slope decreases and the distribution becomes somewhat irregular to the right of the break in slope. The "excess" number of craters near the break in the slope of the curve where the upper segment tends to flatten out is interpreted as an effect on crater formation of the transition from regolith to bedrock. It is not obvious whether this effect occurs near or below the approximate base of the regolith. Based on accepted estimates offregolith thickness, it would appear to occur somewhat below the transition zone (caluclated from depth/diameter ratios).

If this explanation is correct, the break in the curve should move toward larger diameters as both the surface age and regolith thickness increase. A complication could be introduced if an older regolith were buried beneath a few tens of meters of younger flows, or if some other stratigraphic variation were present.

Figures 2 and 3 show comparisons of curves for several different surfaces at similar sun angles. The most significant observation resulting from these comparisons is that progressively older surfaces, as inferred from the number of larger craters 300 to 500 m in diameter, show a pronounced decrease in the number of smaller craters as well as a gradual decrease in the slope of the curve above the break in slope. This does not appear to have been specifically predicted by either the equilibrium model of Gault (1970) or the crater erosion model of Soderblom (1972).

A possible explanation of this effect utilizes the recent calculations by Schultz and Gault (1975). They propose that impact-generated ground motions (shock waves and surface oscillations) from larger impacts should have a significant effect on the degradation of craters less than 1 km in diameter. Their calculations suggest that formation of a 2 km crater could produce ground movement of up to 1 m within 4 km of the crater center.

If one combines Soderblom's (1970) erosion model and Gault's (1970) model for saturation or equilibrium impact-generated regolith with the Schultz and Gault (1975) seismic modification calculations, it might be possible to explain both the nature of the break in curve slope and the gradual disappearance of smaller craters with increasing age. A greater age is equivalent to a deeper regolith, which indicates a larger number of impacts capable of severely shaking the regolith as it is gradually thickened. For the surfaces in Figures 2 and 3 the diameter at which the break occurs does in fact move progressively toward larger diameters as predicted.

It appears that equilibrium saturation cratering conditions gradually change and evolve toward a smaller total number of craters in the regolith due to the increasing importance of

seismic shaking and the gradually changing nature of the impact process in the thickening regolith. If we examine a much older surface such as Tranquillitatis (Figures 2 and 3), we observe that the numbers of craters decrease even more significantly at the small diameter end of the range, and the break in slope apparent on younger surfaces is not well defined.

H. The Effect of Sun Elevation on Apparent Crater Size-Frequency Distributions

The Tranquillitatis curve in Figure 2 was originally determined for a sun elevation of 46 degrees (for Figure 3, 21° and 23°). This was necessary because most of the Apollo panoramic photography of the eastern maria was acquired at sun elevations generally in excess of 45 degrees. Because sun elevation has an obvious effect on the apparent number of craters that can be readily seen on a photograph, an attempt was made to quantitatively evaluate the effect of changing sun elevation.

Near the Crater Wallace in Mare Imbrium three orbital tracks cross for which panoramic photography is available at sun elevations which range from 4 to 52 degrees. This appears to be the only such mare area suitable for studies of the effect of changing sun elevation on crater size-frequency distributions at a minimum of three sun elevations.

The results of our analysis for the effect of sun elevation in this one area appear in Figure 4. Unfortunately this area appears to be of such an age that the nature of the crater size-frequency distribution curves is starting to deteriorate from the ideal case of two distinct slopes, and the detailed nature of the crater distribution is best defined only by the low sun elevation photograph. The relatively older age of this area is supported by the data of Boyce et al. (1974).

A subsequent recount of this same region late in this study and data from a directly adjacent region (areas 16 and 17, Table 1) produced slightly different results, referred to under the section dealing with "Changes Over the Period of the Study." The effect of sun elevation changes was less marked in the data collected later than in our initial data. As can be seen in Figures 4 and 5, a smaller change in the results was evident for the 4 to 34 degree sun elevations. Both results are presented, and they lead us to the following recommendation: When two curves are obviously dissimilar, it is probably safe to qualitatively compare regions having sun elevations which differ by amounts as great as 10 to 20 degrees. If two curves are very similar, they should be compared at similar sun elevations (and equivalent scales). Changes in individuals' performances over the period of a study should be checked by periodic recounting of a test area.

Detailed analysis of sun elevation effects: A cursory examination of the three curves in Figure 4 suggests that many more craters are in fact visible on the low sun elevation photograph. However, correlation of the raw crater interval data shows a striking similarity between the number of craters near 110 m in diameter on the 52-degree curves, 130 m on the 34-degree curve, and 160 m on the 4-degree curve (the first solid point on each curve, Figure 4). At greater apparent diameters on each curve (shown by the transition to solid symbols) a point was reached where the numbers of craters in each size class were remarkably similar on each curve, allowing for both slight differences in photo scales and the nature of the data collection process. The photographs taken at different sun elevations were carefully compared, and a few subdued and fresh craters on each were measured. It is clear from even a qualitative inspection of these photographs that almost all of the craters seen on the 4-degree sun elevation photograph are present and measurable on the 52-degree photograph, but at lower sun angles the apparent diameters are larger. Our figures suggest that only about 2.5% additional craters were measured on the low sun angle photograph when absolutely equivalent diameter categories are compared. These are presumably very subdued craters which were not apparent on the 52-degree photograph. The remaining additional craters (nearly 1700 more from 52 to 4 degrees) are merely included in the smallest diameter intervals due to the fact that these craters, which had apparent diameters smaller than 100 m on the 52-degree photograph, appeared larger than 100 m on the 4-degree photograph. As previously noted, the lower sun elevation photograph should be the most accurate for determining the true diameter. However, when comparing two photographs in the range between 4 and 52 degrees, careful inspection shows that the same craters are visible on both photographs with few exceptions.

Regardless of the significance of this apparent diameter change, it is obvious that the net effect on the data, as plotted in this paper, was merely to displace the curves approximately parallel to themselves without changing the relative slope of the curve segments. If the data had been plotted as cumulative size-frequency curves on log-log coordinates, as is usually the case, the details of what had actually occurred would not have been obvious.

When the results are plotted in the form of the figures in this paper, it is possible to make a qualitative correction for different sun elevations by merely making a lateral shift in the curve proportional to the amount indicated in Figures 4 and 5. The apparent diameter increase is an average effect produced by all the craters combined and cannot be used to correct diameters of individual craters, which may vary by greater or lesser amounts. Younger craters with steeper, sharper rims change the least, but these "fresh" craters typically comprise less than 5% of the crater population (Chapman et al., 1970).

Our final conclusions regarding the effects of sun elevation changes indicate that sun angle changes do not usually produce curve changes which are likely to be confused with the effects caused by impact gardening (aging) of the surface.

A further problem with regard to the correction for different sun elevations arises from the possibility that mare surfaces differ not only in regolith thickness but also in their probable subsurface stratigraphies. This would imply that each area has a unique surface "texture" formed by the combined action of equilibrium cratering and seismic modification of each unique stratigraphic section. Thus it is possible that slightly different sun elevation corrections would be found for each distinctive mare region.

However, it remains clear that the curve slope, the curve break, and the total number of large diameter craters combined are a sensitive measure of surface age regardless of sun elevation over the interval from 4 to 52 degrees. Most of the measurements presented in this paper were confined to the range of sun elevations between 17 and 38 degrees, which we feel would minimize the relative effects of changing sun elevation. Wherever possible, sun elevations near 34 degrees were used to test the model and to avoid the necessity for counting excessively large numbers of craters at the small diameter end of the range.

If more precise sun elevation corrections are required, either constant revision of sun elevation tests must be done or a stereoscopic analysis should be used, eliminating the sun elevation problem.

I. Saturation and Equilibrium Cratering Conditions

Figure 6 illustrates how the surfaces we determined to have the maximum and minimum size-frequency slopes compare with the calculated equilibrium limits of Gault (1970). Gault suggested that equilibrium values would only approach 1% to 10% of theoretical saturation values. The 1% and 10% curves were obtained by calculating the corresponding fraction of the hexagonal-closest-packing condition for each 100 m diameter interval.

It is apparent that the values of 1% to 10% for equilibrium cratering suggested by Gault are attained for relatively young surfaces at crater diameters below 200 m. On older surfaces the combined equilibrium and seismic modification conditions produce a curve which becomes parallel to the equilibrium curves somewhat below the 1% level. The same result is obtained by using the Tranquillitatis curves from Figure 3. This indicates that equilibrium conditions are not the same for surfaces of different ages. This supports the model in this paper, which suggests that the increase in regolith thickness combined with the related increase in numbers of larger impacts produces a

gradually changing surface response to the flux of impacting objects. The reason for the gradual change, which involves a great reduction in the observable number of small craters from 100 to 300 m in diameter, may be due to the changing physical response of the thicker regolith to impacts and impact erosion as well as the total amount of seismic modification produced by larger impacts over the longer time period. It is logical to expect that craters produced where regolith is thin and most of the crater ejecta is blocky will degrade much more slowly than equivalent-sized craters formed entirely in a thick regolith. This would seem to be the case regardless of whether impact erosion or seismic modification were the dominant mode of crater degradation.

Chapman et al. (1970) also concluded that differences in crater distributions between different lunar regions cannot be produced solely by saturation cratering (impact erosion). However, they assumed that volcanic-collapse craters largely explained the differences. The model presented here is an alternative which is more consistent with the gradual changes observed as a function of relative age.

J. Effect of Secondary Rays on Frequency Distributions

Figure 7 illustrates the effect that obvious secondary rays can have on crater populations. The two curves represent a comparison of crater counts from seven areas near the crater Brayley (nos. 1-7, Table 1), five located on distinct secondary rays, and two located off the rays. We have assumed that the uniform albedo in this region and the location of the sinuous rille, Rimsky Korsakov, demonstrate large-scale lava flooding in this region and a uniform age throughout. The separate areas were counted by only two individuals each, but the different areas were combined, which we assume is just as valid as performing more counts in a single area. We assume that the differences in the curves can be accounted for solely by the impact of ejecta rays. The rays throughout this part of the Imbrium basin are mainly from Copernicus, Aristarchus, and Kepler craters. They all contain large clumps of irregular secondary craters surrounded by more evenly distributed smaller secondaries which are less irregular in shape. The two curves which group together similar areas, exhibit the same general trend that results from the effect of cratering over an extended period of time. The ray areas show an increase in craters greater than 170 m in diameter accompanied by a decrease in craters smaller than 170 m when compared with the regions not located on rays. This further supports our contention that prolonged impact gardening reduces the number of smaller craters within the equilibrium range.

A test of secondary ray areas in Mare Crisium produced slightly different results (compare data for areas 26, 27, Table 1). In this instance there were several complicating factors. 1) The scales of the two photos were different enough

to cause parallel displacement of the curves when plotted. 2) The areas are near two large postmare craters. 3) There is no independent, obvious evidence for or against the ages of the two areas. 4) The Crisium surface flows appear to be covered with a thin dark mantle, which causes small craters which penetrate the surface to appear particularly bright. This condition is present over much of Crisium, and Apollo panoramic photography at appropriate sun elevations is not as good as coverage in the other maria. 5) The obvious rays in much of Crisium appear to consist mainly of relatively small, uniformly spaced craters, without the numerous large irregular clumps of secondaries more common in Imbrium. The net effect of all these conditions, mainly the uniform fine rays, has been to shift curves on ray areas to the right of nonray areas (more craters in all categories). Thus it appears that the absence of large groups of secondaries has not caused obliteration of the smaller craters. However, this conclusion is very speculative in view of all the uncertainties. It is reasonable to expect that all secondary rays may be slightly different and, therefore, may produce slightly different results upon impact.

In either of the areas where rays were examined in this study, the presence of rays gives the surfaces a greater apparent relative age, which is to be expected. The significant observation is that the basic nature of the individual curves on or off rays, is the same.

K. Other Complications of the Idealized Model

Figure 8 is a comparison of a curve representative of three areas measured in Mare Serenitatis with three different areas from Mare Imbrium. The Serenitatis surfaces contain a much higher proportion of craters with very blocky ejecta as described by Young et al. (1974) and as suggested by the radar data of Thompson et al. (1973). Two of the Imbrium surfaces are on the Phase I and Phase III flows defined by Schaber (1973, Schaber et al., 1975) in the general vicinity of the crater Lambert, neither of which appears unusually blocky. If the simple model of regolith production and equilibrium cratering discussed in this paper is correct, then the blockiness of the regolith should decrease as the age and thickness of the regolith increase. The relative positions of the curves in Figure 5 indicate that the surfaces in Mare Serenitatis are intermediate in age between the range of the Imbrium surfaces, in spite of the obviously more blocky appearance of most of the surface in the southern Serenitatis basin. This supports our earlier suggestion (Young et al., 1974) that subsurface stratigraphy, perhaps a regolith buried by younger flows, could explain this difference. More recent filling of the central Serenitatis basin by lavas (similar to the model of Head, 1974a) would fit the buried regolith model proposed here. This interpretation is based on the observation that the transition from regolith to bedrock at present is related to the equilibrium size-frequency distribution below crater diameters of

275 m (Figures 2 and 3) and that the blockiness observed was produced by impacts that penetrated through surface lavas into an older, buried regolith as described by Young et al. (1974) and Young (1975).

If this rather simplified model of the near-surface stratigraphy of Mare Serenitatis is correct, it is reasonable to infer that less obvious stratigraphic differences would produce less obvious, but possibly significant, changes in the slopes of the crater size-frequency distribution curves for other areas.

Another problem associated with crater distributions is the presence of dark "mantle" deposits such as those in the Apollo 17 landing site area. This could produce inverse apparent age relationships either by covering small craters or because dark mantle deposits independently increase the relative thickness of the fine surface material (regolith) and produce a different response to the normal cratering process (Lucchitta and Sanchez, 1975).

We have examined such a dark mantle(?) area in Mare Nubium (Figure 9). When compared with other regions, the number of large craters indicate that Nubium is between the Imbrium and Serenitatis areas in age, yet it has fewer small-diameter craters (100-200 m) than either of the other surfaces. The photograph at 34 degrees for this region shows a distinctly darker surface, as do full moon photographs of the area. It is readily apparent that the smaller craters are difficult to see due to the lack of contrast between the sunlit and shadowed portions of individual craters and the adjacent surface with its dark albedo. In addition, the 34-degree sun elevation curve for this region is somewhat irregular, in contrast to surfaces of similar age, and shows no pronounced break in slope. Viewing and measuring the same area at a 10-degree sun angle eliminates some of these difficulties, and the crater distribution does show the characteristic break in slope. In this instance the dark mantle has not only apparently buried the smaller craters but has made it difficult to see craters at moderate sun elevations by producing a uniformly dark surface, where shadows blend with the darker surface albedo. Our results in this region suggest that some low albedo areas not generally considered to contain dark mantle deposits may be blanketed with such materials and that dark albedos in many instances cannot be assumed to merely represent relatively young lavas. However, it would be difficult to distinguish between the effect of mantling and the potentially different response of the dark mantle to impact erosion.

L. Hypothetical Crater Size-Frequency Distributions for Representative Areas

The results of the crater measurements described in this study can be utilized in the following manner: 1) If a single area is counted at two different sun elevations, the size-frequency distributions can be averaged and assumed to be valid for

a sun elevation intermediate between the actual sun elevations used. 2) If two adjacent or nearby areas can be assumed to be the same age from independent geologic evidence, crater counts for these two areas can also be averaged and assumed to be valid for a sun elevation intermediate between the actual sun elevations utilized. 3) As more areas are counted, the larger diameter portion of the typical curve (Figure 1,C) becomes more regular, if the results are averaged and normalized to the standard 350 km^2 area.

Individual small mare regions may have crater frequencies with irregularities or complications caused by subsurface stratigraphy, secondary rays, dark mantles, and unspecified causes. Because any small mare region used in this study could be atypical, we have chosen several general regions for which we have 2 or more sets of data at sun angles near 30 degrees. These separate counts for each region have been averaged together and plotted on Figure 10 using the conclusions listed in the preceding paragraph. The four curves in Figure 10 represent four distinct surface ages which cover the range of examples encountered in this study (Table 1). To obtain the composite curves, the individual areas were plotted and a "best fit" curve was approximated through all the points. In view of differences between individual results in the data collecting process, it was not considered necessary to use a least squares solution. Expressing curve slopes as decimals implies a greater precision than is warranted. We acknowledge that this is an empirical technique and that each group of individuals might obtain slightly different results.

To obtain data points for each hypothetical curve, an interval was chosen which closely approximated the average diameter interval for all the actual sets of data. The hypothetical data points were then extrapolated from the curves. These four curves are considered to be hypothetical "type areas" for the regions they represent. These four curves can be used to compare with individual data sets for the purpose of determining relative ages compared to these regions. The flows in Mare Imbrium (I_e) were chosen because of their uniqueness and the data available from other studies (Schaber et al., 1975). The central Serenitatis region is important because it appears to have the most uniform crater distribution in this size range of any comparable mare region. The Mare Imbrium surface near the crater Wallace (I_W) is the region used for our sun elevation tests and is also one of the oldest Imbrium surfaces. It appears to represent a transition between the two youngest surfaces and the older Tranquillitatis (T) region. The Tranquillitatis region was chosen because it is one of the few areas in the older maria for which suitable (low) sun elevation photography was available. It is not necessarily the oldest mare region on the moon. We have listed the data points extrapolated from these hypothetical curves in tabular form (Table 3) for ease of comparison with the data on crater frequencies in Appendix 1. The 30-degree sun elevation choice is partly coincidence,

but probably represents the best choice considering the problems related to sun elevation differences. Based on our results for sun elevation tests (Figures 4 and 5), we consider it valid to make direct qualitative comparisons of all the crater frequency data from 4 to 55 degrees except where the curves are very similar. An approximate sun elevation correction can be made by shifting any curve (parallel to itself) by 10 meters for each 30-degree change in sun elevation. The diameters increase as the sun elevation decreases.

Curves which appear very similar after all corrections have been applied are probably so close together in age that any distinction between them would be difficult by any means other than direct information, such as radiometric ages.

Although enlarging the standard area used in this study would improve the statistics, it would also increase the chances that areal or stratigraphic variations were producing composite curves. The purpose of the study was to determine the feasibility of reliably characterizing small mare regions without requiring any additional supporting information. This is the basic difference between our technique and those of Soderblom and Lebofsky (1972), Boyce et al. (1974), and Boyce and Dial (1975). The reliability of the technique is supported by our general agreement with the results of these other studies where our results overlap.

The total amount of time required to complete a crater size-frequency analysis of a 350 km^2 area on the moon using the technique in this report is 8 to 10 man-hours for an area comparable to two and one half 7 1/2-minute terrestrial geologic quadrangles. Considering that little additional information can be obtained about such small areas without other remote sensing data, it is not an overly time-consuming means of obtaining detailed information about an area that would require considerably more time for adequate photoreconnaissance on the earth.

M. Implications of Crater Size-Frequency Distributions Within Selected Mare Regions

The general effect of impact gardening is to obliterate small features on mare surfaces and to make it difficult to observe relationships between the types of features found within the maria. For this reason most of the discussion of the genesis of mare features has been confined to relationships seen in the younger maria, mainly Mare Imbrium, Oceanus Procellarum, and Mare Serenitatis. Most of the features discussed within these regions are common enough that it is presumed they formed in similar ways on the older mare surfaces. Furthermore, we have concentrated on those maria where the geologic framework is understood in the greatest detail from earlier studies.

Mare Imbrium and Aristarchus Plateau Region: The ages of flow units in Mare Imbrium have been summarized by Boyce et al. (1974) and Boyce and Dial (1975) from studies of craters in the 200 to 2000 m range. Our few results agree with the relative ages they obtained for the entire basin surface except that we have not calibrated our technique with absolute radiometric ages. Most of the Apollo landing sites are in areas with complex geology, and assumptions must be made concerning the correlation of crater distributions with radiometric ages. However, using Boyce and Dial's values of D_L (diameter of largest crater eroded to a maximum 1° slope) and comparing it to our curves it appears that the inflection points in our curves correspond to the maximum diameter of the D_L interval defined by Boyce and Dial (1975). Assuming that this correlation is valid, we would extend the area of young Eratosthenian flows near Euler to the region directly east of Lambert and westward to the edge of the Aristarchus Plateau (Figure 11, Areas 1-7, 15). There are a number of young flows east of the crater Lambert which look very similar to the flows near Euler and are mapped as Phase I (oldest) flows by Schaber (1973). This difference of opinion may be explained by the fact that the D_L intervals chosen by Boyce and Dial (1975) have a boundary at 195 m, which is near the inflection point for our curves. Thus a slight age difference may shift an area into one or the other of their categories.

Further evidence of the greater extent of the Eratosthenian flows mapped by Schaber from Apollo 15 photography can be seen on Apollo 17 views. The rille Rimsky Korsakov extends from the crater Brayley C (130 km east of the Aristarchus Plateau) westward to the vicinity of the crater Euler (LT039B3), where it is expressed in a Phase III (youngest) flow mapped by Schaber (1973). Careful analysis of the flow lobe margins on stereo photography suggests that the Phase III flow may have crossed an older lava tube which had not yet collapsed (metric frame AS15-1701). This is suggested by the smaller dimensions of the collapsed lava tube beneath the flow lobe. Moore and Schaber (1975) estimate the flows are on the order of 10 to 20 m thick. It appears probable that Phase I, Phase II, and, possibly, Phase III flows had sources near the margin of the Aristarchus Plateau as well as in

the vicinity of Euler.

The area due west of the Aristarchus Plateau also has an age approximately equal to the Eratosthenian flows mapped by Schaber (1973) as shown by crater counts in Area 30 (Table 1) near the crater Schiaparelli C. Several sinuous rilles on the Nielson topographic map (LTO38B2) show lavas flowed westward from the Montes Agricola region (LTO38B2S1). We believe there is strong evidence that the Aristarchus Plateau region was a general source for late stage (Eratosthenian) flows around the general periphery of the plateau. The large number of sinuous rilles in this region certainly demonstrate that it was very active as a source region earlier.

Flows in the vicinity of the Aristarchus Plateau in Oceanus Procellarum also provide a good measure of the relative effects of shallow lava flooding on crater densities in a young mare region. A low albedo region in the Seleucus Quadrangle (Moore, 1967) northwest of the Aristarchus Plateau (Area 31, Table 1) has been flooded by very thin flow(s). This can be determined by the flooding of small craters and large crater rim deposits on metric frame AS15-2746 and on topographic maps (LTO38B1, 38B4). Contour lines crossing a sinuous rille in the lava suggest it is thin, as does the very minor flooding of large craters. Craters the size of Meteor Crater (1.2 km) have been breached and barely flooded. This implies flow thicknesses less than 50 m to breach the rims and form shallow lava tubes. The crater counts for Area 30 (Table 1) lie outside the margin of these flows and demonstrate an Eratosthenian Age, whereas Area 31 on the flow has significantly fewer craters. Because the flows in this region filled 1 km diameter craters, the flooded area should show a complete "resetting" effect on the crater counts for craters in the range from 100 to 500 m. When the curves for Areas 30 and 31 are compared (see Appendix 1), they produce two parallel curves similar to I_e (Figure 10) separated by 35 to 40 m. This demonstrates that flooding of surfaces does not produce an effect which is likely to be confused with impact gardening when two regions are compared. The parallel offset of the curves is as great as the maximum sun effect observed over a 48-degree range (Figure 4), although the sun elevations are close in this case. In this instance, because the two areas are very close in age, the curves are different but parallel with inflections near 215 m diameters.

Subtraction of the two sets of data for Areas 30 and 31 gives the relative distribution of crater-producing objects for the interval from 100 to 500 m over a finite period during Eratosthenian Time. Although this is a rather imprecise measurement without radiometric age control, it can provide a better idea of the relative distribution of crater sizes for a finite interval during the latest stages of mare filling. Similar measurements for other regions with similar histories of flooding could provide a measure of the relative uniformity of the meteorite flux through time. Some geologic constraints are required to compare

the regions, such as superpositional relationships.

However, viewed from another perspective, the younger area has approximately 58% fewer craters than the older (unflooded) region adjacent to it. Since both curves have slopes and inflection points indicative of an Eratosthenian Age (flows near Euler), they probably lie in the age range of 2.5 ± 0.5 BY (Boyce et al., 1974). Therefore, the great difference in crater densities implies either a rapid flux decrease during the interval or a large age difference between the two surfaces. Geologic evidence over the whole moon suggests there has not been any significant volcanism since the eruption of the Eratosthenian flows in Mare Imbrium. Other evidence supporting their relatively close age is the parallelism of the curve segments which all other data in this report show to be a sensitive indicator of relative age.

Other general conclusions from our studies of the Imbrium basin indicate that the crater counting technique can discriminate between the ages of Schabers Phase I, II and III flows (see data for Areas 8-14 in Appendix, Figure 11). We also support a model which implies more recent filling of the central basin as is obvious in Serenitatis (Boyce and Dial, 1975). The Apollo 15 Site is on one of the older flow areas in the basin but is distinctly younger than the surface near the crater Wallace, Areas 16 and 17, Figure 11.

Mare Serenitatis: Our crater measurements in Mare Serenitatis, combined with other evidence, imply that a shallow regional subsurface discontinuity exists in southern Mare Serenitatis.

Several characteristics of south-central Mare Serenitatis are unique to this basin and indicate that an unusual history may be recorded in the basin fill. Geologic evidence strongly supports a regional discontinuity beginning at depths greater than 40 m below the surface and extending to 250 m depths in some places. The following observations concerning the basin are pertinent to the discussion which follows: 1) The central portion of Serenitatis (brownish gray lavas) represents much younger flooding than that which produced the older flows which ring the basin and form the highly cratered darker annulus of bluish gray lavas and mantling materials. Although the brownish gray lavas are approximately equivalent in age to large portions of the Imbrium basin surface (crater counts), most of the mare ridges in Serenitatis experienced much later growth and deformation as demonstrated by their very sharp morphology and the unusually large number of postmare craters filled by flows along the ridge flanks. 2) Despite the obvious 2-stage flooding of the basin, there are few remnants of old flooded craters or ring structures, indicating either that the late stage filling was relatively deep or that some other deposit covered the surface before the most recent flooding. 3) The overturned strata in the rim flap of Bessel have exposed the bluish gray lavas found beneath the younger brownish gray surface rocks (Muehlberger, 1974). The low depth/diameter ratio for Bessel (0.11) indicates

that the contact zone must lie at a depth considerably shallower than the 1000 m depth of the crater floor below the surrounding surface. This is a significant deviation from the estimate made by Muehlberger (1974) prior to completion of detailed topographic maps for the minimum thickness of the younger lavas. 4) The flooded craters, Finsch and Bobillier, located 100 km northeast and 85 km southwest of Bessel, indicate a buried surface at a depth of 150 to 200 m based on rim height-diameter ratios of unflooded craters in the same basin. 5) Phillips et al. (1974) suggested the existence of a subsurface interface near 100 m in Mare Serenitatis about 80 km southwest of Bessel from the Apollo 17 Lunar Sounder Experiment. 6) Bessel D, near the center of Serenitatis, also shows layering (overturned flap?) in the upper 200 m of its rim. 7) Most craters with diameters up to 1 km in southern Serenitatis have conspicuously larger and more numerous ejecta blocks than in any comparable mare region covered by panoramic photography. This has been interpreted as indicating a buried regolith or ejecta deposit beneath the surface lavas (Young et al., 1974).

Our detailed crater size-frequency measurements on 34 mare surfaces in 8 different maria show the overall distributions in southern Serenitatis to be the most uniform of any maria in the diameter range from 100 m to 600 m (Table 1, Appendix 1). The discontinuity in the typical crater size-frequency slope at the upper limit of the equilibrium cratering range for Serenitatis occurs near diameters of 250 m throughout the southern part of the basin. Mare Serenitatis crater frequency distribution curves all show a somewhat more pronounced irregularity in the number of craters in this transition zone when contrasted with the other maria. In addition to the normal change in the size distribution near 250 m, there are abnormally high numbers of craters with diameters near 250 m, approximately 50% more than would be predicted by extrapolation of the numbers of craters both larger and smaller. Although some irregularities are normal near this zone of transition from fractured rock (regolith) to more coherent bedrock, the Serenitatis region shows a significant anomaly in this interval (240 to 260 m craters). Depth/diameter ratios indicate a discontinuity which is "sensed" by craters penetrating to a depth of 30 to 50 m. There is also an abundance of flat-floored craters and flat-floored craters with central mounds in south central Serenitatis with diameters between 250 and 700 m. Although this morphology is common for craters which penetrate through the surface regolith to bedrock, craters with 700 m diameters should be too deep to represent the surface regolith/bedrock boundary in Mare Serenitatis. The largest craters in this range (700 m) suggest the presence of a 2nd coherent layer beneath an intermediate unconsolidated horizon near a depth of 100-200 m by analogy with model studies of impacts in layered media (Quaide and Oberbeck, 1968) and terrestrial craters.

For both Meteor Crater (1.2 km) and Ries Crater (23 km) Stöffler et al. (1974) have shown that nearly 99% of the ejecta surrounding these craters came from rocks originally occurring

in the upper 30 to 35% of the depth of the transient cavity immediately after impact. Bessel Crater has a shape similar to that of Meteor Crater in that their rim heights (uplift plus overturned flap) above the original ground surface average 33% of the present crater depths, ignoring the younger sediments now filling part of Meteor Crater. Based on these terrestrial examples and assumed gross similarities, the bluish gray lava on the overturned flap of Bessel can be assumed to have been excavated from depths not much greater than 400 m. A significant amount must have been present at shallower depths in order that enough material was ejected to still be obvious from orbit in the impact-gardened surficial deposits around an Eratosthenian Age crater.

All the foregoing evidence indicates the presence of a discontinuity or unconformity containing a significant amount of unconsolidated material at depths close to 100 m, probably between 50 and 300 m, which lies between the older bluish gray maria visible around the edge of Serenitatis and the brownish gray lavas in central Serenitatis. Spectral images (Johnson et al., 1975) show dark-mantle-type material "mixed" with the more crystal-rich soils in central Serenitatis. This could be material excavated by craters <1 km in diameter. The evidence for 50 m or more of black, orange, and red pyroclastic(?) deposits on the old dark bluish basalts all around the southern edge of Serenitatis (Lucchitta and Schmitt, 1975) would provide the necessary thickness of material between the flows in the central basin. The thickness required is on the order of 50 to 100 m in order to account for both the absence of older large crater rims protruding through the thin surface flows of brownish gray lava and the shallow nature of the 250 m crater diameter anomaly.

A dark layer (mantle?) is present in Bessel ~430 m below the rim (Figure 14). From crater counts, correlated with published ages for surfaces with equivalent crater distributions, there appears to be at least a 0.5 BY interval separating the two filling episodes (Boyce et al., 1974; Boyce and Dial, 1975; Lucchitta and Schmitt, 1975). This provides ample time for significant cratering of the buried surface of the bluish lavas. The surfaces appear to be roughly equivalent to the ages of Apollo 15 and Apollo 17 basalts. Although the surface lavas and pyroclastics beneath them are probably not of uniform thickness, a reasonable model for the subsurface layering would include 50 m to 150 m of brownish gray surface lavas overlying 50 to 100 m of regolith and pyroclastics above the bluish gray lavas. The constraints on the surface elevation of the bluish gray lavas in the vicinity of Bessel indicate that the relatively steep gradient on the dark annulus around southern Serenitatis must level off to a nearly horizontal surface with a probable elevation between 4450 and 4600 m near the center of the basin.

If correct, this shallow discontinuity places constraints on models for mare ridge formation which invoke thick sections of

cooling lavas or horizontal stresses transmitted across mare surfaces. It appears likely that the relief across mare ridges in Serenitatis is in some cases significantly greater than the thickness of the surface lavas in which they have formed.

Other results from our work on Mare Serenitatis are discussed at length in Young (1975) and Young et al. (1974).

A caution about the use of crater counts on the young lavas in central Serenitatis should be considered. Boyce and Dial (1975) state that their method of crater age determination using D_L (the largest diameter crater which has been degraded to maximum slopes of 1°) assumes that flat-floored to concentric craters (usually small craters in the regolith) have little effect on their results because the craters they use are too large. In the case of Mare Serenitatis, there are large numbers of concentric and flat-floored craters with diameters up to at least 700 m caused by the subsurface stratigraphic section discussed in the preceding pages. It is our view that although the surface of Serenitatis has a crater count age similar to the Apollo 15 Site area, it is slightly younger according to our method of plotting size-frequency distributions. Boyce et al. (1974) indicate a correspondence in ages of the Apollo 15 Site and south central Mare Serenitatis, in addition to a distinct range of ages in Serenitatis which we cannot see in our data. In view of the very uniform and regular crater distribution for our four Serenitatis areas (Figure 12), it is possible that the stratigraphic discontinuity we feel certain exists is responsible for the difference between our conclusions and the age assignments by Boyce et al. (1974).

We have not attempted to complete crater frequency analyses for the Apollo 17 Site due to the complex geology of that region (Lucchitta and Schmitt, 1975).

Oceanus Procellarum and Mare Nubium: Apollo 16 Photography: Our few measurements in the Mare Nubium region (Figure 15) are discussed in Section K, p. 15 with regard to dark mantle deposits. It is generally agreed that Oceanus Procellarum (including Mare Nubium) is one of the younger maria and that it is not like the isolated circular maria. Our few crater counts bear out its general age, in spite of the dark-mantle problem (see Areas 32 and 34). Area 32 (Figure 15) coincides almost exactly with the curve for I_e on Figure 10, whereas Area 34 is approximately the same age as the Apollo 15 landing site (Area 18). Area 34 appears to show the effect of the same dark-mantle deposit as Area 33 (Figure 9), although to a lesser degree. It is parallel to curve S on Figure 10 but displaced 30 to 50 m to the right. This does not fit the normal progressive change in our proposed aging model, but the origin and effect of dark-mantle deposits are not completely certain. The method of its emplacement, its thickness, the timing of its emplacement, and how it responds to impacts could all affect the rate of crater erosion and the total number of craters visible at present. More significant information will

be discussed concerning Oceanus Procellarum in the section dealing with mare ridges, rilles, and surface features.

Mare Crisium: The geology of Mare Crisium is discussed under part J of Section I dealing with the effects of secondary rays and dark mantles. Further discussion is contained in the section dealing with multiringed basins. It is difficult to add any further detail concerning the surface geology in addition to that which is included in the geologic map of Mare Undarum (Olson and Wilhelms, 1974). Our crater counts (Figure 16, Table 1) indicate a probable age intermediate between the Eratosthenian flows in Mare Imbrium and the Apollo 15 Site flows, but the presence of a dark mantle may be affecting these results. It is clear that the center of Mare Crisium has subsided and been filled by younger lavas as is the situation in Mare Imbrium and Mare Serenitatis.

Mare Tranquillitatis: Crater counts on the older mare surfaces such as Tranquillitatis, Fecunditatis, and Nectaris are limited due to the generally high sun elevations encountered on Apollo photography of these areas. Photogeologic comparisons of all of these maria demonstrate they are generally older and contain many more craters with diameters from 300 to 600 m. Our results in the Sinus Amoris portion of Tranquillitatis suggest that it would be difficult to determine relative ages on surface in this range (Figure 12, Areas 23, 24, 25; Appendix 1). The character of the curves (see Figure 6) is such that there is likely to be a great deal of overlap from one curve to the next for a range of ages. We attribute this to the effects of prolonged impact gardening and seismic modification of older surfaces as discussed under Section G. For the same reasons, studies of surface morphology are less productive due to the much greater thickness of regolith.

Tsiolkovsky: The small amount of mare material flooding the floor of the farside crater Tsiolkovsky has an age slightly younger than the Apollo 15 Site. A single analysis of this region was completed merely to ascertain that the obvious volcanism on the farside was more or less contemporaneous with similar events on the frontside. It is likely that the flooding of Tsiolkovsky was determined largely by the relatively young age of the impact. The general elevation of the farside indicates that volcanism might not have occurred in that specific region if the crater Tsiolkovsky had not provided a conduit for the lavas to reach the surface.

N. The Validity of the Eratosthenian and Copernican Systems as Regional Lunar Time-Stratigraphic Units

Certain age relationships shown on published U.S.G.S. Lunar Geologic Quadrangle maps produced from telescopic and Orbiter photography can be seen to be in need of revision, especially features designated as Copernican and Eratosthenian. A prime example is the crater Euler (Carr, 1965) in Mare Imbrium. The

northwest portion of the ejecta blanket from the crater Euler is partially obliterated by the Eratosthenian flows mapped by Schaber (1973). However, Euler was mapped as a Copernican age crater by Carr (1965) and by Wilhelms and McCauley (1971). In this case a direct superpositional relationship can be demonstrated. Euler does have many of the characteristics considered to be typical of Copernican craters without obvious rays.

This single example in an area that has been studied by many individuals in great detail indicates that the characteristics of Eratosthenian and Copernican features are not distinctly different enough to allow discrimination between the two ages in all cases. It appears that the characteristics of old Copernican craters overlap in time the episode of Eratosthenian lava flooding on the moon. Thus caution is necessary in assuming that all the relatively simple(?) designations published for the ages of major mare units and young craters are absolutely certain. If these relationships are not always obvious in the Imbrian basin, they may be even less obvious in the highlands and other mare regions. Maps produced subsequent to the acquisition of Orbiter photography should be superior, but even the example cited above is not obvious on Orbiter frames. For this reason we have avoided using the terms Eratosthenian and Copernican for age relationships except where the terms have been previously applied to well-documented geologic features. If one were to use the crater Copernicus to define the base of the Copernican System, it is clearly younger than the flows which postdate Euler, as shown by superposition of secondary ray clusters. However, this does not alleviate the problem of correctly assigning other craters to the Copernican or Eratosthenian Systems.

0. Summary: Crater Measurements and Related Studies

The following conclusions are of significance with regard to our studies of mare surface ages defined by crater distributions.

1) Areas as small as 350 km^2 may be discriminated with regard to relative age using the size-frequency distribution of craters between 100 and 600 m in diameter.

2) Crater distributions in this range define (bracket) the equilibrium diameter for most, if not all, mare surfaces on the moon.

3) Impact gardening produces a gradually changing surface response to impact and crater preservation as the regolith thickens with time. All surfaces older than the Eratosthenian flows in Mare Imbrium show a decrease in the absolute numbers of craters in the diameter range from 100 to ~300 m with increasing age. Craters with diameter >300 meters show the expected increase in numbers with increasing age.

4) The simple model of regolith production and crater destruction demonstrated by the curves in Figure 10 can be complicated by the presence of dark-mantles, subsurface stratigraphic discontinuities, shallow flooding by lavas, rays, and marked sun elevation differences. However, the method of plotting used in this report generally allows identification of and allowance for the simple complications of the idealized model.

5) Our independent results agree generally with those of Boyce and Dial (1975) regarding relative age determinations of mare surfaces. Our technique can be used in areas that are so small that they contain (statistically) only a single crater as large as 500-600 m. Our method is not likely to be affected by primary crater shape anomalies such as are present over much of southern Mare Serenitatis.

6) Although there is a need for rapid and efficient methods of studying large mare regions, detailed studies of small (350 km^2) areas can provide significant data on surface and subsurface geology which is lacking in methods that do not involve precise measurements of small craters (100-500 m).

7) Crater counts by single individuals, regardless of how conscientiously performed, contain individual bias which prevents them from being meaningfully compared with the data of other single individuals. If a single individual can be shown to perform in a consistent fashion, his or her data may be compared safely only with results for his or her own earlier work. Comparison of data between groups should only be attempted for measurements made using the same technique and preferably using averages of at least 3 persons.

8) Detailed measurements of small craters (0-200 m) for which the sun elevation effect has not been considered should be used with caution, especially if photographic scales are not precisely known.

9) If detailed panoramic photography at favorable sun elevations were available for a greater portion of the lunar surface, many individual stratigraphic problems could be solved with greater precision. Of particular interest is the possibility of recognizing subsurface discontinuities, which may be of significance for the accurate interpretation of remote sensing data (see discussion of Mare Serenitatis).

10) Although time consuming, the method of crater analysis used in this report is a relatively inexpensive and efficient means of photogeologically examining regions on the moon of a size that would require a far greater effort and expense for comparable results on the earth.

11) It is evident that the Eratosthenian and Copernican Systems used for age comparisons on geologic maps have shortcomings which should be carefully evaluated before published age criteria are assumed to be absolutely valid in individual cases.

12) It appears likely, from relative crater frequencies on closely related Eratosthenian Age flows, that there has been a significant decrease in the number of 100 to 500 m crater-producing objects since the youngest significant flows were erupted on the moon. (From data on Areas 30 and 31.)

13) A summary of our relative age estimates for the regions on Table 1 appears on Table 1A.

Captions: Figures 1-17

Figure 1. Crater size-frequency distribution curves based on apparent diameters for Imbrium flows (Areas 13 and 14, Table 1; Figure 11). All curves on Figures 1-10 represent 350 km^2. Craters plotted at centers of intervals (Table 1). Linear segments of curve A and C show significant discontinuity near B, interpreted as bedrock transition effect. Lower curve slope (C) approximated with line merely to draw attention to change in slope representing change from equilibrium conditions at small diameter end of curve (A). Log log plots of same data included for comparison. Error bars omitted for clarity on all other Figures. See Appendix 1.

Figure 2. Comparison of crater size-frequency distributions for several 350 km^2 areas plotted as in Figure 1. Areas not photographed near 34° sun elevation were corrected by lateral shift proportional to sun effect shown in Figure 3. Bullseye: (no curve drawn) Tranquillitatis, Area 24. Square: Crisium, Area 27. Triangle: Serenitatis, Area 20. Dot: Imbrium flows, Area 10. Dashed line (no points plotted) Mare Imbrium near crater Wallace, Area 17, data shown on Figure 4. Note decrease in slope of small diameter segments corresponding to increase in 300 to 500 m craters. Discontinuity between segments shifts toward larger diameter with increasing age.

Figure 3. Similar plot to Figure 2 for 5 different 350 km^2 regions. Three of these curves include averages of more than one 350 km^2 area, and are likely to be more reliable than Figure 2. The same progressive change in the segments of the curves is shown. Older surfaces have noticeably fewer small diameter craters and more large ones. I_E, Area 10. S, Area 22. P, Areas 33a and 34. I_W, Areas 16c and 17c. T, Areas 23 and 25. Symbols stand for Imbrium, Serenitatis, Procellarum, and Tranquillitatis initials. Symbols on Figure are listed with youngest at top, oldest at bottom, except that the Procellarum curve (P) is in a dark mantle region and is not indicative of the true relative age.

Figure 4. Effect of changing sun elevation on apparent crater diameters for a single area (Table 1, 17 a, b, c) in Mare Imbrium near the crater, Wallace. Dashed line is least squares fit for 34° sun elevation points. Note that craters shift essentially parallel at small diameter range toward increased diameters as sun elevation decreases. Open symbols represent new craters not counted at 52° sun elevation which appear large

enough to be above 100 m limit as sun elevation decreases. The additional craters on each curve (open symbols) represent a >100% increase in the total craters counted from 52° to 4°.

Figure 5. Two curves for sun elevation comparison in Area 16 (Table 1) immediately adjacent to Area 17 (Figure 11). These curves show basically same sun elevation effect as Figure 4 but were completed later in the study to check the consistency of results. Absolute effect of sun angle change seems to have diminished but is still noticeable. Data for 52 degree sun elevation in same area (Table 1, 16a) is almost identical to 34 degree data (see appendix). We interpret results of Figures 4 and 5 to indicate improvement in individuals ability to measure crater diameters on high sun elevation photographs. Average correction to be applied to curves when comparing different sun elevations is estimated to be parallel shift of curve by 10 m per 30 degree change.

Figure 6. Comparison of Imbrium curve (Area 10) and Tranquillitatis curve from Figure 2 with theoretical saturation curves of Gault (1970). Young surfaces approach equilibrium saturation in the range suggested by Gault (1-10%), but older surfaces such as Tranquillitatis become parallel to the saturation curves below the 1% level. Curves were corrected to true diameter using Figure 4 and thus are slightly displaced from their positions on Figure 2. Change in numbers of small craters is due to increased thickening of regolith and seismic modification of older surfaces.

Figure 7. Contrast of several areas on and off rays near crater Brayley in SW Imbrium. Open circles represent average of Areas 1 through 5 (Table 1) which lie on rays from Aristarchus(?). Solid dots are areas on same flows which are unaffected by rays. All surfaces are considered to have been flooded by flows which produced Rima Rimsky Korsakov. This sinuous rille traverses the entire area and appears to be expressed in a Stage III flow of Schaber (1973). Superposition of ray across flows has same effect as impact gardening over longer period, reduction in number of small craters and increase in larger diameters. (See further discussion in text.)

Figure 8. Comparison of curve representing average of 3 similar but separate 350 km^2 areas across central Serenitatis (Areas 20, 21, 22) with three different curves from Mare Imbrium (Areas 13 and 14; 17; 10;). Although the surface in central Serenitatis is conspicuously more bouldery in the ejecta of craters <1 km, the Serenitatis curve appears equal to or older than the

Imbrian flows represented by the two solid line curves. Bouldery surfaces do not appear to be an absolute criterion of relative age (see further discussion in text).

Figure 9. Effect of "dark mantle" on apparent size-frequency curves for area in Mare Nubium (Areas 33a, 33b) at two different sun elevations. Craters appear to be buried at small diameters, and at 34° sun elevation the curve loses its characteristic shape due to the difficulty of distinguishing crater shadows from the surrounding dark surface (see further discussion in text).

Figure 10. Hypothetical curves (averaged) calculated for 30° sun elevation for selected areas representative of the range of surface ages examined in this study. I_W, Areas 16 and 17. I_e, areas 10 and 15 on Eratosthenian flows in Imbrium. S, average of areas 19, 20, 21, and 22 in central Serenitatis. T, Areas 23 and 25 from Sinus Amorus in Mare Tranquillitatis. (See locations on Figures 11, 12, 15, 16, 17) See text for method of construction of curves, and Table 3 for data represented by points. This set of curves is designed to be used as a reference with which to compare other areas listed in Table 1 and data from Appendix 1.

Figure 11. Location of crater count areas (350 km^2) in Mare Imbrium. Eratosthenian flows (E_m); Craters, Lambert (L), Euler (E), Timocharus (T), and Apollo 15 landing site (star). After Wilhelms and McCauley, 1971. See Table 1 and Appendix 1. Brayley Crater (B).

Figure 12. Location of crater count areas (350 km^2) in Mare Serenitatis and vicinity. Dark mantle units (D) taken from compilation of geologic quadrangle maps (U.S.G.S.) B designates crater Bessel. See Table 1 and Appendix 1.

Figure 13. Fresh and partially degraded 1 km craters in southern Mare Serenitatis (A,B). Apollo 17 panoramic frames 2325, 2333. Fresh and partially degraded 1 km craters near Aristarchus plateau along southwestern edge of Mare Imbrium (C,D). Apollo 15 panoramic frame 0330. Contrast much higher proportion of large blocks (up to 60 meters long) around craters in Mare Serenitatis. Sun elevation is 10° in Serenitatis, 16° in Imbrium.

Figure 14. Crater Bessel interior and rim (inset). Apollo 15 pan frames AS15-9330 and AS17-2345. Crater Bessel wall on WSW side is approximately 1300 m high (south at top). Inset shows layering in upper rim (A to B) above dark layer at low sun elevation. Larger view shows dark layer (dark mantle?) beneath overturned rim flap. Dark layer (M) is interpreted as dark mantle material similar to dark annulus around SE Serenitatis basin which apparently extends throughout the southern Serenitatis basin beneath the young flows in the interior (see Figure 12). Bessel diameter is 16 km.

Figure 15. Location of crater count areas in Oceanus Procellarum and Mare Nubium. H indicates location of Herigonius rille vents. R is flooded crater rim shown on Figures 20, 21. Irregular-shaped patches are highlands within flooded mare regions. See Table 1 and Appendix 1.

Figure 16. Location of crater count areas and features in Mare Crisium area. P is crater Peirce; D is Dawes, J is Jansen, M is Miraldi D, and T is Taruntius. See Table 1 and Appendix 1.

Figure 17. Location of crater count areas and features in Mare Smythii. Crater symbols: Haldane (HA), Runge (R), Warner (WA), Kiess (KS), Widmannstätten (W), Kao (K), Helmert (H). See Table 1 and Appendix 1.

FIGURE 1

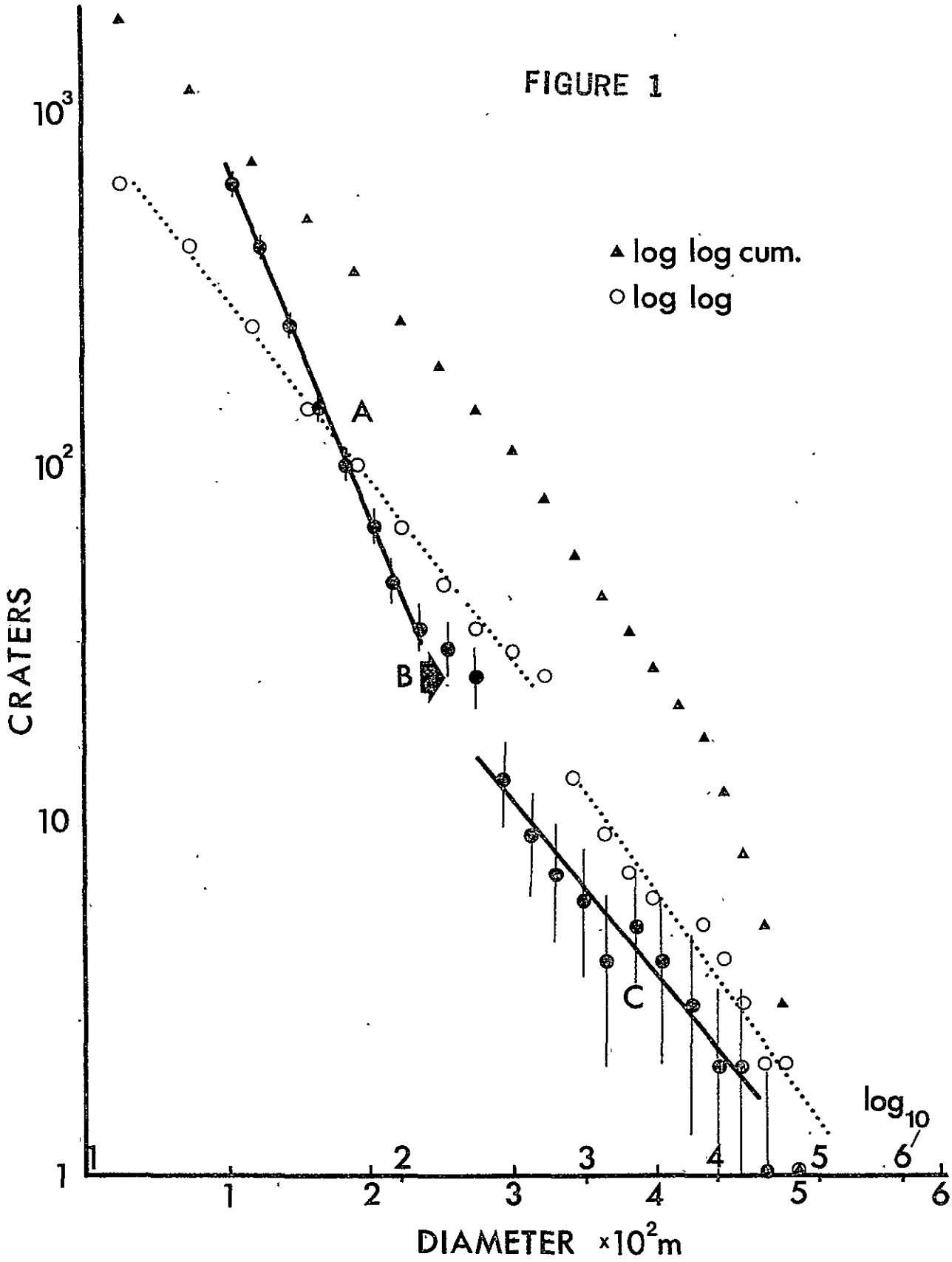
log log cum.
log log
A
B
C
CRATERS
10^3
10^2
10
1
1
2
3
4
5
6
$\log_{10}$
DIAMETER $\times 10^2$m

FIGURE 2

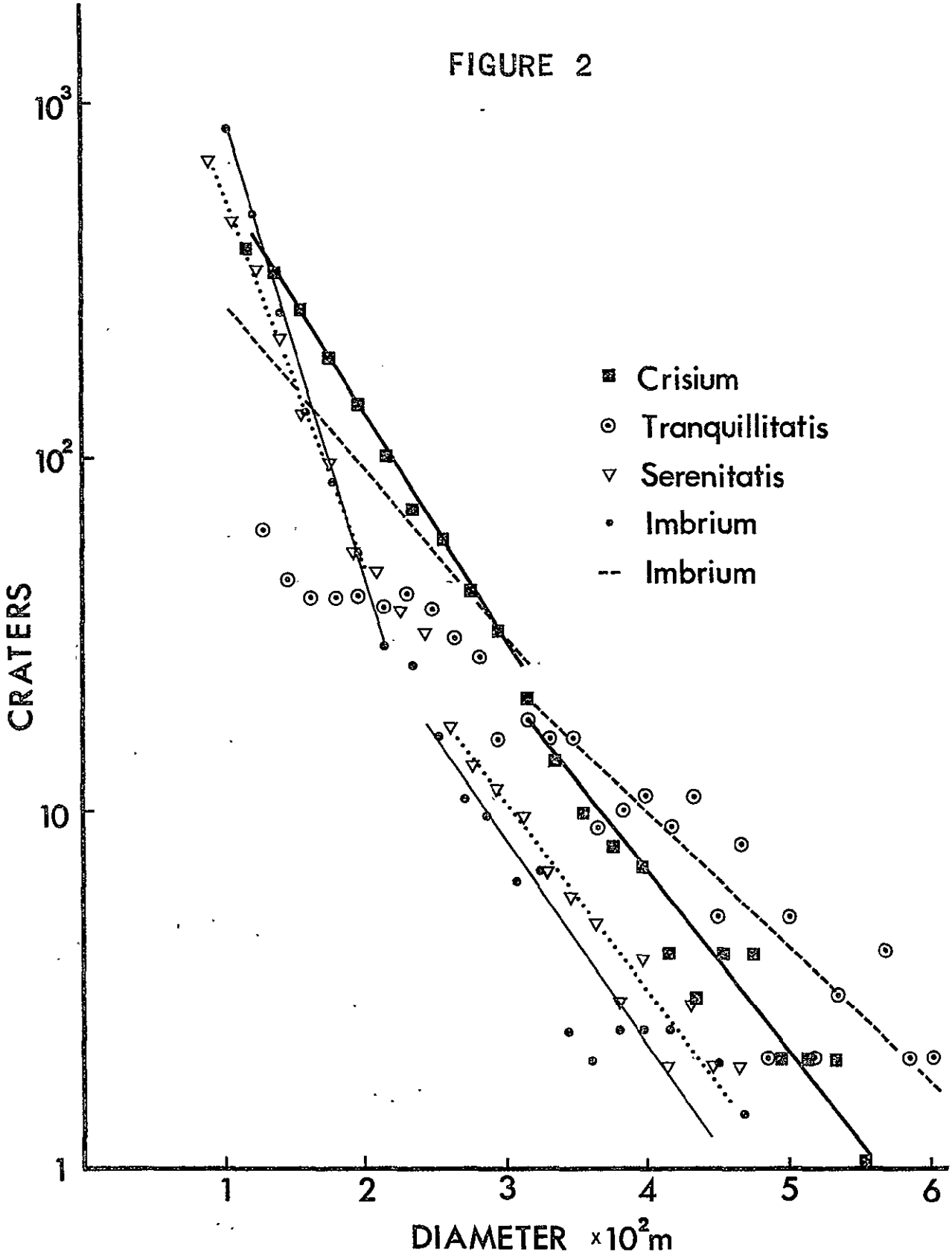
10^3
10^2
10
1
CRATERS
1
2
3
4
5
6
DIAMETER $\times 10^2$m
Crisium
Tranquillitatis
Serenitatis
Imbrium
Imbrium

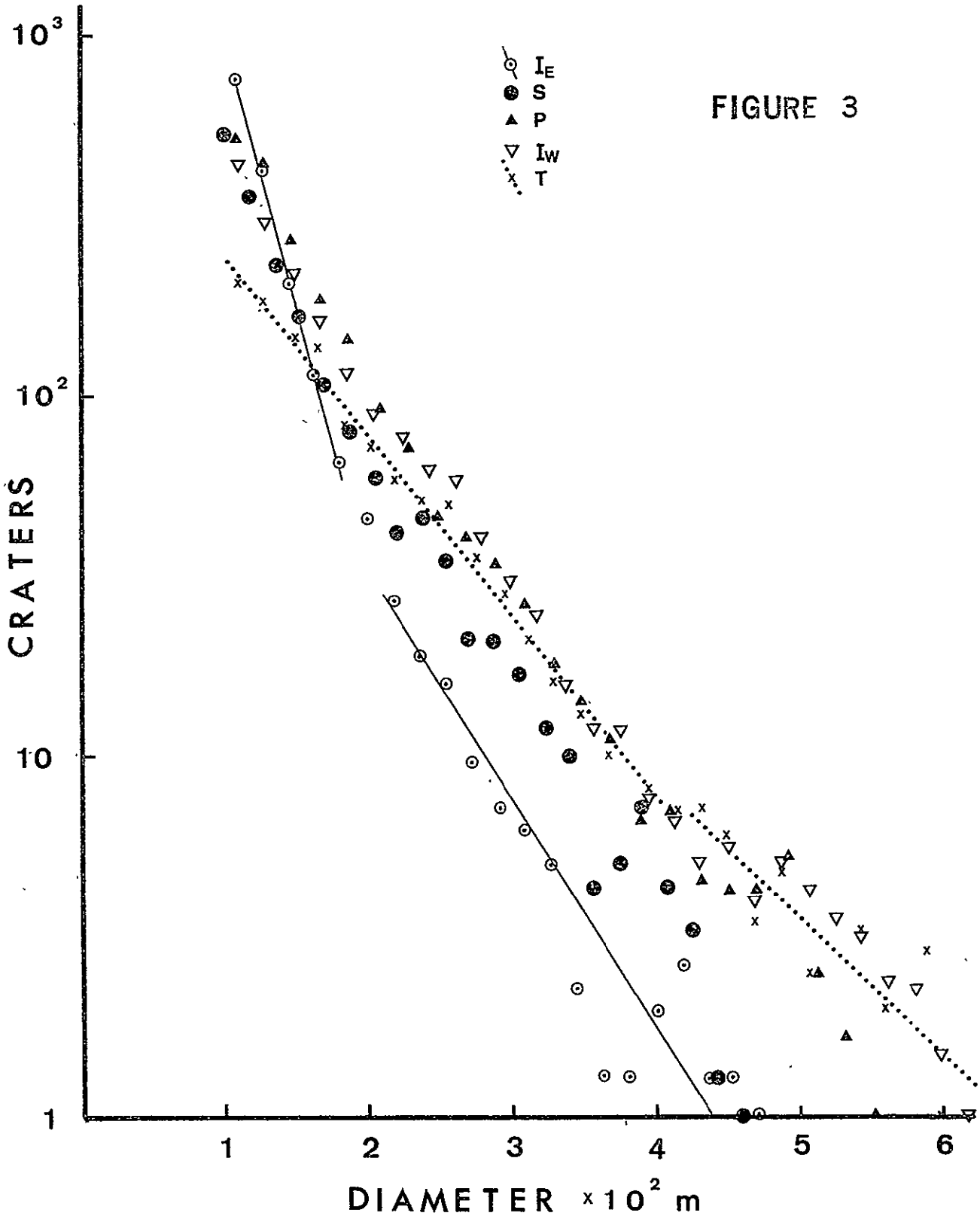

FIGURE 3

FIGURE 4

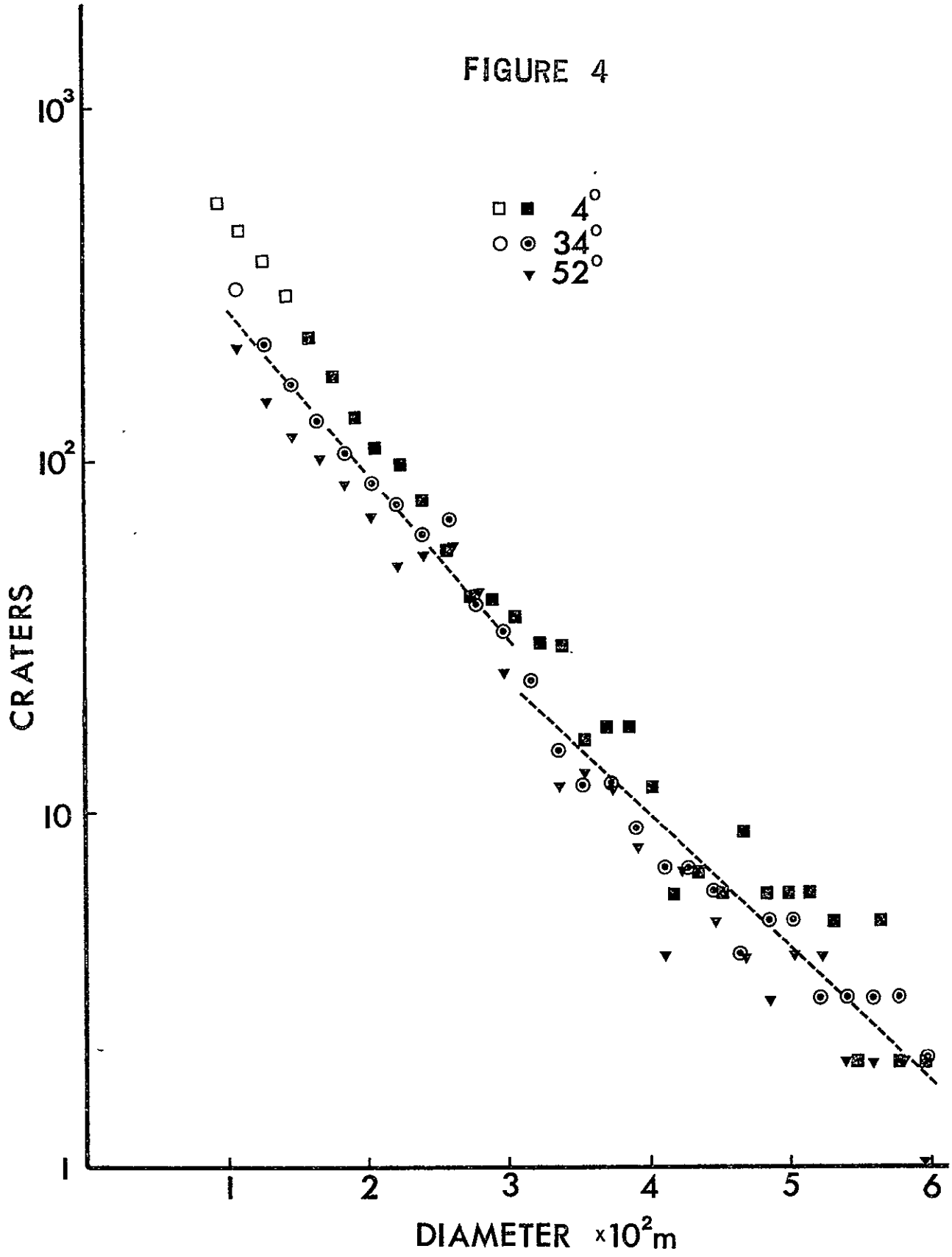

FIGURE 5

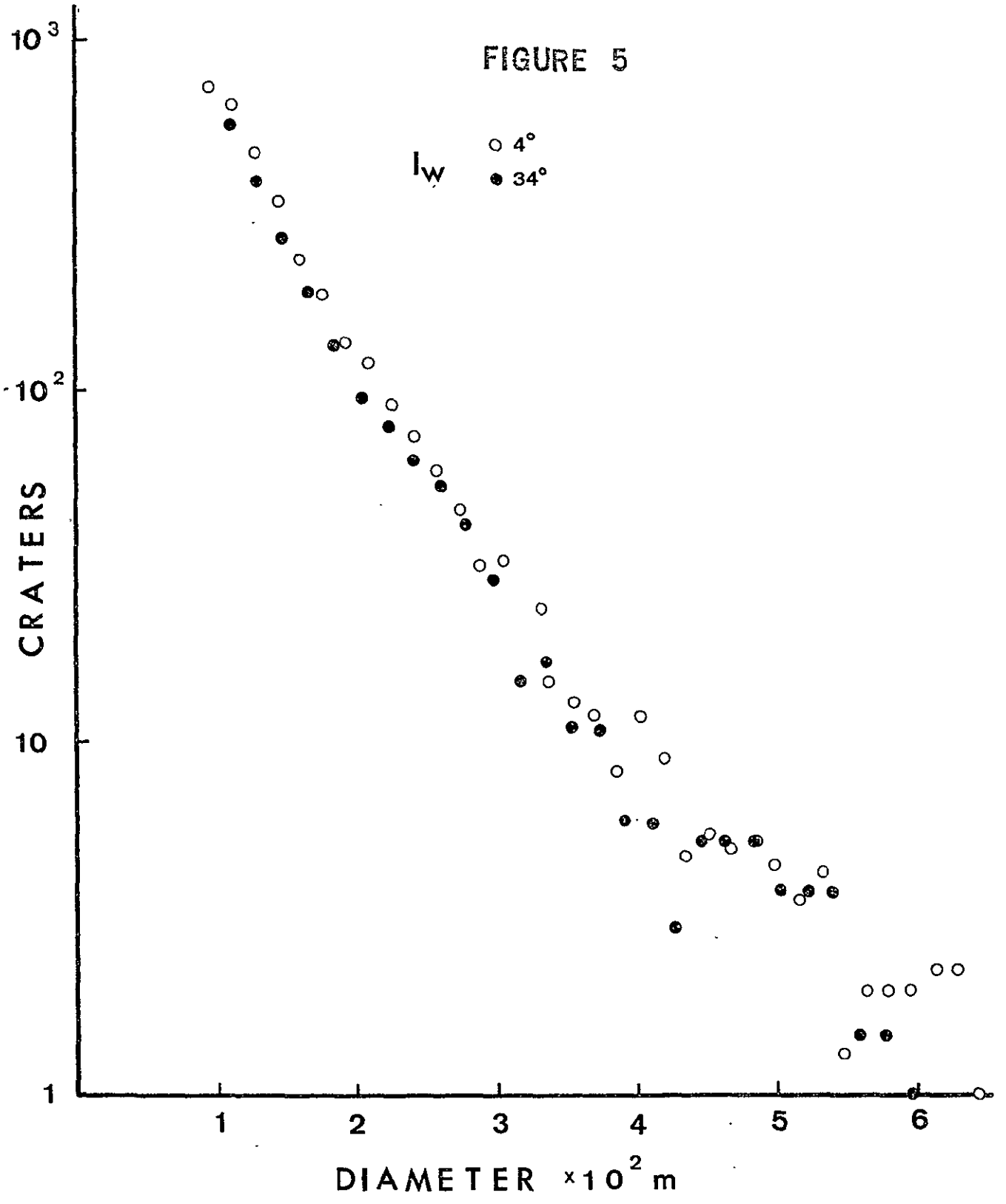

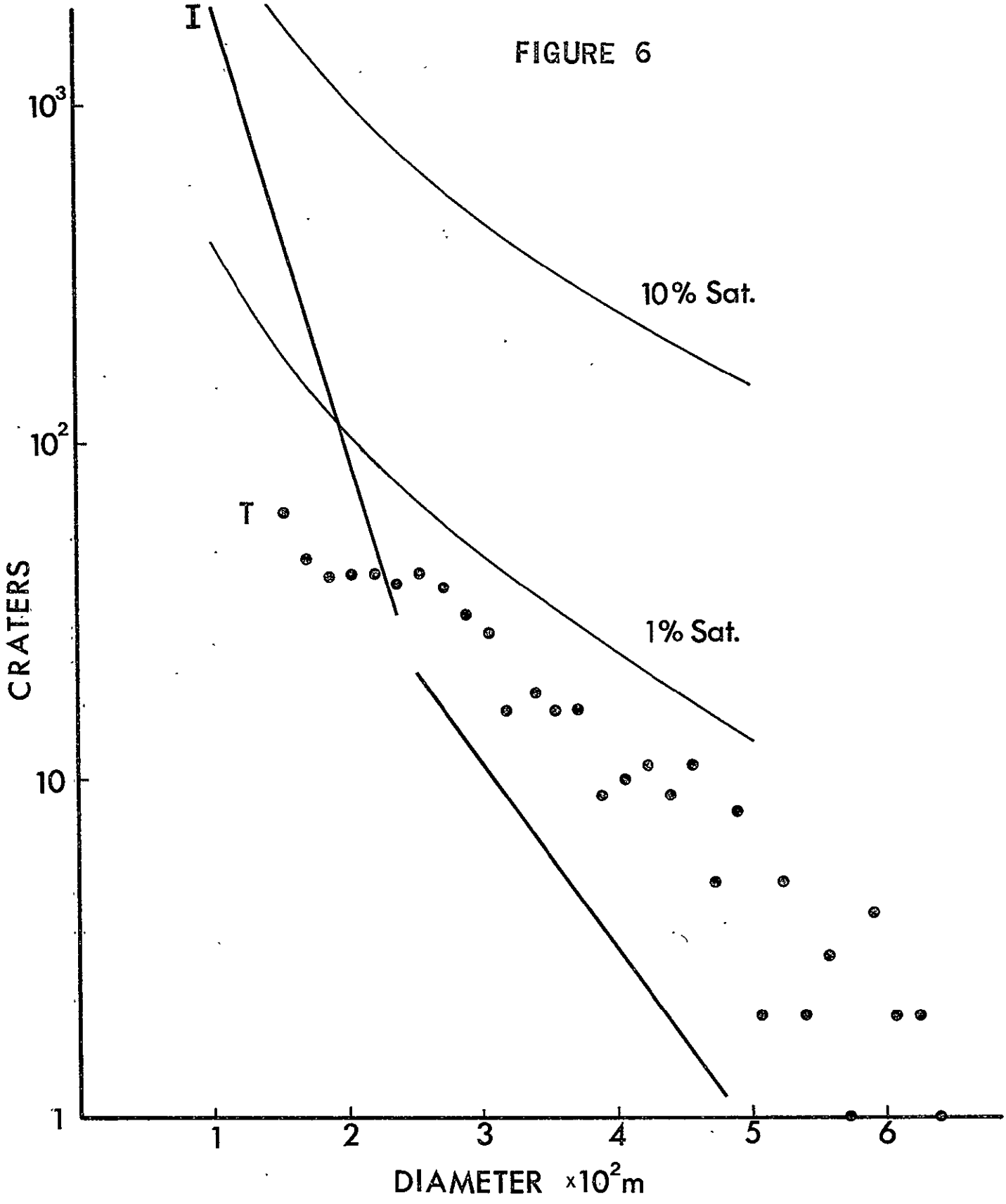
FIGURE 6
I
T
10% Sat.
1% Sat.
CRATERS
10^3
10^2
10
1
1
2
3
4
5
6
DIAMETER $\times 10^2$m

FIGURE 7

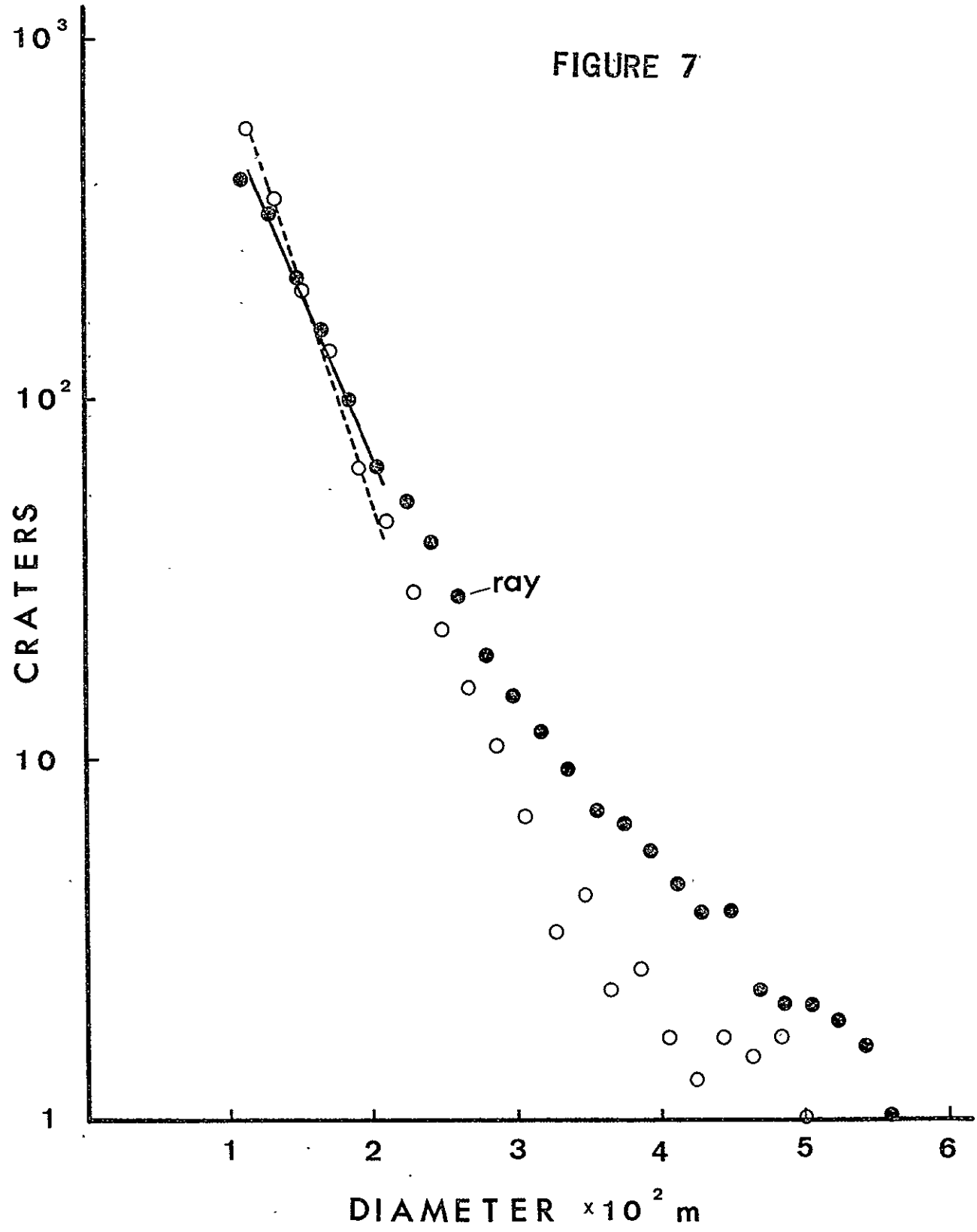

FIGURE 8

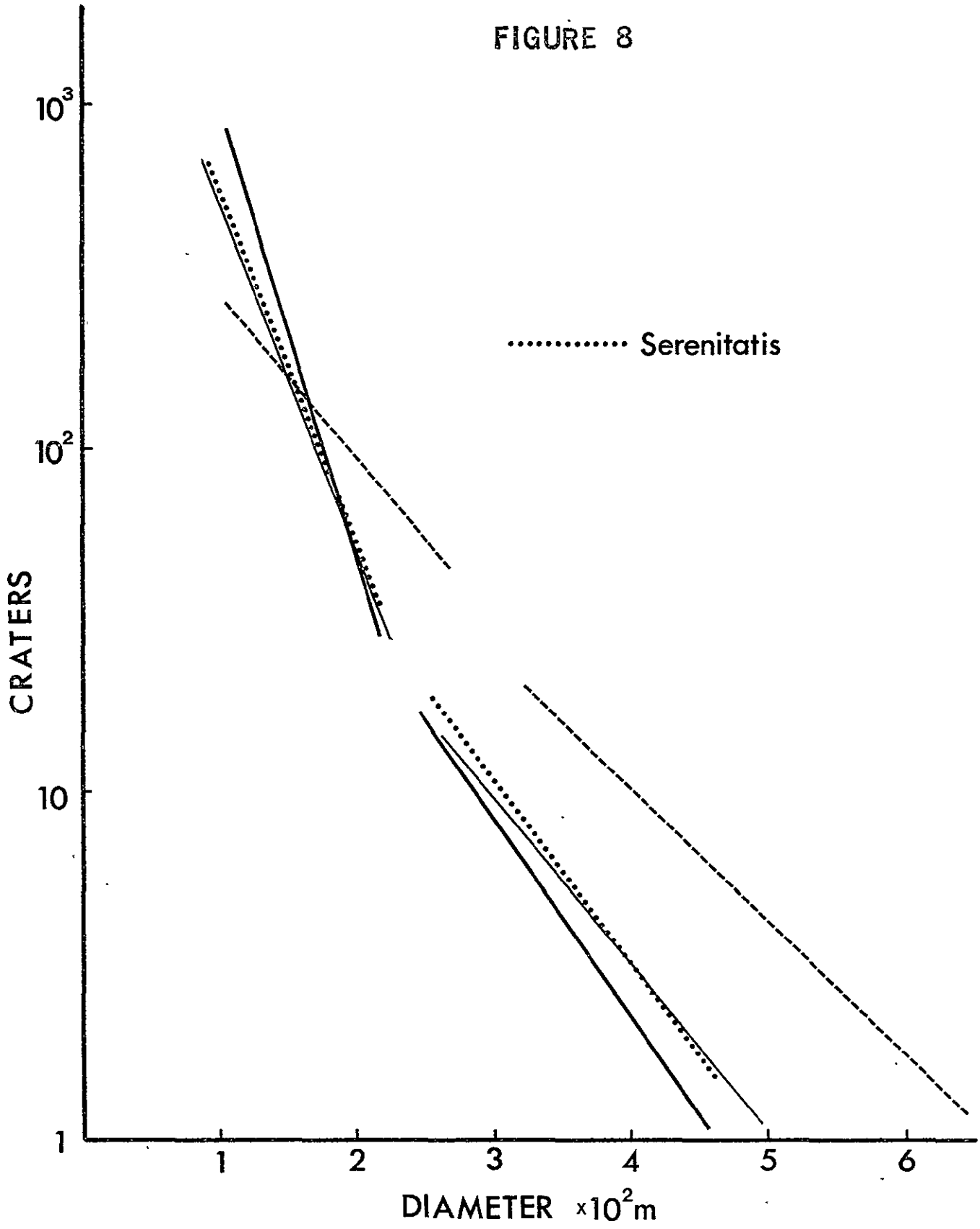
10^3
10^2
10
1
CRATERS
1
2
3
4
5
6
DIAMETER $\times 10^2$m
Serenitatis

FIGURE 9

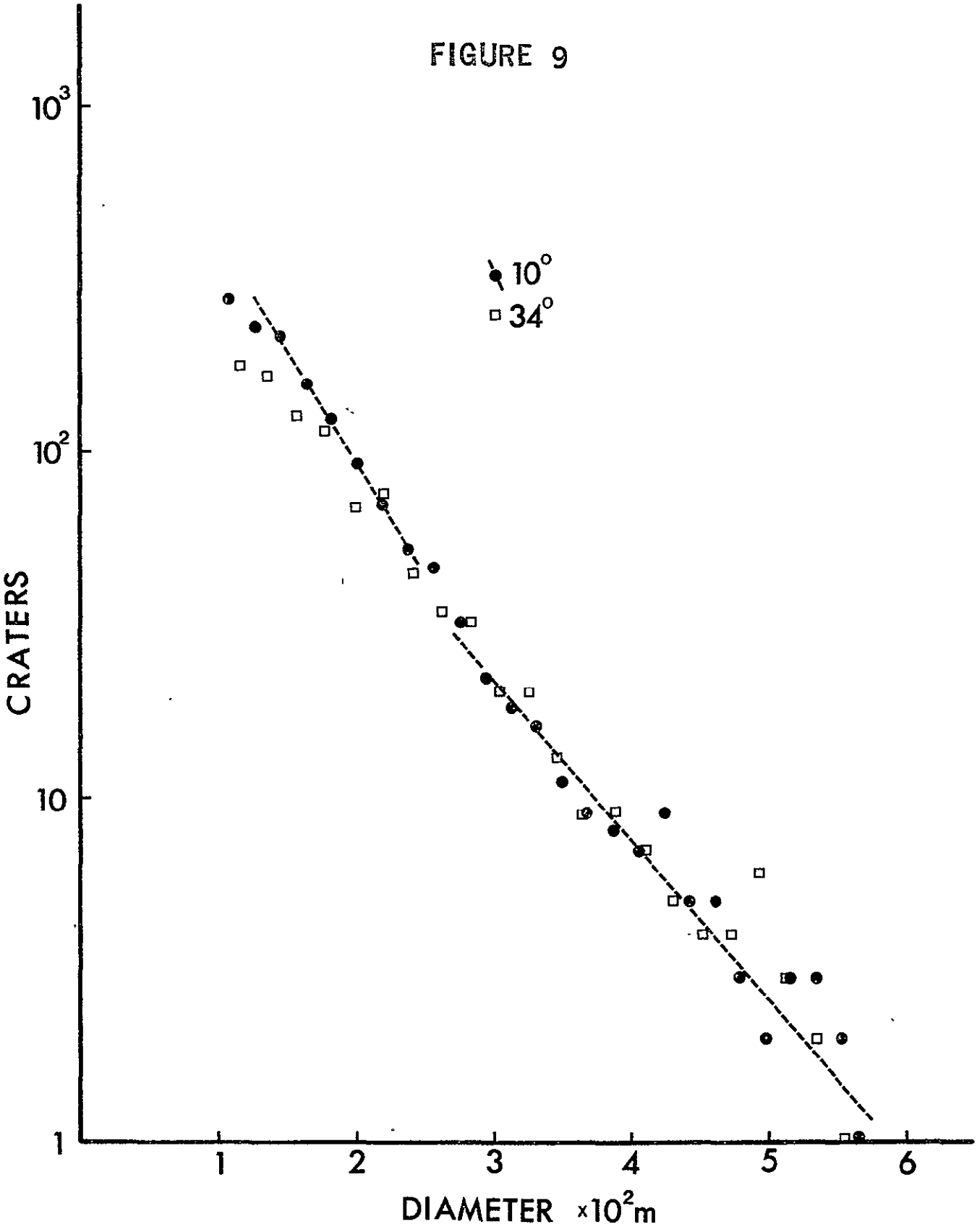

FIGURE 10

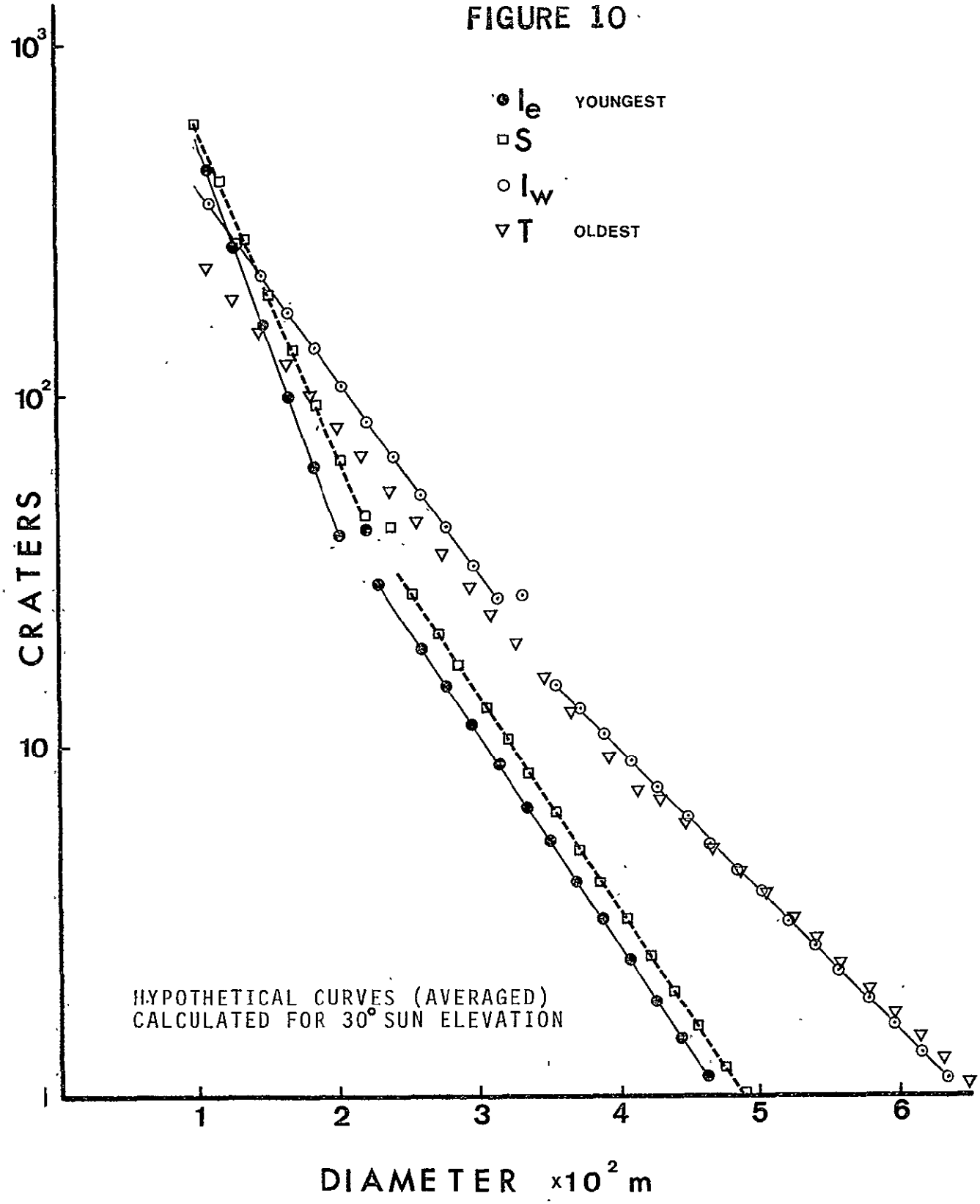
10^3
10^2
10
1
CRATERS
l_e YOUNGEST
S
l_w
T OLDEST
HYPOTHETICAL CURVES (AVERAGED)
CALCULATED FOR 30° SUN ELEVATION
1
2
3
4
5
6
DIAMETER x10² m

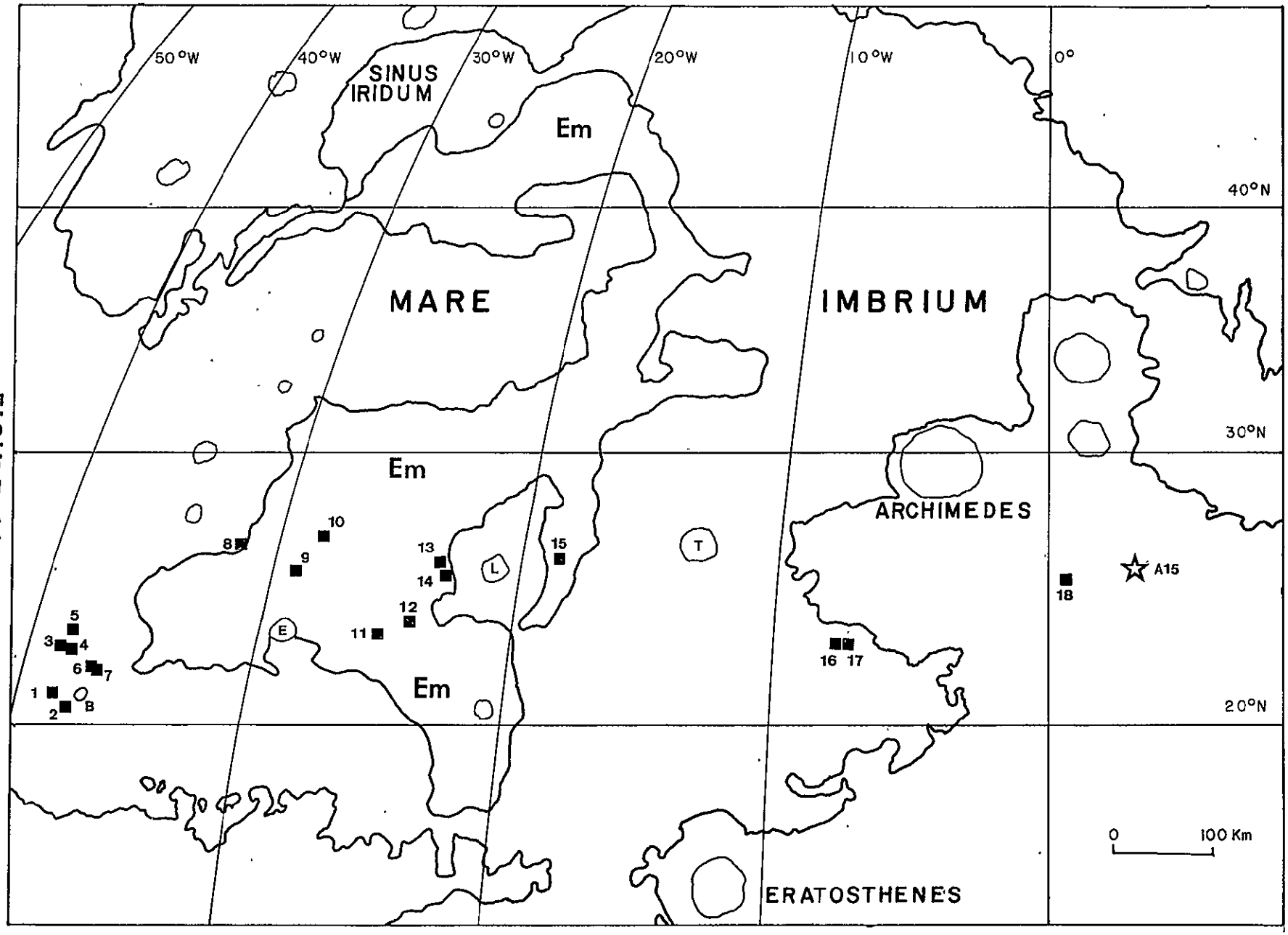
50°W
40°W
30°W
20°W
10°W
0°
40°N
30°N
20°N
SINUS IRIDUM
Em
MARE
IMBRIUM
Em
Em
ARCHIMEDES
ERATOSTHENES
A15
1
2
3
4
5
6
7
8
9
10
11
12
13
14
15
16
17
18
B
E
L
T
0
100 Km

FIGURE 11

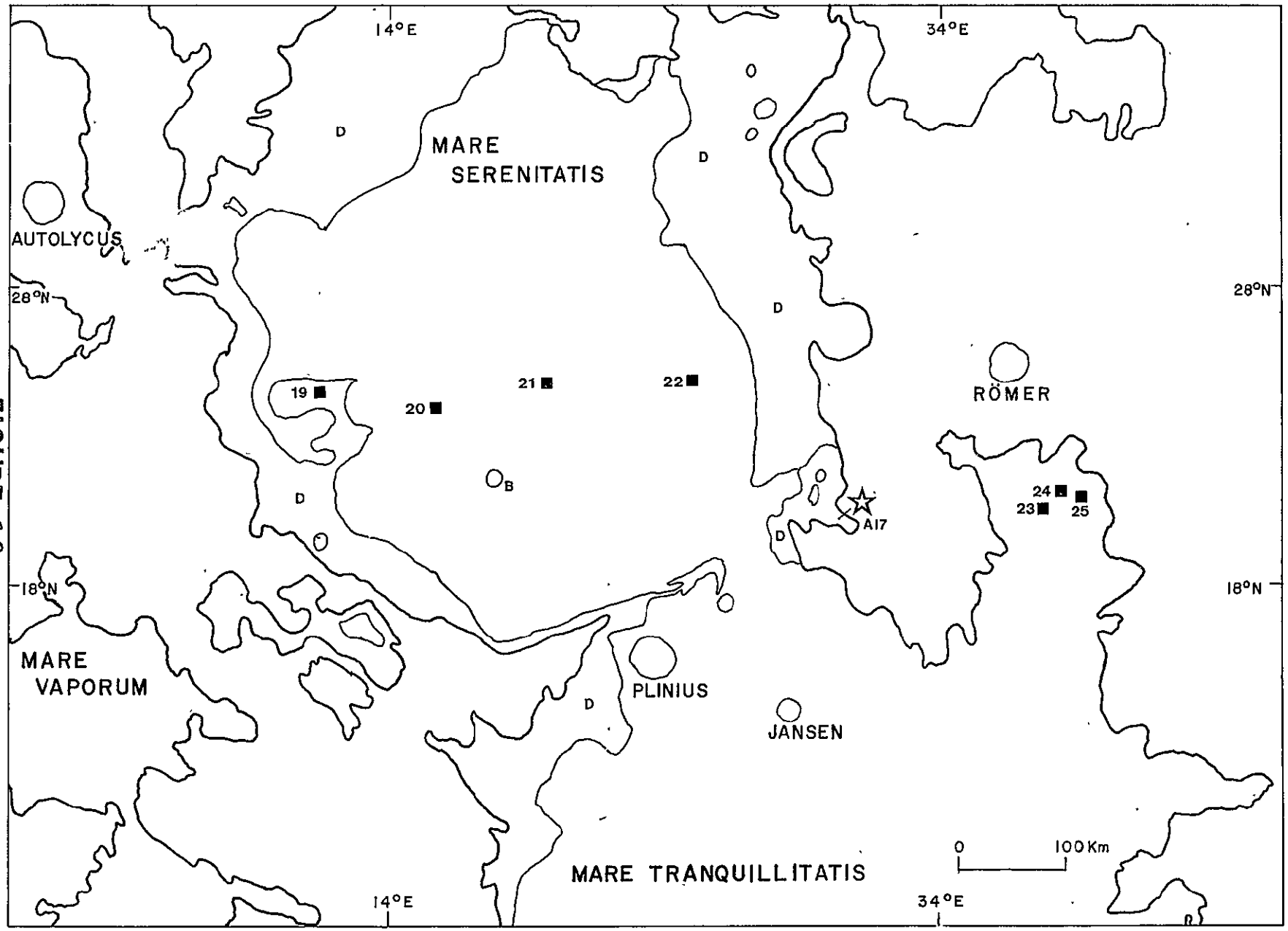
14°E
34°E
MARE
SERENITATIS
AUTOLYCUS
28°N
28°N
D
D
D
19
20
21
22
B
RÖMER
24
23
25
A17
D
D
18°N
18°N
MARE
VAPORUM
PLINIUS
JANSEN
MARE TRANQUILLITATIS
0
100Km
14°E
34°E

FIGURE 12

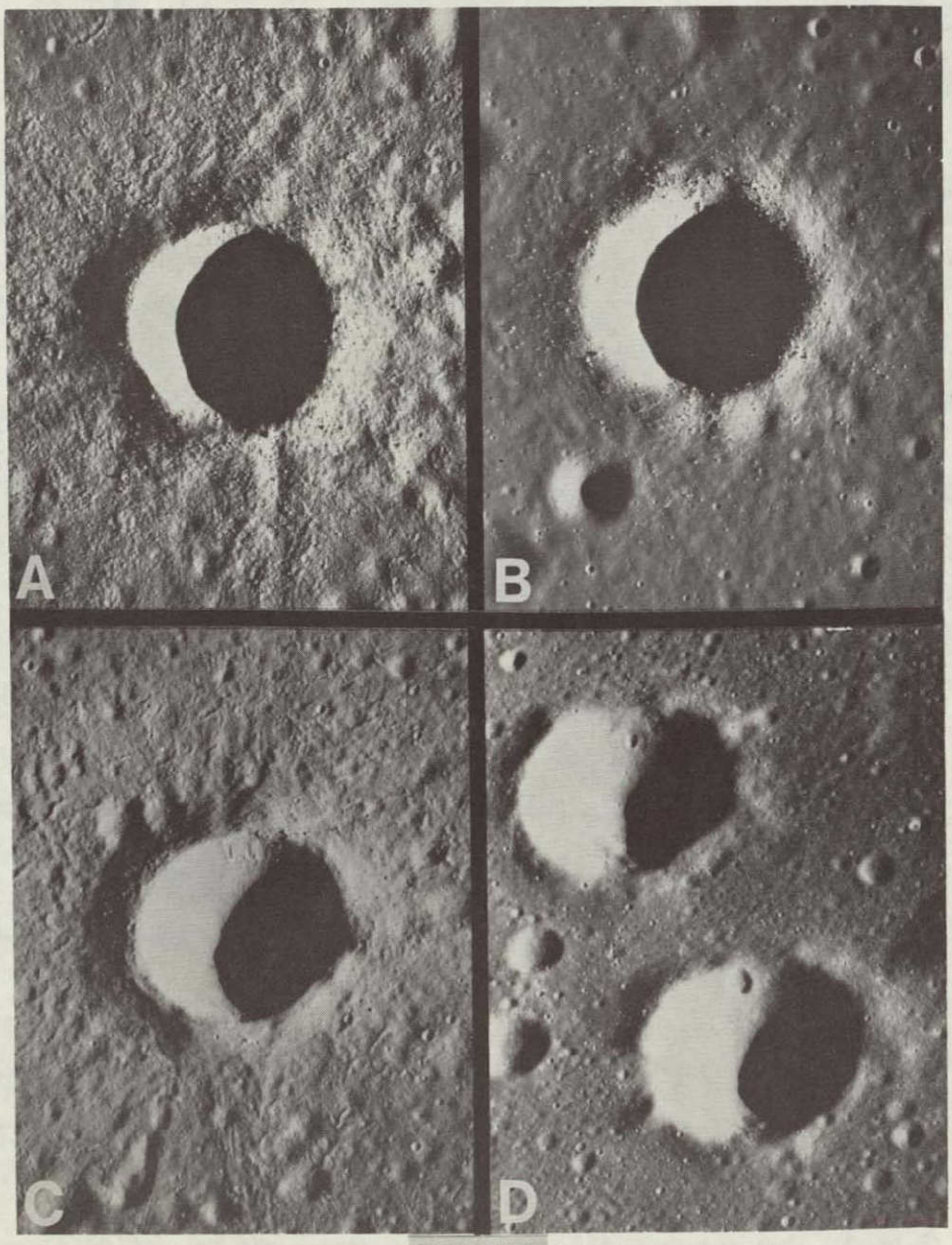

FIGURE 13

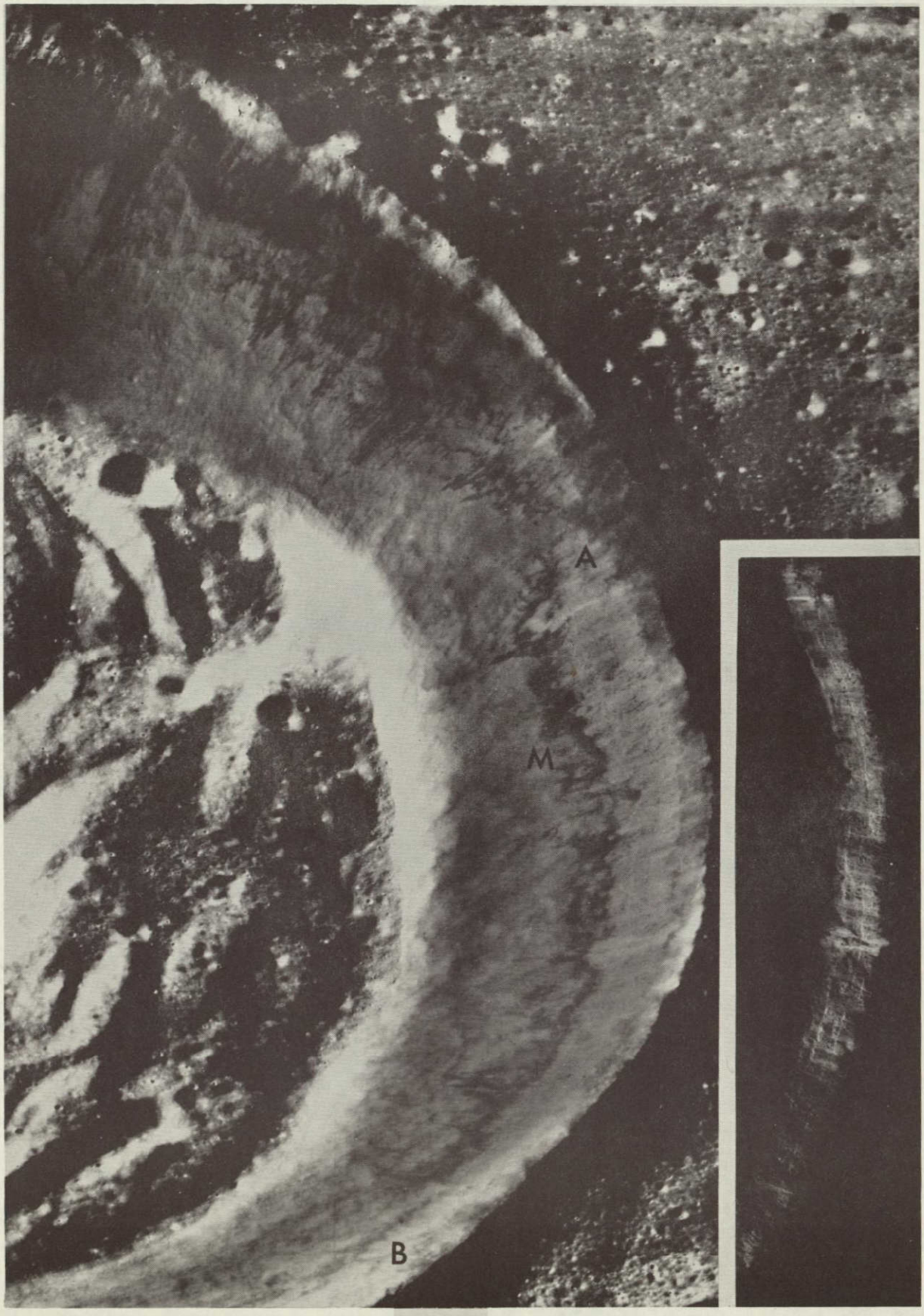

FIGURE 14

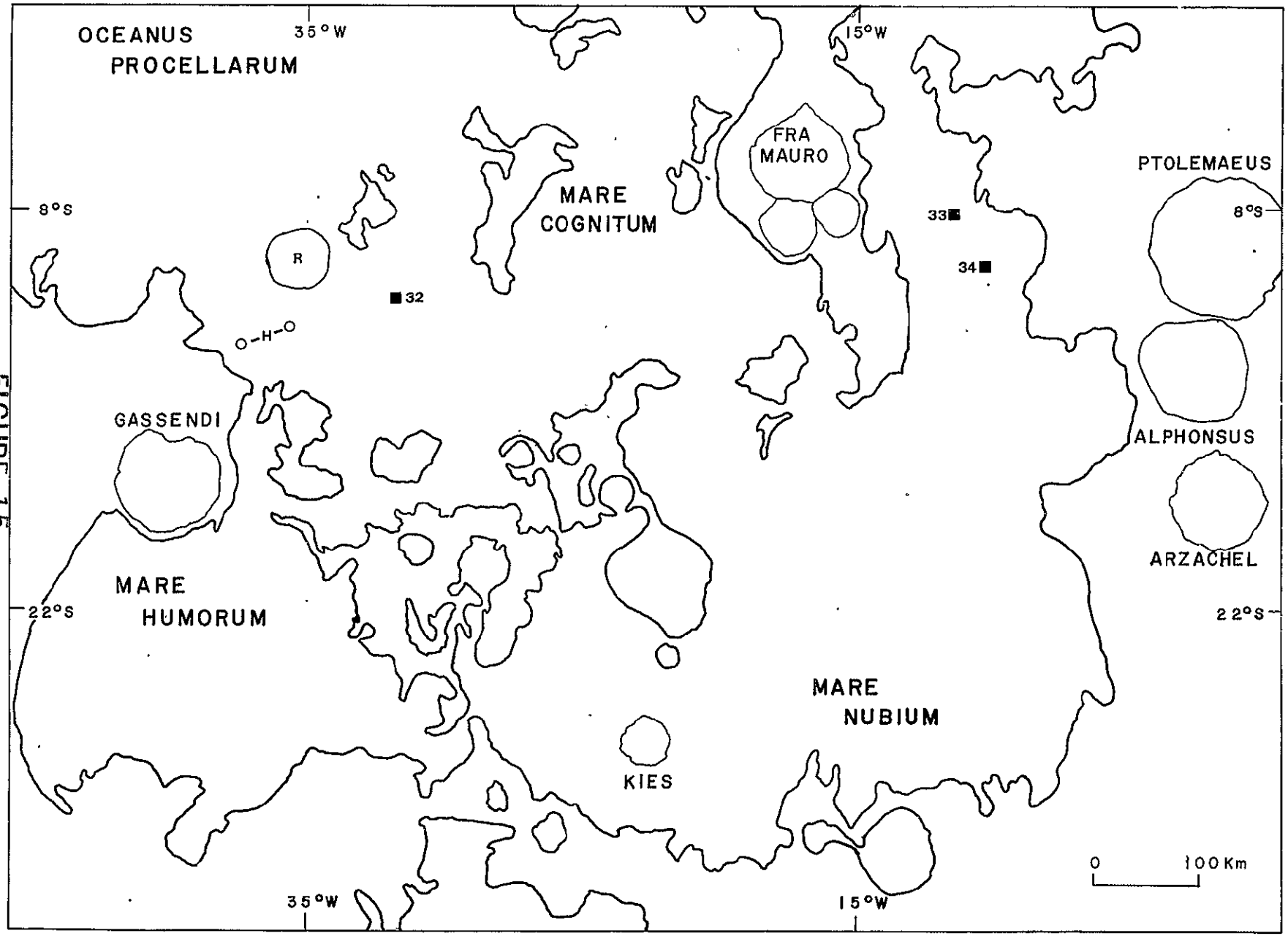
OCEANUS PROCELLARUM
35°W
15°W
FRA MAURO
PTOLEMAEUS
MARE COGNITUM
8°S
33
34
R
32
O-H-O
GASSENDI
ALPHONSUS
ARZACHEL
MARE HUMORUM
22°S
MARE NUBIUM
KIES
0
100 Km

FIGURE 15

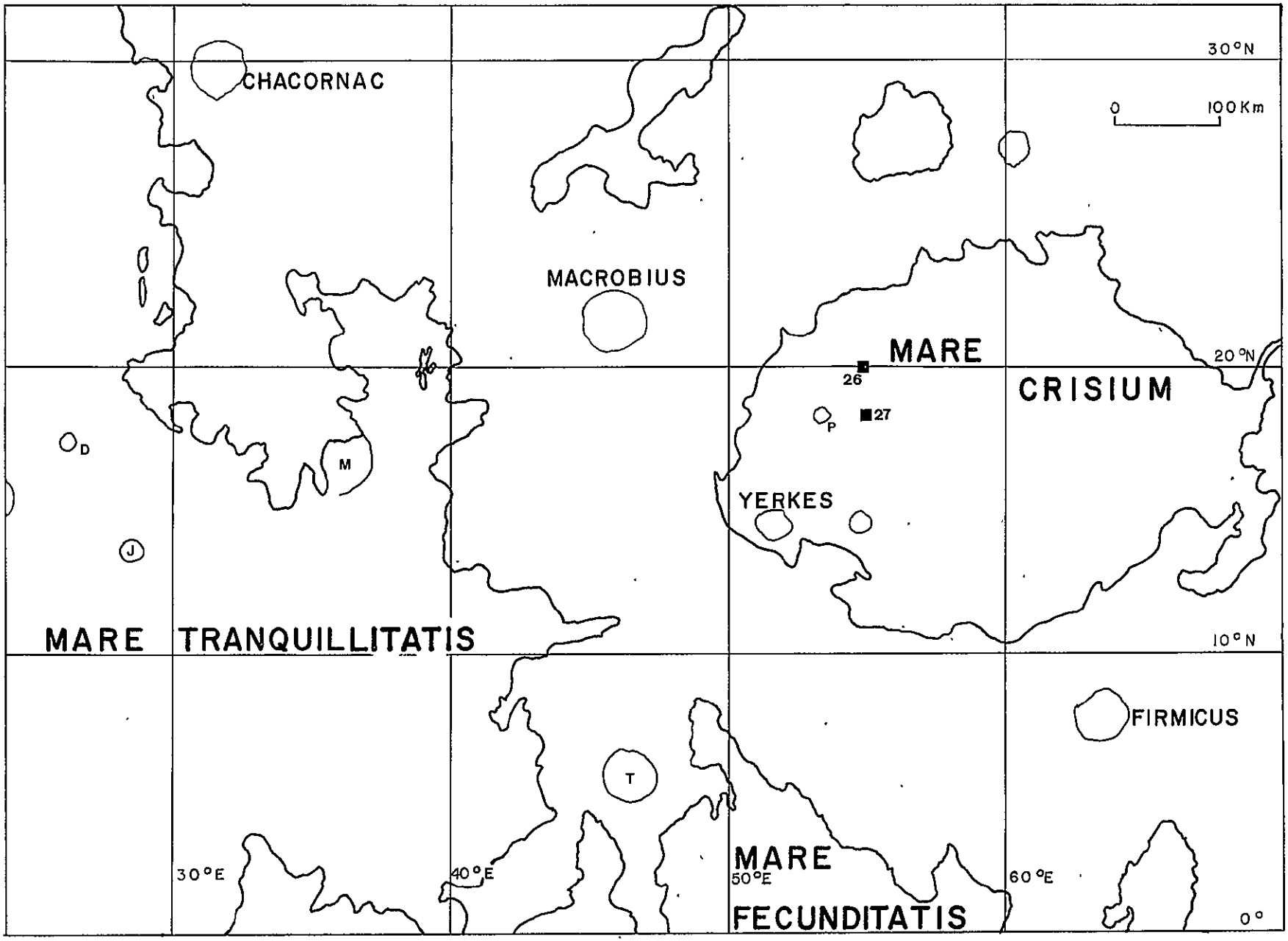
30°N
CHACORNAC
0 100Km
MACROBIUS
MARE
CRISIUM
20°N
26
27
P
D
M
J
YERKES
MARE TRANQUILLITATIS
10°N
FIRMICUS
T
30°E
40°E
MARE
50°E
60°E
FECUNDITATIS
0°

FIGURE 16

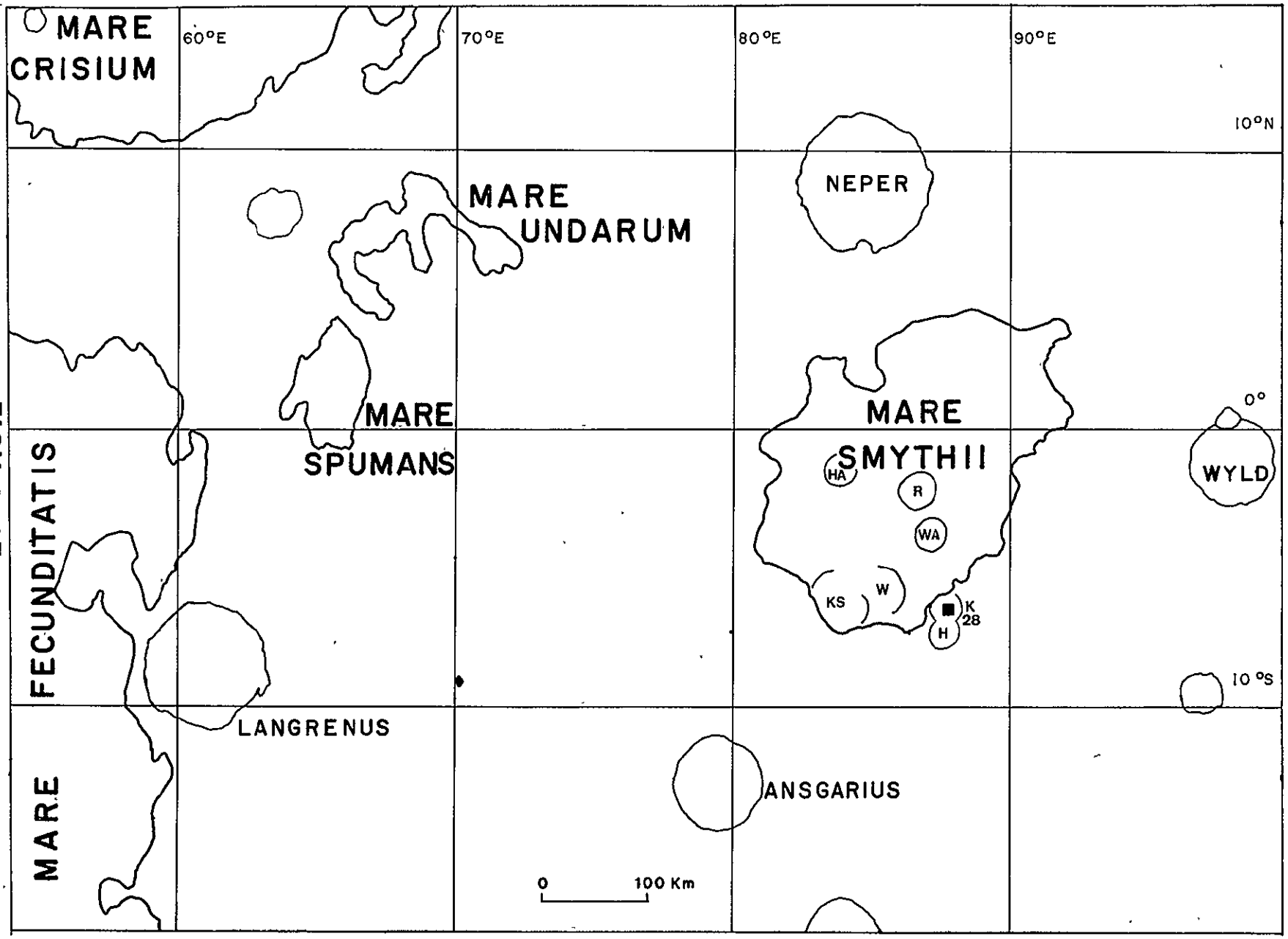
MARE CRISIUM
60°E
70°E
80°E
90°E
10°N
NEPER
MARE UNDARUM
MARE SPUMANS
MARE SMYTHII
HA
R
WA
KS
W
K
28
H
WYLD
0°
10°S
FECUNDITATIS
LANGRENUS
ANSGARIUS
MARE
0
100 Km

FIGURE 17

II. RILLES

A. Linear and Arcuate Rilles

Linear and arcuate rilles are widely distributed on the lunar surface. Unlike sinuous rilles they are present in the highlands as well as the maria, and many extend from mare surfaces into highland areas. In some cases they are concentric to mare basin structures as in Mare Serenetatis, Mare Imbrium (Hackmann, 1966), Mare Humorum (Titley, 1967; Trask and Titley, 1966), and Mare Tranquillitatis (Carr, 1966; Morris and Wilhelms, 1967), while many others follow trends that appear to be unrelated to the structural fabric of single impact basins. Examples of the latter can be seen in the Bonpland area, as well as all of the areas cited above (Figure 18).

In length, linear and arcuate rilles may be as long as several hundred kilometers. The Sosigenes 1 and Ariadaeus rilles (Morris and Wilhelms, 1967) are between 300 km and 400 km in length. Widths are much smaller than length. The widest portion of the Hyginus rille is approximately 4 km (Wilhelms, 1968) that of the Ariadaeus rille about 6 km (Morris and Wilhelms, 1967). Most other examples range from less than 1 km to 2 km in width.

The depth of most examples shown on LTO maps at a scale of 1/250,000 or 1/50,000 is less than 100 m. The maximum depth measured was approximately 200 m in Mare Tranquillitatis (LT061A3) and Mare Serenitatis (LT042C4).

Most who have studied linear and arcuate rilles interpret them as grabens (Baldwin, 1963; Quaide, 1965; McGill, 1970). McGill (1970) has measured slopes of rille walls in order to approximate the orientations of the boundary faults. His results indicate that most such rilles are true grabens bounded by inward dipping faults and that they are conjugate shears which result from stress systems in which the maximum principal stress is compressive and vertical and the intermediate principal stress is oriented parallel to the length of the rille. A few rilles are apparently bounded by vertical faults (Hyginus rille) which are interpreted by McGill as extension fractures produced by the same stress system.

Several examples of linear and arcuate rilles which exhibit superposition and cross-cutting relationships with other features can be seen on Apollo metric and panoramic photography. The rilles illustrated in Figure 18 are clearly younger than the craters which they transect but are older than the surface of the Mare Cognitum. The Ariadaeus rille is another example of a rille which is covered by younger mare flows. (Morris and Wilhelms, 1967). It is apparent that linear and arcuate rilles range widely in age from premare to postmare.

B. Sinuous Rilles

Unlike linear and arcuate rilles, sinuous rilles are found only in the maria, but not throughout the maria. In the areas covered by Apollo photography, the sinuous rilles are best observed in Mare Imbrium and the Oceanus Procellarum. They are not abundant in Mare Crisium, Mare Smythii, Mare Serenitatis, or Mare Fecundatatis. One large rille, Rima Jansen does occur in Mare Tranquillitatis. Sinuous rilles are elongate and range in length from a few kilometers to several hundred kilometers. Rima Rimsky Korsakov near the Crater Brayley in Mare Imbrium extends over a distance of 340 km (Young et al., 1973a). The greatest depth measured in sinuous rilles was 600 m (Vallis Schröteri, LT038B3), although most smaller rilles have depths of less than 100 m. Both the Rima Prinz (LT039A3) and Rima Hadley (LT041B4) are approximately 400 m deep. Scott et al. (1975) have compiled a map of the distribution of lunar rilles, faults, and scarps.

Several morphological types of sinuous rilles can be recognized. Examples of sinuous rilles without levees include the Herigonius rilles (Figure 20), Rima Rimsky Korsakov (Figure 23), and Rima Hadley in Mare Imbrium. Rilles of this type are characterized by high sinuosity, abrupt changes in direction, and lengths as great as several hundred kilometers. Rilles with levees (Figure 18) differ by having lower sinuosity, an absence of abrupt changes in direction, and conspicuous levees, but may also have lengths in excess of 100 km. Most examples of both types have widths of a few tens to a few hundred meters, but they may be as wide as two kilometers (Rima Hadley LT041B4). A third type of sinuous rille can be seen in Figure 19. This type is most abundant in the Aristarchus region of the Oceanus Procellarum and is characterized by high sinuosity, abrupt changes in direction, a conspicuous decrease in width in the downslope direction, and an absence of levees. Such rilles may be as wide as 10 km (Young, et al., 1973a), nearly always originate in vent-like craters, and sometimes smaller rilles are present within larger ones (Vallis Schröteri).

Sinuous rilles of all three varieties may extend from vent-like craters on or near mare ridges or highland margins (Figures 19, 20, 22). In some cases (Rima Hadley) they extend from fracture systems. Both leveed and non-leveed sinuous rilles may decrease in width and depth at both ends and gradually terminate without a link to any other surface feature.

Although some investigators have explained the occurrance of sinuous rilles as the result of stream erosion (Schubert et al., 1970; Leonardi, 1972) or erosion caused by gases escaping from the interior of the Moon along fractures (Schumm, 1970), most have concluded that they result from volcanism (Howard et al., 1972; Oberbeck et al., 1972; El-Baz et al., 1972). Greeley (1972), Greeley and Hyde (1972), and Cruickshank and Wood (1972) have related the formation of sinuous rilles to similar terrestrial analogues of volcanic origin (lava tubes and lava channels),

which are common in areas of widespread volcanic activity (oceanic islands, and basalt plateaus). Greeley (1971) and Murase and McBirney (1970) have discussed the conditions on the Moon which would result in the formation of lava tubes. The restriction of sinuous rilles to the basaltic maria indicates that they are most probably volcanic (Scott, 1975).

Origins and Spatial Relationships of Rilles to Associated Features: The maps prepared by Scott et al. (1975) demonstrate that sinuous rilles and mare ridges (Section III) are both confined essentially to the lunar maria. Because it is now documented that the lunar maria are filled with volcanic rocks and veneered with a relatively thin regolith, models which attribute sinuous rilles to nonvolcanic fluid erosion subsequent to the formation of the maria can be disregarded. We conclude that it has been adequately demonstrated that nearly all sinuous rilles are probably the result of channelization of flow within molten lava flows both as tubes and open channels, and that they have been subjected to the same meteorite flux which has produced the regolith. Therefore, the relative size of existing rilles which originated as lava tubes is controlled by the depth to which they were eventually buried as well as their actual dimensions. For a given diameter, more deeply buried tubes would appear smaller if exposed by impact gardening.

Within the maria, many sinuous rilles exhibit obvious genetic relationships to mare ridges, craters, faults or fracture zones, and flooded highland borders. For ridges, craters, and fractures, it is clear that lava would move to the surface along fracture zones produced by impact and tectonism. The relationship to flooded highlands is more indirect but equally significant. Tubes and channels are likely to develop in regions of most rapid flow (Young et al., 1973a). Preexisting surface irregularities channel the flow and may provide evidence of preexisting topography and slopes. In the more obvious cases (Figures 19, 37) flow has been channeled by and along highland contact zones and through gaps in highland ridges. Fissure eruptions along grabens and faults followed by collapse of crusted-over surfaces can readily account for those sinuous rilles which appear to have linear segments aligned with regional fracture patterns (Figure 19). It is likely that some rilles were localized in buried grabens or along buried fault scarps.

In many instances rilles show the effect of having been deformed or intruded by subsequent volcanism along mare ridges (Figures 20-25). Specific examples of this activity are discussed by Young et al. (1973a, 1973b) and described in the captions for Figures 20 through 25. The significance of these relationships is further considered under the topic of mare ridges (Section III).

Significance of Sinuous Rilles for Geologic Studies: Rilles are one of the few indicators of the direction of lava flow during widespread flooding, the probable source regions of significant volumes of lava, and the great distances over which individual eruptions spread. The dimensions of collapsed tubes place approximate lower limits on the thicknesses of individual flows, although flowing lava can erode through underlying solid surfaces (Greeley and Hyde, 1972).

For the purpose of comparing mare surface ages or demonstrating continuity of time stratigraphic units, any region traversed by a single rille can be assumed to have a uniform age equivalent to the episode of flow represented by the rille (see discussion of Brayley region, Section I). Relative age relationships of discrete surface features (craters, ridges, rays, faults) can be demonstrated by their cross-cutting and superposition relationships to rilles.

Although closed lava tubes could theoretically act as siphons if they were closed systems, the mechanics of lava tube formation and the style of lunar eruptions imply that they normally developed on existing slopes and flowed toward lower elevations. Tubes and channels normally get smaller toward their terminal ends and may disappear abruptly where subsurface flow is ponded. Conversely, tubes may originate where restricted flow escapes from a ponded "lake". Thus rilles which have no apparent source or termination should not be considered unusual. Nor should the end of a rille be assumed to always represent either the origin or termination of discrete lava flow units. Where dimensions and directions of flow are obvious, existing surface topography can be examined for postrille structural warping of the surface, assuming that all major rilles required a level or slightly sloping surface in the direction of flow. An example of the use of rilles to explain the details of the regional geology is contained in Section III dealing with the Montes Agricola region northwest of the Aristarchus Plateau and the Crater Isaev (Figure 25) on the farside (LTO102B2).

The significance of sinuous rilles is summarized along with the conclusions at the end of Section III because of the interrelated nature of mare ridge and rille genesis in mare regions.

III. MARE RIDGES

A. Introduction

Ridge-like landforms are widely distributed features which are found almost exclusively in the maria (Quaide, 1965, Scott et al., 1975). They characteristically vary in width and height above the surrounding mare surfaces, and individual ridges vary in width, height, and cross-sectional shape along their lengths (Colton et al., 1972). Some mare ridges consist of a ridge complex superimposed upon a broad gentle arch (Strom, 1971). Figure 26 illustrates topographic profiles of several typical mare ridges constructed from 1/250,000 scale LTO maps with a contour interval of 100 meters. Only the broad gentle arches are consistently recognizable at this scale. In general, the ridges are arcuate, discontinuous, en echelon, or sinuous in form and many are bifurcated. In some portions of the maria the distribution of the ridges appears to reflect a circular mare-related fracture pattern (Hartmann and Wood, 1971, Scott et al., 1975) as in the southeastern portion of Mare Serenitatis (Figure 36), where the largest ridges follow trends that are concentric or radial to the center of the basin. Others (Tija, 1970) have concluded that a uniform arrangement of mare ridges confirms the existence of a regional stress system on the Moon. However, regional patterns are not always apparent. In western Oceanus Procellarum Scott et al. (1975) have shown that the ridges coincide with positive gravity anomalies.

B. Ridge Morphology

Dimensions: Mare ridges or, more appropriately, mare ridge systems extend for great distances within the lunar maria. In Mare Crisium a ridge system extends around the interior for a distance of approximately 1200 km. In the Oceanus Procellarum several more nearly linear ridge systems, including that located adjacent to the Herigonius rilles, extend for distances of the order of 500 km. In some instances individual ridge-like features may be as short as 10 km.

The widths of mare ridges are much smaller than their lengths. In general, the widths are of the order of a few tens of kilometers or less. The mare ridge whose profile is illustrated at A (Figure 26) is one of the largest examined in this study, its width is at least 40 km. Since mare ridges often exhibit broad gentle arches it is sometimes difficult to locate with certainty their lateral margins. Hence most estimates of width are minimum values. The remaining mare ridge profiles (B through H) in Figure 26 have widths of 20 to 30 km and are representative of most other ridges in the maria. For most mare ridges width is smaller than length by approximately one order of magnitude.

The relief across mare ridges is highly variable. The ridge profile illustrated at A (Figure 26) has a height of approximately 700 m, the greatest of any examined in this study. Since the margins of ridges are difficult to locate with certainty, the estimates of ridge height (like ridge width) are minimum values. Heights of 200 to 350 m (profiles B through H in Figure 26) are representative of the maximum heights of most ridges. Where broad gentle arches are absent, ridge heights may be as low as 20 m.

Symmetry: Mare ridges typically exhibit an asymmetry that is apparently related to differences in elevation of the mare surfaces on either side of each mare ridge. The elevation differences vary from near zero to 200 m (Figure 26, B-H). Many ridges also exhibit steep escarpments along one side (Figure 26, C, D, E, F, H) with relief of up to several hundred meters (Figure 26, D, F). This seems difficult to explain without the presence of high angle faults. The occurrence of faulting in ridge formation has been discussed by several investigators (Strom, 1971; Colton et al., 1972; Young et al., 1973a; Young et al., 1973b). Several of the mare ridges examined in this study show clear evidence of faulting aligned with ridge crests (Figure 27), especially where ridges terminate at highland boundaries, (Figure 28, Figure 30, Figure 22). Since the maria are sites of thick accumulations of basaltic lavas, it seems likely that the elevation differences across mare ridges represent lower limits of throw on the associated faults and that the mare surface relief is a much subdued replica of that on the surface beneath the lava. However, large scale vertical displacement is not considered to be necessary to ridge formation, but is rather a commonly observed or inferred phenomenon.

Morphological Variations: The morphology of mare ridges changes frequently and abruptly along their lengths. Dorsa Aldrovandi (Figure 31) is a typical example of a mare ridge in this respect. It changes in width, height, and trend, and also bifurcates along its length. Many of these same variations (excluding variations in height) can be observed in the fracture system (Fossae Pavlova, Figure 31) which lies just to the east of Dorsa Aldrovandi. The close similarities in the areal patterns of the two features supports the previously cited evidence of the roles faulting and fracturing in ridge formation.

Additional changes in morphology along the lengths of mare ridges include the occurrence of small (in both vertical and horizontal extent) "wrinkle-like" features which have been termed "squeeze-ups" (Colton et al., 1972) because they resemble much smaller extrusions of magma from cracks in the hardened crust of terrestrial lava flows. The small scale of such features allows them to be obliterated by meteorite bombardment. For this reason they are best preserved on mare ridges in the relatively young maria, such as the Oceanus Procellarum, Mare

Imbrium, and Mare Serenitatis. Many such features, including one illustrated at c (Figure 32, A) have flowed into and partly filled small craters (Young et al., 1973a). Hodges (1973) has described several examples of similar features elsewhere in the maria. Their low vertical relief is illustrated at c on profile A (Figure 32) where one "squeeze-up" appears as a small nondescript prominence despite the fact that the profile was constructed from a 1/50,000 scale map with a 20 m contour interval and a 5x vertical exaggeration. It is evident from the ease with which they are recognized on photographs and the poor representation on the best lunar topographic maps that many of the "squeeze-ups" are less than 20 m in height.

Small scarp-like landforms which resemble the Lee-Lincoln scarp at the Apollo 17 landing site (Scott, 1973) can be seen along many ridges including the Dorsum Aldrovandi. Two are illustrated at a and b on profile A (Figure 32). The relief of both is approximately 40 m. Another good example can be seen at x and y on Figure 29 and other areas where ridges terminate against the highlands. The distances over which they can be traced into the highlands is variable, ranging from less than 1 to more than 10 km. We believe they are fault scarps caused by high angle faulting prior to and during ridge volcanism (see Part B).

Profiles B and C (Figure 32) represent two views of Dorsum Zirkel in Mare Imbrium. Dorsum Zirkel is bounded on both sides by steep escarpments (d and e on profile B) which suggest that it is a horst mantled with lavas extruded, at least in part, along the bounding faults. The prominance at f on profile C is interpreted as a constructional volcanic landform analagous to a small, two-dimensional shield volcano. All three profiles in Figure 32 illustrate, when contrasted with both smaller scale profiles (Figure 32, A, B, C) and metric and panoramic photographs, the wide range in vertical relief among landforms associated with mare ridges.

C. Evidence for Origins and Relative Ages in Selected Regions

Mare ridges that are relatively isolated in the central portions of the maria can be described only as to their morphology and regional trends or patterns. Several authors previously mentioned have described the regional patterns of mare ridges. In this section we discuss specific examples of regions where mare ridges exhibit clearly discernible relationships to craters, faults, sinuous rilles, subsidence features, and highlands which allow conclusions to be drawn regarding ridge genesis.

Relation to Sinuous Rilles: In several places sinuous rilles originate near the summits of mare ridges (Figures 20, 21, 22, 28V, 31F). This is strong evidence that volcanic vent areas are closely associated with ridges. At the Herigonius rilles (Figure 21) the rille vents (E, F) must have developed after the ridge segment between E and N (Figure 21), because both

of the rilles were apparently deflected along the ridge to join at N. Lava flowing out at G was most likely shifted to a new vent at F by ridge growth, although flow was apparently maintained toward the southwest across the ridge. Alternatively, the shift of the vent from G to F may have caused formation of the smaller (deeper?) lava tubes leading northwest from B (see regional view, Figure 20). The smaller rilles on Figure 20 leading northwestward from the main vent (H) have been completely obliterated in two places by ridge deformation or intrusion (s-s'). Regardless of the precise sequence of events in this region, any explanation of the observed relations between the features requires multiple episodes of alternating ridge deformation (growth) and rille development. Topographic contours (LT075C1) show that the surface to the northwest of the vent, F, has been deformed so that lava would not presently flow in that direction. All relationships suggest contemporaneous volcanism, ridge development, and tectonism.

Rima Jansen (Figure 22) occupies a similar position at the summit of Dorsa Barlow (LT060B2, 61A1). Ridge growth subsequent to rille formation is necessary to account for the existing topography along the rille. Rima Jansen also crosses the edge of a volcanically modified buried crater rim at N (Figure 22) similar to the feature at M. This relationship also requires deformation of the crater rim subsequent to rille formation to account for existing surface topography. Two related irregular volcanic vents occur at E and southwest of H along the ridge. All of these relationships combined with the fault trace at A and K, the volcanic domes (L) and the modified craters demonstrate that volcanism, ridge formation, and tectonism were closely related in time.

In many other locations on the moon where ridges and sinuous rilles intersect, it is generally observed that ridge deformation (faulting or intrusions) has followed rille formation (Figures 19, 23, 24, 25, 37, 44B). It can be inferred that rille development is mainly associated with the widespread flooding of the maria, whereas ridge growth was intermittent and continued for longer periods, perhaps representing the final pulses of major mare volcanism.

Relations to Craters: Small ridge elements and flow-like lobes along the flanks of ridges partially fill or overlie impact craters (Strom, 1971). Most of these occurrences are best preserved in the younger maria (Figures 31, 33, 38). Although some authors have suggested that the lobes in craters are slumps related to a thrust-fault origin for ridges (Bryan, 1973), the thin regolith in the younger maria make this hypothesis difficult to support. Because the small flows have not caused ponding on crater floors in all cases, they must be relatively viscous and/or of small volume. The large number of craters which have been filled along ridges in Mare Nubium, Mare Cognitum, and Mare Serenitatis demonstrate that ridge volcanism continued considerably after the major surface flows were formed and subjected to prolonged impact gardening.

Complex relationships of sinuous rilles, ridges, and subsidence structures can be seen in the floor of the crater Isaev (Figure 25) on the lunar farside (LTO102B2). The 4-km-wide depression shown on Figure 25 is on the floor of a 90 km impact crater (inset). The small crater is 200 m deep, has no rim, is not circular, and is probably a volcanic subsidence depression in the lavas which fill the floor of Isaev Crater. Formation of the subsidence structure destroyed part of the sinuous rille which formerly crossed the subsidence depression, and which can still be seen on either side of the subsidence structure. Following formation of the subsidence crater, a mare ridge developed trending north-south across the mare surface and through the depression. This clearly illustrates the commonly observed association of volcanic vent areas, volcanism, and ridge formation, with ridge development definitely continuing after lava flooding and distinctly separated in time from volcanic events which are clearly older than the ridge.

Relations to Faults, Grabens, and Arcuate Rilles: Ridges in Mare Serenitatis have been cited by several authors who attribute the formation of mare ridges to regional compressive stress systems (Muehlberger, 1974; Bryan, 1973; Howard and Muehlberger, 1973; Hodges, 1973). Much of the detailed discussion in these analyses concentrates on the morphology of Dorsa Aldrovandi, Dorsum Gast, and other ridges which are basically concentric to the basin margins. Much of the evidence for suggesting a thrust fault origin has been based on the morphology of the ridge extensions into the highlands near the Apollo 17 Site and at C, Figure 31 (enlarged in Figure 35). The abrupt change of ridge morphology in these regions is striking, but not unique. In fact, in almost every example where ridges trend obliquely into highlands, there is evidence of this same abrupt morphological change. There are abundant examples along the groundtrack of the Apollo 16 Mission in the western maria and in the general vicinity of southwestern Mare Serenitatis (Figures 22, 30, 33, 34, 35, 37). Many of these features in the highlands have morphologies very similar to the Lincoln-Lee Scarp near the Apollo 17 Site.

It is inconsistent to explain the origins of Dorsa Aldrovandi and its extension (Figure 35) as the result of eastward thrusting of the mare surface, in view of the fact that a similar highland feature has formed in western Serenitatis (Figure 29) where the main ridge meets the basin margin at nearly a right angle. In several other cases the main mare ridge elements are aligned along obvious structural trends whose highland extensions predate the most recent flooding by mare lavas (Figure 29, M, 2; Figure 28, M; Figure 30; Figure 31 A-D-E and F-D-G).

The formation of mare ridges and the development of associated highland scarps in all of these examples can best be explained by a model which depends upon the reactivation of older high-angle faults and grabens as vents for fissure

eruptions at lower elevations. The abrupt change in morphology of the ridge structures at highland margins is due to the absence of volcanism at higher elevations (above the mare surfaces). The subdued relief of these fault scarps and their continuity across steep highland slopes is attributed to both the thicker regolith in the highlands and to the slow rate of postmare slope erosion (Section IV). In most cases the sense of offset on the faults in the highlands is the same as the relative elevation differences on the mare surfaces adjacent to them. The elevation difference on the Mare Serenitatis surface on Figure 31 from A to B is approximately 300 m (lower on west) and is inconsistent with the concept of the maria being thrust toward the highlands. In addition, many grabens in the highlands (G, H, Figure 31) suggest that the earlier deformation was generally opposite in sense to that required by the thrust models. If the dark mantle in Serenitatis is everywhere roughly equivalent in age to the Apollo 17 Site ages, then tensional faulting occurred until at least 3.7 to 3.8 BY ago. Likewise tensional faulting at B (Figure 31) continued subsequent to the flooding by the younger lavas (~3.3 BY) in central Serenitatis.

Elevation differences on the mare surfaces in Figure 29 (Z) are 100 m (lower to north) in the same sense as the offset of the highland fault between X and Y. Often these highland faults (covered with regolith) exhibit opposite-facing scarp elements and bifurcations. Both features can be explained as scissors, graben, and horst displacements representing one or more episodes of displacement and, possibly reversals in the relative motion on individual faults. The alignment of ridge and fault trends and the sense of displacement on Figure 30 are obvious.

The relationships of faults, ridges, rilles, and volcanism on Figures 19 and 37 near the Aristarchus Plateau are very instructive because of the clearly demonstrable geologic relationships. On Figure 37, Rima Chopin (A-J) has been offset by ridge deformation or faulting at section H-I. The elevation difference between H and I is ~200 m (lower at H). Regional geologic evidence shows that all rilles in this region (A,B,C,D) flowed westward, yet A and D could not have done so given the present surface elevations. Displacement along the fault, D E, is also ~200 m and a volcanic vent lies on the same structural trend at G. In this region lava flooding and rille development have clearly preceded development of the ridge along structural trend DEFG. Rille D appears to originate in or extend from the fault zone, DE. If the offset on the fault continues in the same sense near K and G, it is not apparent in the existing topography. The presence of cross-cutting structures parallel to the massif (F) might account for the abrupt termination of the offset across the ridge between H and I.

Similar colinearity of faults and ridges can be seen on Figures 28, 29 (m,g,d,e,f) and Figure 22 (K).

Although multiple displacements along older basement faults cannot be proven, the premare age of many flooded highland structures (Figure 31, E and H) combined with obvious elevation difference across mare ridges that are colinear with highland faults suggest that multiple displacements (premare and postmare) are very likely. It would be very unusual if mare lavas did not utilize basement fracture zones as vents for fissure eruptions including emplacement of viscous intrusives and extrusives associated with the final pulses of mare volcanism. It is also reasonable to expect that the final pulses of mare volcanism might have included lavas that could have been more viscous, silicic differentiates from the large magma bodies which produced the widespread mare flooding

D. Probable Modes of Origin

The preceding discussion of individual mare ridges leaves little doubt that the formation of ridges is inseparable from faulting and magmatic activity in the maria. The fact that ridges change to faults where they enter the highlands and that large sinuous rilles of probable volcanic origin (Herigonius and Jansen rilles) extend from the summits of ridges demonstrates that the ridge sites and their associated faults are primary sources of fissure volcanism. The absence of ridge morphology along highland extensions of faults aligned with mare ridges is attributed to the high elevations of the fault traces. Hydrostatic considerations suggest that fissure eruptions would occur along the lower portions of faults and graben systems. This relationship and the measurable offset of highland fault scarps demonstrates that volcanism along faults rather than displacement is the primary process responsible for ridge morphology. This is further supported by the presence along some ridge systems of positive gravity anomalies (Scott et al., 1975), which are the probable result of the emplacement of basaltic dikes beneath thin mare lavas. Plutonism in the form of two dimensional laccolithic bodies is almost surely a major cause of the development of broad gentle arches. This is best illustrated by rilles such as Rimsky Korsakov and the Rima Chopin where flexuring of the mare surface has clearly occurred after the last widespread episode of flooding (uppermost lava flow) in which the rille must have formed.

Most large, complex ridges apparently develop over a considerable period of time or at least require more than one volcanic, plutonic, or structural event in order to develop. The deflection of the directions of flow of the Herigonius rilles by some of the ridges in the complex from which they issue, and the similar deflection of the Eratosthenian lava flows (Schaber, 1973) of southern Mare Imbrium through gaps in mare ridges, followed by redevelopment of ridge elements in the gaps, are unequivocal examples of the growth or deformation of mare ridges throughout more than one episode of volcanism. In contrast, the presence of mare ridges in the western portion of the incompletely flooded Mare Orientale suggests that individual ridges do not require a complete sequence of mare filling to develop.

The widespread occurrence of "squeeze-ups" on mare ridges and in postmare craters demonstrates that intermittant small scale volcanism followed the last major episodes of lava flooding and, by inference, occurred between earlier episodes of flooding. The same inference is made with respect to small scale volcanism which has reestablished mare ridge segments across rilles, as at Lambert R and in the Aristarchus region.

Figure 39 illustrates three hypothetical cross-sections of mare ridges. All are envisioned to be the results of intermittant faulting, volcanism (from large to very small scale), plutonism, and regolith development. For purposes of clarity the cross-sections have been simplified and made diagrammatic so that the number and dimensions of flows, intrusives, layers of regolith, and the number of small scale volcanic features, such as the "squeeze-up" on cross-section A, should not be construed as accurate values. The cross-sections are drawn beneath scaled topographic profiles (Figure 26, D and E; Figure 32, C) of existing mare ridges, with consideration given to reasonable estimates of flow thicknesses and fault displacements.

All three ridges are of the complex type in that they exhibit broad gentle arches and at least one or more complex features such as escarpments, "squeeze-ups", or other constructional volcanic landforms. Much simpler examples of ridges are found which lack broad gentle arches and consist usually of one ridge element such as a "squeeze-up", some other small scale extrusion, or a small scarp. Such ridges could be the result of single rather than multiple episodes of volcanic and/or tectonic events.

We conclude that mare ridges form as the result of faulting, volcanism and plutonism along submare fractures, and that they have generally formed over an extended period of time rather than in single short periods of activity. Most ridges document the waning phases of the latest volcanic and tectonic activity within the maria where they are found.

IV. LUNAR SLOPES AND SLOPE EROSION

A. Lunar Slopes

Slopes on the moon where highlands are in contact with mare surfaces generally range from 5 to 30 degrees. There is a reasonable correlation between slope steepness and the heights of the highland fronts adjacent to the maria. Highlands with low relief (100-200 m) have slopes in the range of 5 to 10 degrees, whereas those with high relief (1000-2000 m) have slopes of 16 to 28 degrees. These generalizations are based on 130 selected measurements of simple highland slopes on all of the published lunar topographic maps. Slope measurements were made where there were no complications introduced by craters or by compound scarps with benches or obvious irregularities. This relationship can be partially explained by assuming that low relief is indicative of more complete flooding of the adjacent highlands so that only the summits protrude above the maria (regardless of the initial relief differences). Because all highland summits suffer net erosion through time all peaks will tend to be flattened.

There is also a very crude relationship between the age of the mare basins and the steepness of the basin margins. This relationship is also probably dependent on the degree to which each slope has been inundated. However, the younger maria seem to have a greater abundance of steeper, higher massifs adjacent to mare surfaces.

Neither of the two very general relationships appear unusual or difficult to understand, but they should be kept in mind when considering slope erosion processes on the moon as contrasted with the earth.

The steepest slopes in large lunar craters (5-50 km) of postmare and Copernican (highlands) ages average 28 degrees based on our measurements of 108 crater slopes. No compound slopes were measured. The range of slopes was between 20 and 33 degrees with the exception of Proclus (38.5°), and 60% of these craters had slopesin the range of 26 to 31 degrees. All of this data on postmare slopes is presented merely to establish what the range of relatively fresh slopes on the moon actually is.*

The natural angle of repose for general materials on the moon has been estimated at 32 to 35 degrees, not very different from the steepest talus slopes measured on earth (36°) (Choate,1966).

---

*It is interesting to note that a number of craters (4) with very steep slopes (33 to 38 degrees) are located in the small area of Mare Smythii. This might indicate something about the subsurface structure in that basin.

B. The Morphological Evolution of Mare-Highland Contacts: A Potential Measure of Relative Mare Surface Age

Erosion of lunar slopes in postmare time has been accomplished mainly by ballistic sedimentation and related seismic shaking of the surface caused by the flux of meteorites which has produced the regolith on the maria. On a uniform slope the net volume of material moved through equal cross-sectional areas over the entire slope will be the same, regardless of the actual detailed mode of movement, as long as the flux distribution is uniform when averaged over long periods of time. These conditions are met everywhere except at the top and toe of uniform slopes. The impact process will cause net erosion at the summit and net deposition at the toe (Figure 40A). It is important to note that in this "conveyor belt" model the length of the slope is not significant as long as the rate of downslope transport is slower than the rate of regolith production. The same-sized deposit will accumulate at the base of all equal slopes composed of similar materials for a range of slope lengths. Significant landslides appear to have been relatively rare (Young, 1976b).

Where a highland slope adjoins a smooth mare surface, there will be no large-scale transport of slope material by impacts for any significant distance out onto the mare surface. Mass wasting deposits overlying mare-highland contacts are all younger than the adjacent mare lavas, and because postmare regolith depths are generally less than 15 m, an upper limit can be placed on the amount of material which has moved down most slopes onto the mare surfaces. Assuming a depth of 10 m (for illustration only) of postmare regolith formation on a 5 km slope, the maximum accumulation of debris at the base, if all the material were transported downward, would be a 320 m high wedge sloping at 45°. With a more realistic slope (30°), and if half the regolith moved downslope, the debris would form an apron 170 m high extending 300 m from the original toe of the slope.

These figures are probably high for the rate of transport down most lunar slopes since the last major mare flooding, but they illustrate that very little material should have accumulated at the toes of highland slopes where they are in contact with the younger maria. The actual morphological form of the lower slope deposits is not specified in this discussion, but the younger maria do exhibit distinctive talus aprons of uniform width which are not discernible along older mare-highland contacts. It is assumed that all highlands are composed of complexly brecciated rock and that typical slopes are less than 30°. Talus aprons are more prevalent than is apparent on many photographs because typical illumination angles produce photographically underexposed slopes on high contrast prints. The features are often subtle and must be brought out by careful photoreproduction (Figures 40B, 41).

Houston et al. (1973) have shown that relatively little material is transported by impact-induced vibrations down lunar

slopes by regolith-forming impacts. In the range of slope angles below 30°, they imply that a maximum of 5 m of surficial material has probably moved downslope throughout postmare time.

From surface exposure ages and erosion of boulder tracks on 10° to 25° slopes at the Apollo 17 site, Arvidson et al. (1975) have determined limits for regolith transport into shallow depressions by all processes. Extrapolation of their rates back to 3 BY produces a range of 6 to 24 m of regolith movement down similar slopes, assuming a constant meteorite flux.

The theoretical evolution of lunar slopes adjacent to mare surfaces may be similar to the diagrammatic sketch in Figure 40A. All else being equal, the size and shape of the deposit of transported material at the base of the slope should be a function of the meteorite flux, the slope angle, the nature of the parent material, and the age of the adjacent mare surface. Relatively young (based on crater counts) mare regions such as Oceanus Procellarum show abundant evidence of small uniform talus aprons, whereas the older mare-highland slopes are more degraded with no sharp break discernible at the toe. The absence of a complete range of talus apron sizes is probably due to the limited number of distinctly different mare surface ages and the probability that the aprons gradually evolve into smooth slopes after passage of a critical period of time.

The relatively uniform appearance and persistence of the distinctive talus aprons in young mare regions indicate that the impact flux has produced a uniform deposit under similar conditions along highlands regardless of slope length differences and little affected by small slope angle differences.

The lack of an obvious correlation between steeper slopes and greater talus apron volumes means that the effect of slope angle must be relatively small compared to the total volume of material moved down typical slopes (15°-30°) in postmare time. Calculations suggest that net downslope ballistic transport of ejecta for a 1 m radius impact should approximately double with a slope increase from 15° to 30° (Soderblom, 1970). Thus a slope-angle dependency is to be expected, but it is not readily visible or easily measured on existing topographic maps and photographs. In fact, the absence of any appreciable slope dependency appears to be demonstrated on individual photographs, where seemingly uniform talus aprons continue unbroken for 50 km along the foot of highland scarps, which vary in height from 300 to 1300 m and slope from 11° to 22°. A compensating factor is related to the slight decrease in numbers of impacts per unit area as slope increases (∿9% per 15°) caused by reduction of the effective target area exposed to the flux. Because slope angle does not appear to be a sensitive variable in slope erosion, the talus aprons in the different maria must be reflecting mainly the age of the adjacent mare surfaces as related to the cumulative flux of impacts.

Another compensating factor which reduces the net amount of material moved downslope by larger impacts can be explained as follows. Although large impacts on slopes throw a large quantity of material downslope and cause a severe seismic disturbance, they also create sizeable traps for all material moved downward from above by the smaller impacts. Thus the greater erosive effect of a large impact is somewhat balanced by the necessity to fill the resulting crater before material upslope can effectively resume its downward migration. The efficiency with which these large craters are filled is obvious from the relative scarcity of craters on highland slopes. In summary, the lack of many large craters on highland slopes need not be considered as evidence that all material down to the depth of large craters (100 to 500 m in diameter) has been moving en masse down lunar slopes.

In the lunar highlands, basal slope deposits are older and slopes meet in complexly intersecting curves. The lack of horizontal surfaces adjacent to these slopes prevents slope erosion debris from developing into obvious, uniform talus aprons. In highland areas, where photography has high resolution and sun angles are favorable, talus deposits are visible in gully-like clefts and along junctions of opposing slopes. These deposits demonstrate that similar processes do operate on all slopes, although only the highland-mare contact zones have simple enough geologic constraints to permit relative age comparisons (Fig. 41).

Meteorite erosion on the moon produces very uniform landforms along the bases of slopes, unlike the highly variable situations for slopes on the earth. Therefore, observations of lunar slope characteristics along contacts with mare surfaces should provide an additional means of comparing the relative ages of mare surfaces over broad regions.

Occasional large impacts, severe seismic shaking, landslides, or unusual geologic conditions can be expected to produce exceptions to this model along individual mare-highland slope contact segments, but the regional similarities apparent on Apollo photographs imply a close correlation of relative mare surface ages with the morphology of talus apron deposits.

Summary: Unlike terrestrial slopes, lunar slopes do not develop stable profiles of equilibrium and undergo parallel retreat. Because of the nature of impact erosion material accumulates at the bases of steep slopes and is continually eroded from summit areas. Uniform transport on smooth segments of slopes results in a gradual decrease of slope angles as talus accumulations cover the lower slope while the upper reaches suffer net erosion. The initial stages of this process produce a distinctive, uniform talus apron along mare contact zones in the younger maria.

Because limits can be placed on postmare regolith formation, based on crater size-frequency distributions, a similar limit

can be placed on the total amount of erosion of slopes in contact with mare surfaces. This qualitative measure of slope differences could provide some indirect information on the relative flux of meteorites for intervals between known mare surface ages.

Captions: Figures 18-41

Figure 18. Area SW of Bonpland Crater (B). Bonpland D Crater (A) is enlarged in Figure 27. Crater at E is enlarged in Figure 38 (B). Lava channels with levees (C); grabens or straight rilles (D); Metric frame Apollo 16-1687.

Figure 19. Aristarchus Plateau (A,H) near Montes Agricola (C). Sinuous rilles A, D, G, H indicate lava flow toward west (left) through gap at F. See crater counts for Areas 30, 31. Area ABCD enlarged in Figure 37. Large crater north of A is 6 km. LT038B2. Apollo metric frames 15-2484 and 2480. Volcanic vents E, D, A, A'.

Figure 20. Herigonius rilles area located on Figure 15. Rille vents (H,H'); Rille deformed by ridges (S,S'). Crater rim (R) reactivated by intrusion along mare ridge (M); Graben(?) between two mare ridge features (G); Rille junction (J); Crater with mare ridge element superimposed (C) is enlarged in Figure 27 (C). Crater at F has impact melt(?) feature seen enlarged in Figure 47. Ring structure (R) is 70 km. LT075C1. Apollo metric frame 16-2990.

Figure 21. Enlarged portion of Herigonius rilles from Figure 20 showing detail of rille/ridge relationships. Discussion of labeled features is in text (Sections II and III). Insets are enlargements of roof remnant in rille (A) and possible volcanic cone filling sinuous rille (L). M is enlarged in Figure 27 (C). LT075C1. Apollo metric frame 16-2990.

Figure 22. Mare Tranquillitatis south of Vitruvius Crater (V). Enlargement of fault trace (A); Mare ridges (B, C, R, J); Volcanic vents near E, H; Reactivated (modified) crater rims at M, N; Jansen rille (H-N) crosses rim of crater near N, indicating postrille deformation; Volcanic domes (L); Continuation of ridge structural trends along highland faults (K,F); Mare highlands contact (G). Refer to discussion of ridges and rilles in text. LT060B2 and LT061A1. Apollo metric frame 17-0306.

Figure 23. Crater Brayley (B) and rille Rima Rimsky (A, C, D) in Mare Imbrium. Deformation of rille by ridge at (D) is enlarged in Figure 24. Discussion of rille area in text, Section I, Parts J and M. Arcuate to sinuous rille R changes abruptly to normal fault F. Tension fractures radiate from buried highland R due to isostatic adjustments or subsidence of adjacent mare surface. Volcanic subsidence depressions (S,S'). Crater Brayley is 14 km. LT039B3 and LT039B4 (parts). Apollo metric frame 17-2928.

Figure 24. Enlarged view of rille interrupted by ridge intrusion or extrusion from Figure 23 (D). Scale 1 cm is 970 m. Apollo panoramic frame 17-3122.

Figure 25. A. Small scale inset of Crater Isaev floor on far-side (LTO102B2) showing location of collapse crater (C) enlarged in part B of Figure. Crater Isaev has 90 km diameter.

B. Enlarged view of 4 km diameter, rimless collapse crater (C). Rille indicates lava flow from R to R' to R". Collapse of crater followed development of rille. Mare ridge (M) development is younger than subsidence crater at C and younger than impact crater F. See discussion in text, p. 57. Collapse crater C has 4 km diameter. Apollo metric frame 17-1567 (oblique) and panoramic frame 17-2381. Views are looking south from orbit.

Figure 26. Topographic profiles of representative mare ridges. (a) Ridge just northeast of Jansen Rille in Mare Tranquillitatus; (b) Ridge in southern Mare Serenitatis; (c) Ridge in southwestern Mare Serenitatis; (d) Dorsa Ewing in the Oceanus Procellarum; (e) Ridge in northwestern Mare Crisium; (f) Ridge in southeastern Mare Crisium; (g) Dorsa Harker in Mare Crisium; (h) Dorsum Oppel in Mare Crisium; All profiles are constructed from Lunar Topographic Orthophotomaps at a scale of 1/250,000. Vertical exaggeration = 5X. An arbitrary topographic datum is given for each profile.

Figure 27. Two examples of mare ridge elements (M;R) extending into postmare impact craters. Top is same as crater C on Figure 20 or M on Figure 21. (1.75 km diameter) Morphology suggests extrusive origin for ridge element. Bottom (F) is same as crater A on Figure 18 (Bonpland D). Fault through crater at F has clearly offset rim along structural trend of mare ridge (R). Crater F has 1 km diameter. Apollo panoramic frames 16-5477 and 16-5435. LTO map references same as larger views.

Figure 28. Vertical higher sun angle view of portion of Figure 29. Letter locations are the same in Figures 28, A and B, and Figure 29. (Western edge of Mare Serenitatis.)
A. Mare ridge M is colinear with fault traces c, d, e, f. Note flooding of faults by mare.
B. Enlargement of area g, h, d shows development of small mare ridge element south of fault trace (g) on mare surface. Length of highland shown in view A is 80 km (top to bottom). Apollo panoramic frame 15-9358; metric frame (A) is 15-0583.

Figure 29. North oblique view of western edge of Mare Serenitatis showing colinearity of mare ridges (M,Z) with highland fractures (g, X-Y). Symbols are the same as on vertical view in Figure 28.
A. See description of Figure 28 for significance of ridge and fault trend m, g, e, f.
B. Enlarged portion of ridge system Z and highland fault scarp X-Y on panoramic frame. V is irregular volcanic vent on mare ridge. See discussion in text on page 58. LT041B3. Apollo metric frame 17-0955, panoramic frame 15-9358.
Craters either side of V are both 4 km in diameter.

Figure 30. South-looking oblique view across Mare Vaporum with Manilius Crater (M) and Hyginus rille near horizon, H. D Caldera is near lower right. Unnamed mare ridge (MR) exhibits obvious colinearity with fault scarp (F) in highlands. Elevation across mare ridge shows displacement in same sense as highland fault scarp (radial structure to Imbrian basin) which has 300 m of relief. Graben (G) terminates at junction with major structure. Younger lavas of Mare Vaporum embay older lavas near Hyginus rille.
LT041C3 and LT041C4 (parts). Crater near G has 9 km diameter, Manilius has 40 km diameter. Apollo metric frame 17-1671.

Figure 31. Dorsa Aldrovandi region of eastern Mare Serenitatis. North oblique view with Posidonius crater (P) near horizon (diameter 100 km) and Clerke Crater in right foreground (6.5 km).
(A) Lava surface is 300 m lower on west side of Dorsa Aldrovandi than at (B). The rift at (B) could be an analogue of the kind of irregular fissure above which some mare ridges form. Note colinearity of ridge L, A, C with ridge D and graben E in highlands. Similar colinearity of ridge F, D and graben G. Intermediate age of tensional rifting shown in Area H. View of highland portion of ridge at (C) is enlarged in Figure 35. LT042B3 and LT042C2. Apollo north oblique metric frame 17-0940.

Figure 32. Mare ridges showing paired topographic profiles (a) Dorsa Aldrovandi; (b) Dorsum Zirkel; (c) Dorsum Zirkel. Upper profiles constructed from Lunar Topographic Orthophotomaps at a scale of 1/50,000, lower profiles constructed from Lunar Topographic Orthophotomaps at a scale of 1/250,000. Vertical exaggeration at both scales is 5X. An arbitrary topographic datum is given for each profile.

Figure 33. A. Compound (mare/highland) ridge system just south of Bowditch on farside (LT0100C1). Bowditch is one of the few craters exhibiting true "high lava marks"

just north of this view. Mare ridge (M) trends into highland fault scarp (F) similar to Lincoln-Lee Scarp at Apollo 17 Site. Similar scarps develop where other mare ridges intersect highlands (see text, p. 57, 58). Apollo metric frame 15-2358. Large crater at left has 17 km diameter. LTO100C1 and LTO100C1S1 (part).
B. Shows mare ridge segments (R) trending into reactivated (modified) crater rim (C). Enlarged view of Figure 22, M. Crater rim diameter is 20 km. LTO61A1. Apollo metric frame 17-0306.

Figure 34. Mare ridge morphology in highland regions showing trends from extrusive/intrusive mare ridge to highland faults. H is highland in mare region southwest of Fra Mauro (also shown in Figure 40B). Highland scarp across H also looks similar to Lincoln-Lee Scarp at Apollo 17 Site. Thin dark mantle appears to cover mare surface and ridge with lighter outcrops showing through. Width of view is ∿5 km. Apollo panoramic frame 16-0534.
A. Change in ridge morphology near gradational mare/highland contact (parallel to ridge). Crater (A) is 2 km in diameter. Area is southwest of Fra Mauro on view in Figure 18 between features labeled C. Length of view is ∿20 km. Part A of this Figure compared with the same region on Figure 18 is a graphic comparison of the exaggerated effect of low sun elevation. The mare ridges in the center of Figure 18 have relief of 100 m. Apollo panoramic frame 16-5431. No LTO map.

Figure 35. Enlarged view of highland segment of Dorsa Aldrovandi in eastern Serenitatis seen on Figure 31 at C. Part B is continuation north of A. Note that typical mare ridge morphology is present north and south of highland (F). Ridge (R) shows extrusion into several postmare craters. Highland fault scarp (F) is similar to Lincoln-Lee Scarp at Apollo 17 Site. See discussion in text, p. 57, 58. In this particular case some slight intrusive activity may be present along highland contact due to low elevation of scarp near mare surface (suggested by small features along scarp). LTO map 42B3.Crater C is ∿1 km. Apollo panoramic frames 15-9296 to 9303.

Figure 36. Radial and concentric mare ridges in SE Mare Serenitatis near crater Brackett (B). Subdued form of ridges in dark anulus (lower right) is probably due to intrusive origin below thick regolith in contrast to extrusive and intrusive form on younger maria to north. Inversion of crater frequencies near 200 m diameters on younger and older surface can be seen here on careful examination (somewhat complicated by ejecta from relatively younger large craters directly south of view (lower right corner). Crater S is 1250 meters in diameter, 290 meters deep and shows bright blocky ejecta facies similar to Figure 13A. This crater probably samples dark mantle beneath young flows and has ejecta related to subsurface stratigraphy discussed in Section I, p. 20-22. Apollo metric frame 17-0601. LT042C4S1 and LT042C4. Crater Brackett (B) has 9 km diameter.

Figure 37. Enlargement of portion of northern edge of Aristarchus Plateau and Montes Agricola seen on Figure 19. See detailed discussion in text of significance of structural trend D, E, F, G (faults, mare ridge, and volcanic vents) as related to timing of displacement, formation of rilles and mare ridges. Letters referred to in text, p. 58. For scale and other data see Figure 19.

Figure 38. Enlargement of mare ridge flow lobes in craters from Figure 18E (near Fra Mauro region). Mare ridge (A) shows definite filling and flow into postmare craters at C. D suggests proximity of fault to trend of ridge through crater with movement postdating crater impact. Apollo panoramic frame 16-5435. LT07602.

Figure 39. Hypothetical cross sections of mare ridges: A Dorsa Ewing, B ridge in northwestern Mare Crisium, C Dorsum Zirkel. (See scaled topographic profiles in Figures 26 and 32.

Figure 40A. Slope erosion model for young mare/highland contact zones. Model explained in text, Section IV.

Figure 40B. Talus apron (A,B) in mare region east of Fra Mauro on highland immediately west of Figure 18 (continuation of ridge at west central part of Figure 18). Ridge (C) crossing highland as fault (D) is on edge of Figure 18, due west of crater A. Subtle change in slope at talus apron (A) is difficult to see except at certain intermediate sun elevations. These talus aprons have been confused with "high lava marks" which are quite dissimilar. Highland is 11.5 km long, 4 km wide. Apollo panoramic frame 16-0534. LTO76D2. (See also Figure 34, H)

Figure 41. Talus aprons on east side of Riphaeus Mts. (Mare Cognitum). Two different exposures illustrate the difficulty of showing subtle talus aprons along mare-highlands contacts. Talus accumulation in highland cleft (B) demonstrates that deposits are slope controlled, not "high lava marks". Talus aprons A, C, D are uniformly developed on range of slope angles and slope lengths. See text, Section IV. Length of view is 12.5 km. Apollo panoramic frame 16-5455 (sun elevation is 18 degrees) LT076D1.

FIGURE 18

ORIGINAL PAGE IS
OF POOR QUALITY

FIGURE 19

FIGURE 20

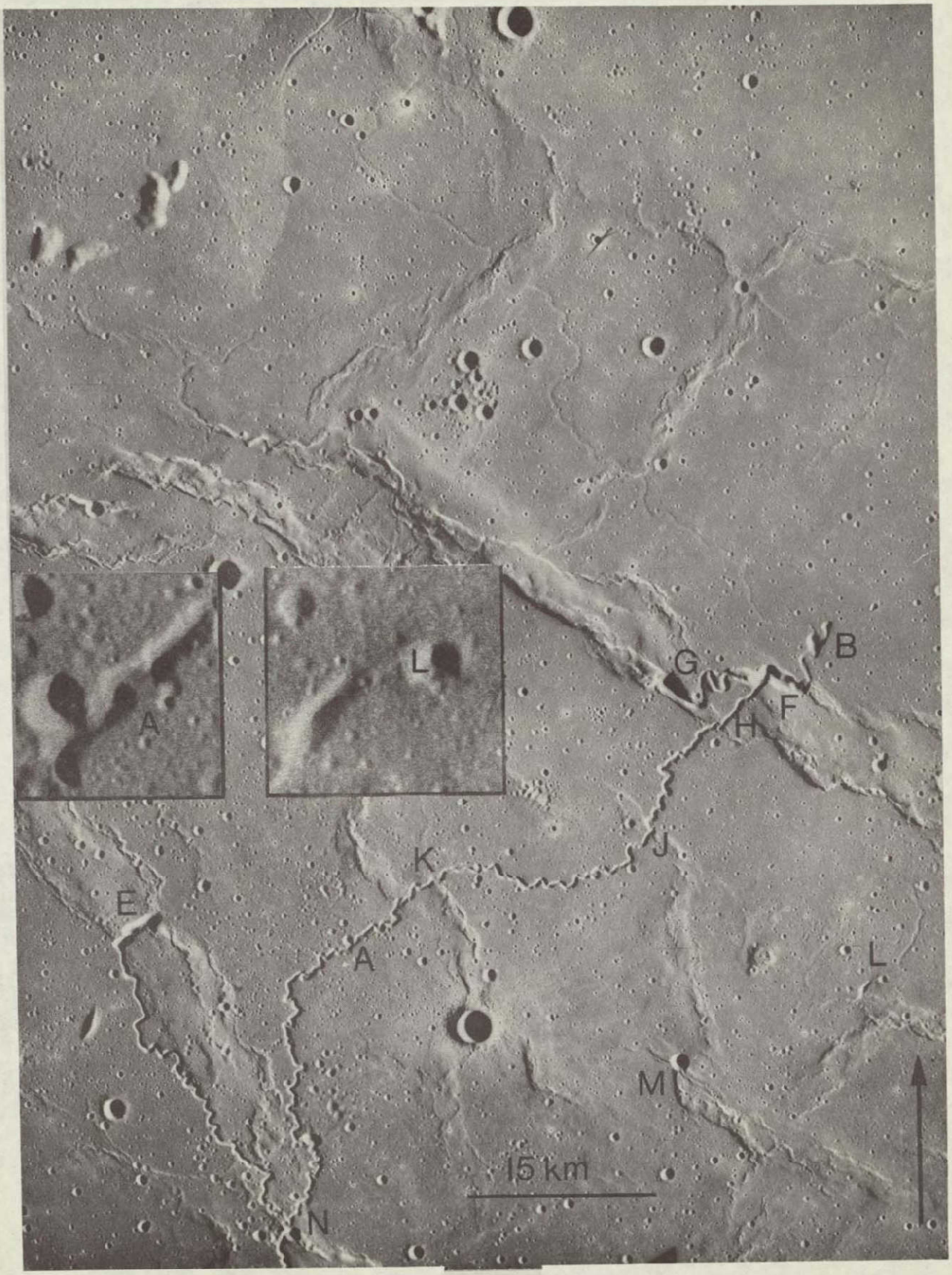

FIGURE 21

FIGURE 22
77

FIGURE 23

FIGURE 24

FIGURE 25

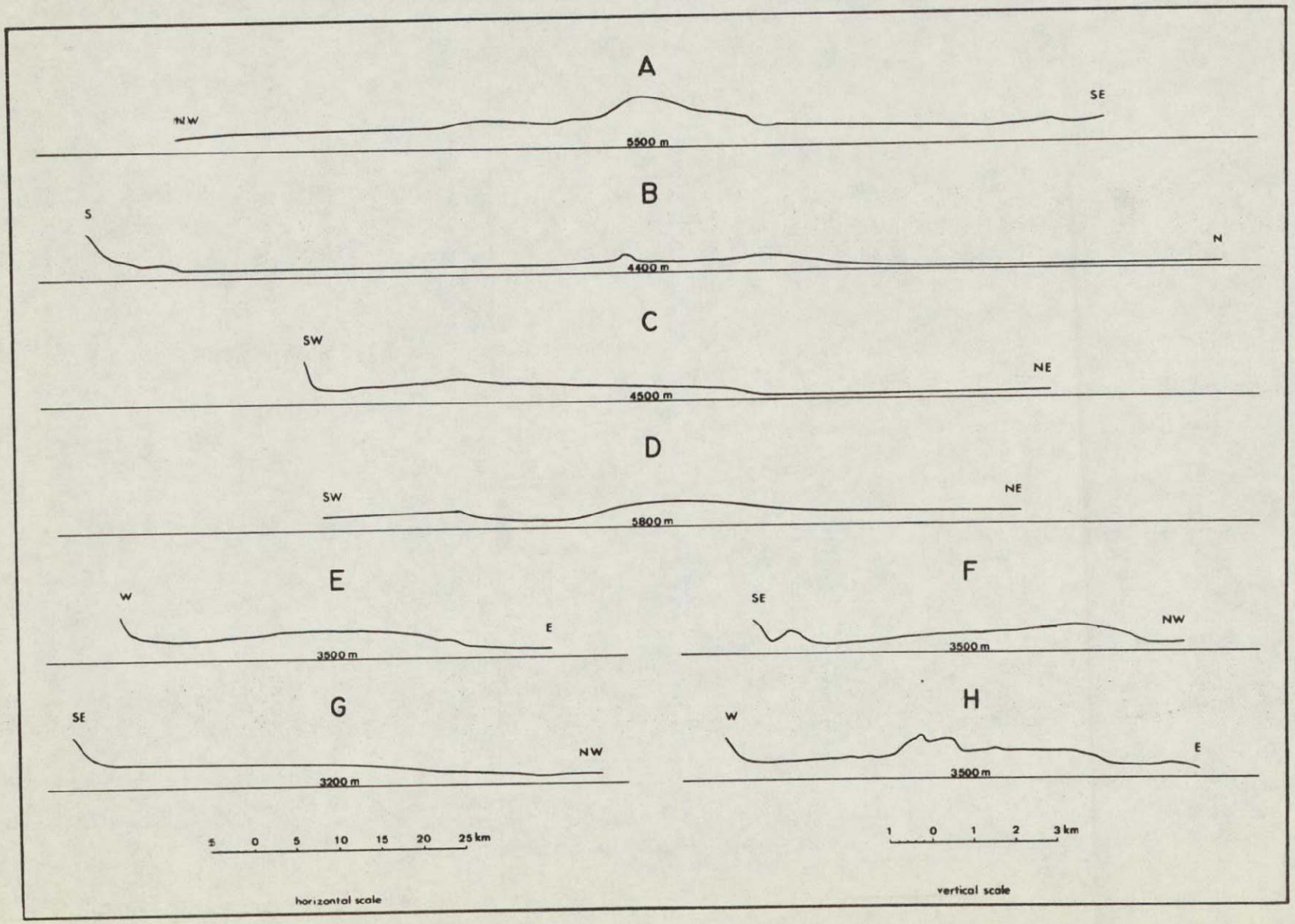
A
NW
SE
5500 m
B
S
N
4400 m
C
SW
NE
4500 m
D
SW
NE
5800 m
E
W
E
3500 m
F
SE
NW
3500 m
G
SE
NW
3200 m
H
W
E
3500 m
5 0 5 10 15 20 25 km
horizontal scale
1 0 1 2 3 km
vertical scale

FIGURE 26

FIGURE 27

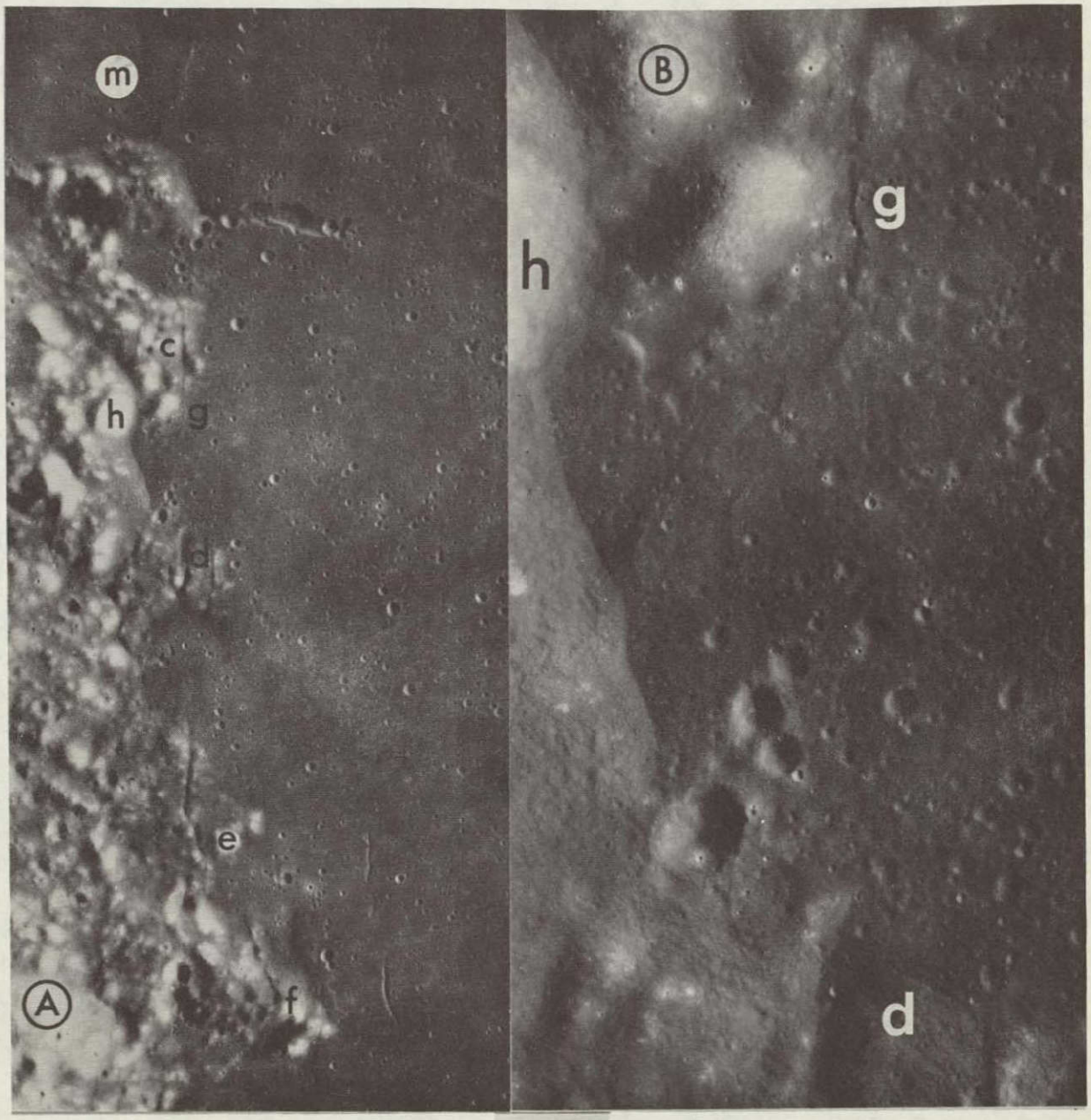

FIGURE 28

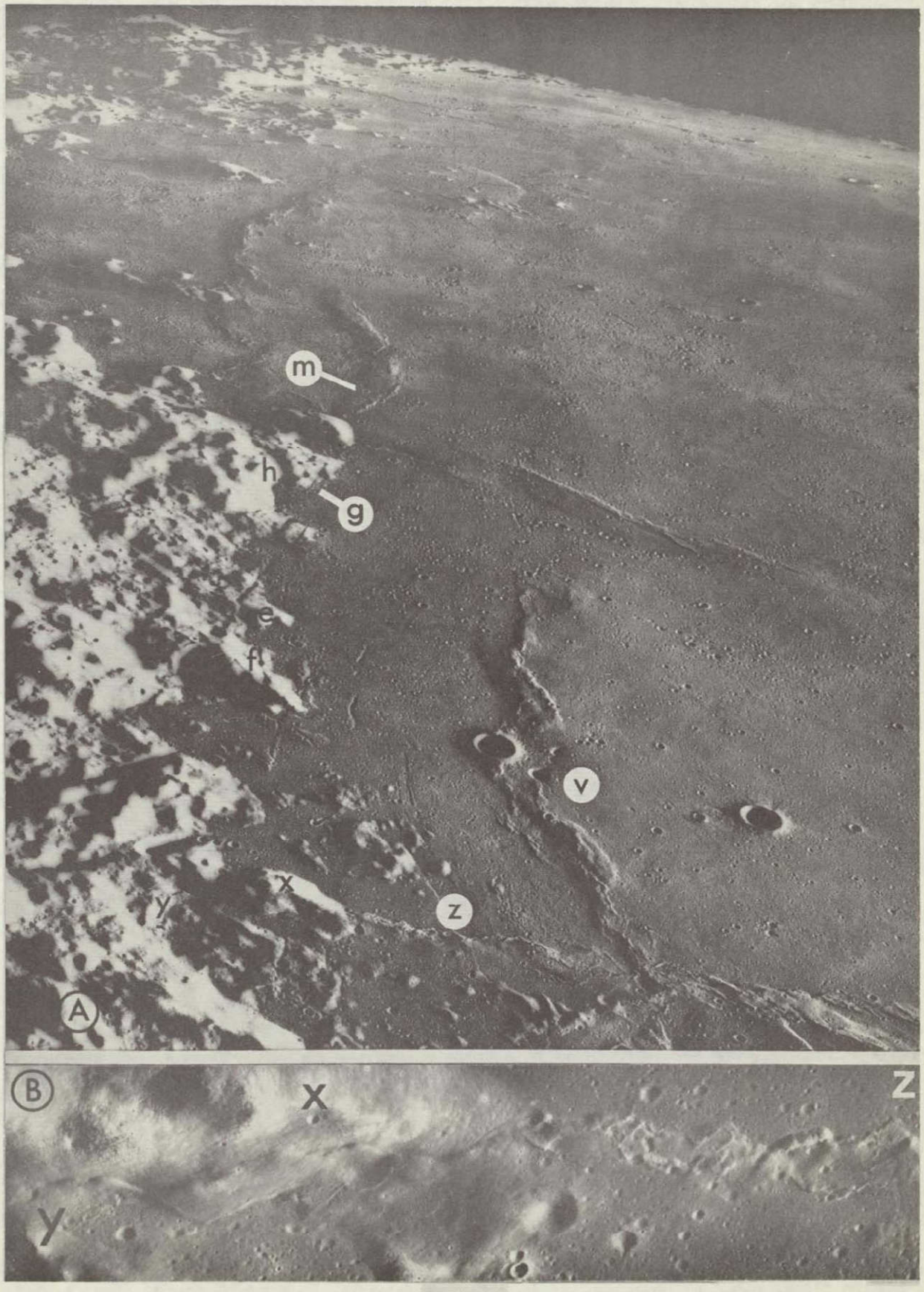

FIGURE 29

FIGURE 30

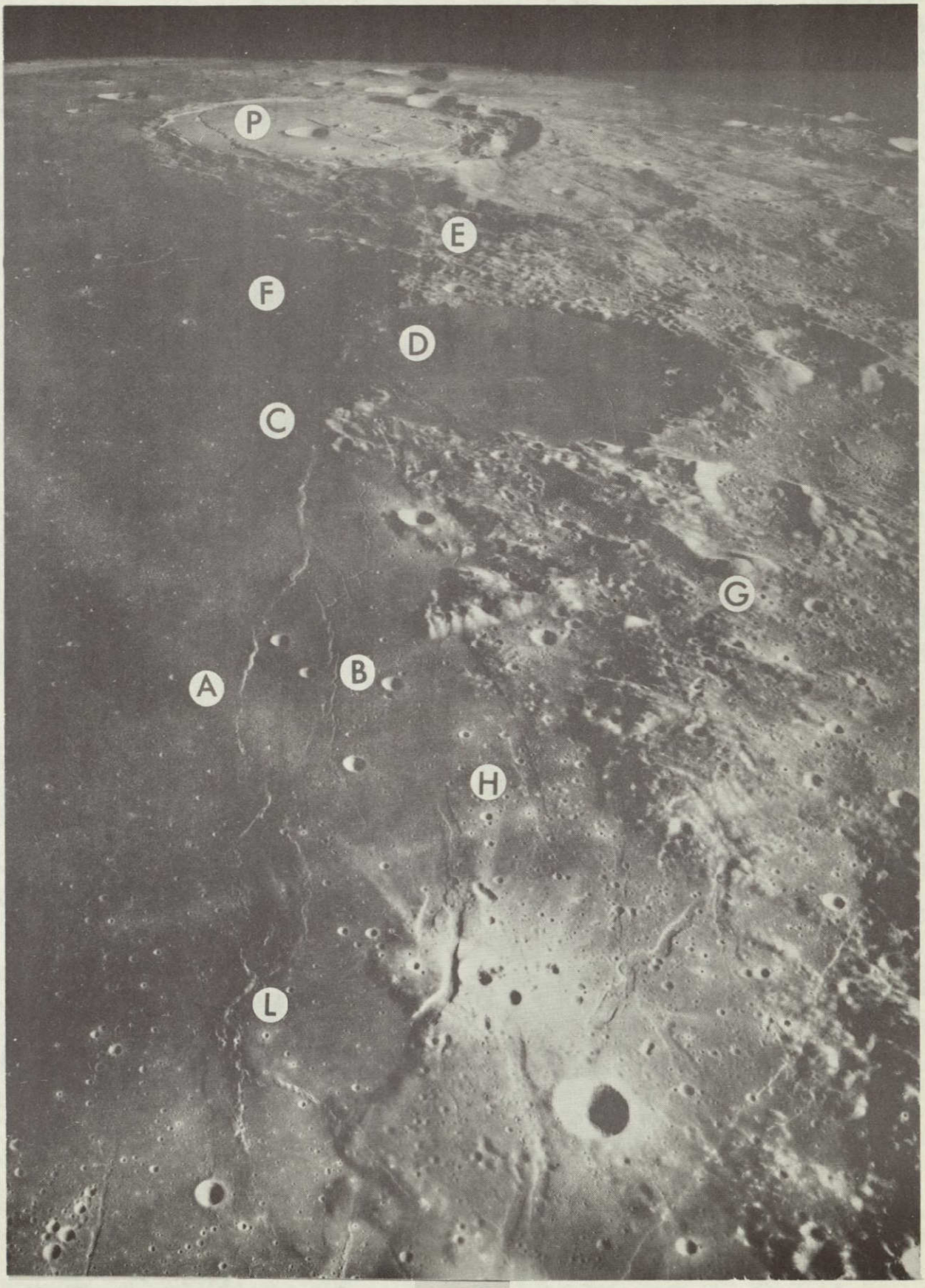

FIGURE 31

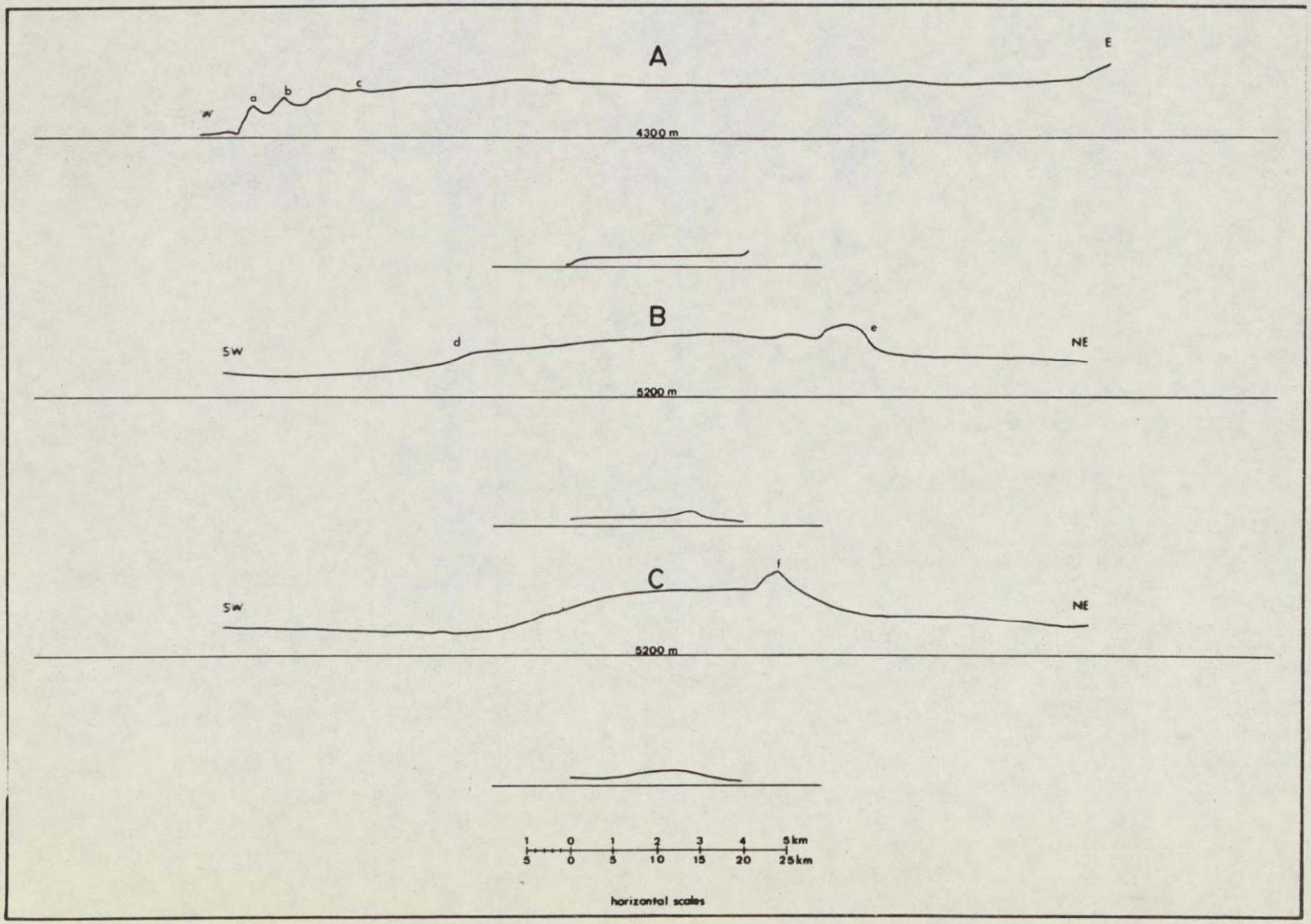
A
E
W
a
b
c
4300 m
B
SW
d
e
NE
5200 m
C
f
SW
NE
5200 m
1 0 1 2 3 4 5km
5 0 5 10 15 20 25km
horizontal scales

FIGURE 32

ORIGINAL PAGE IS
OF POOR QUALITY

FIGURE 33

FIGURE 34

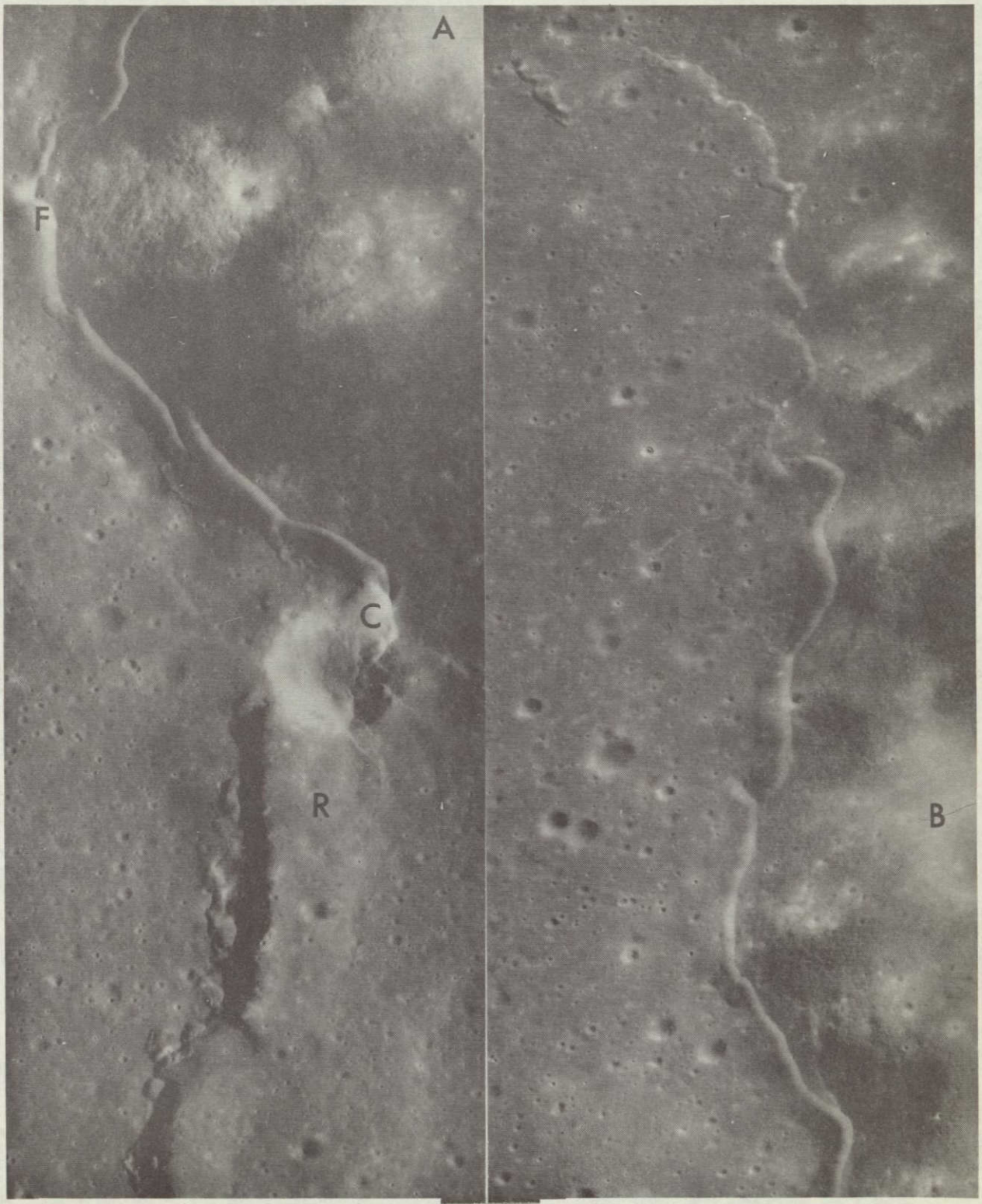

FIGURE 35

FIGURE 36

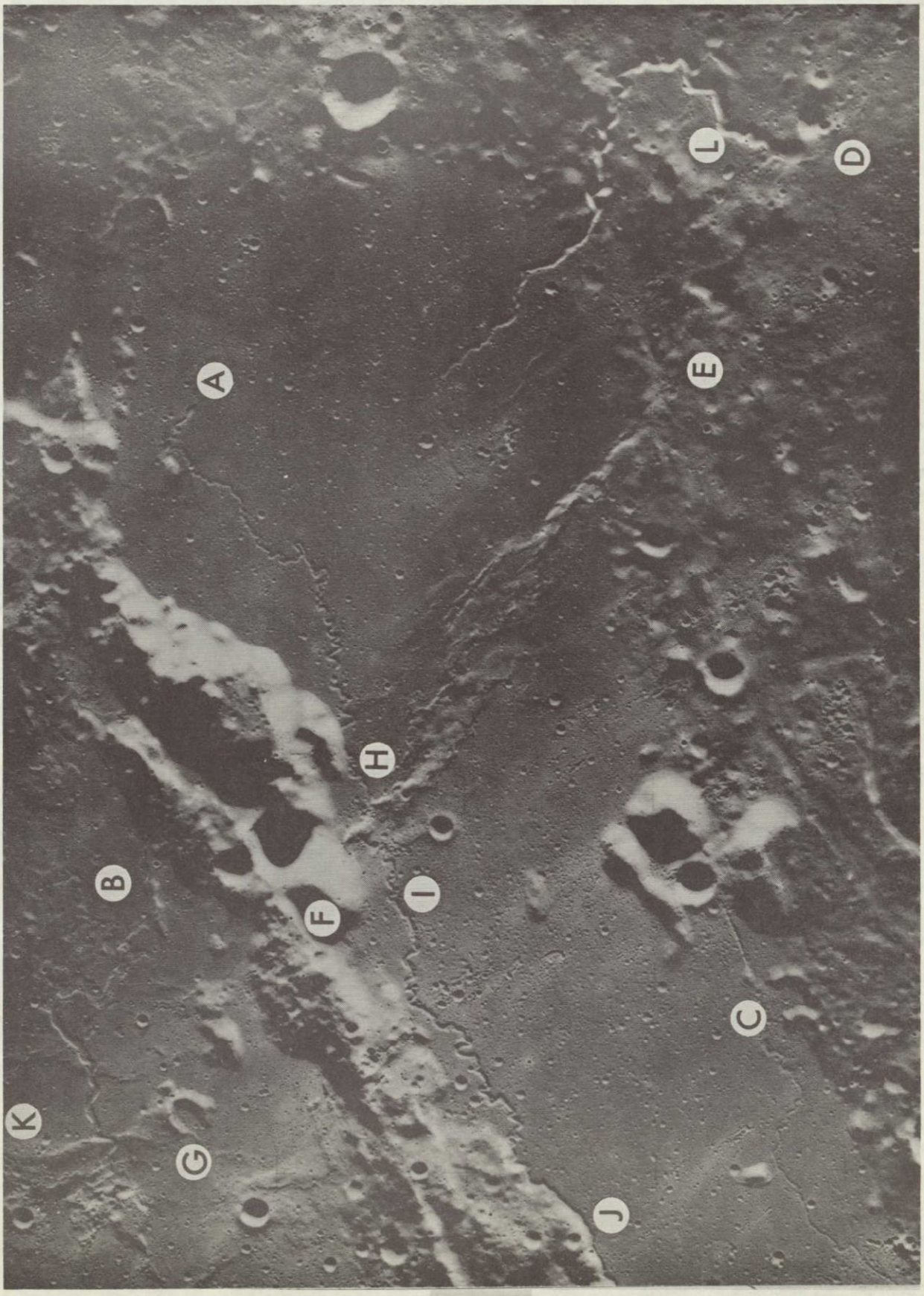

FIGURE 37

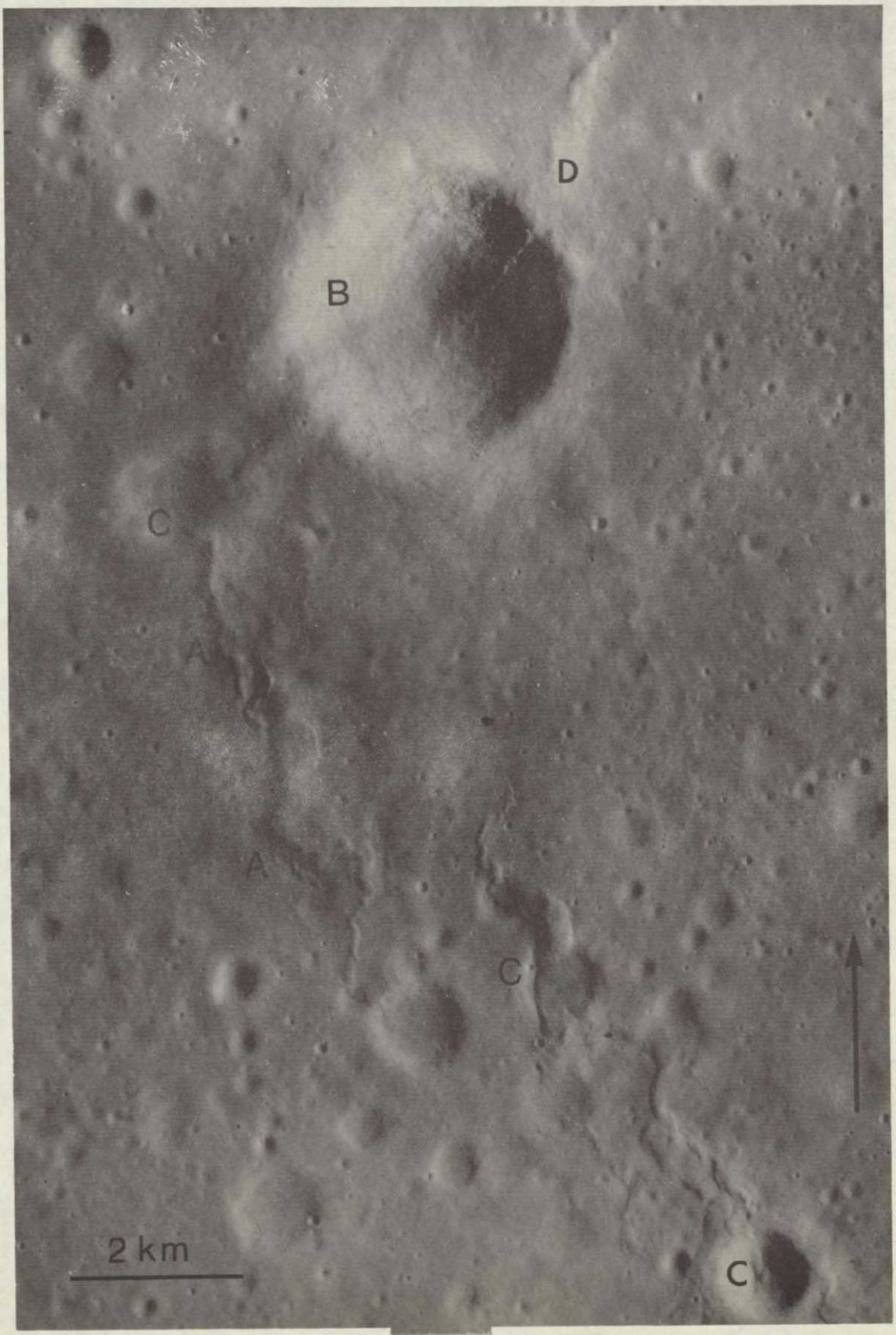

FIGURE 38

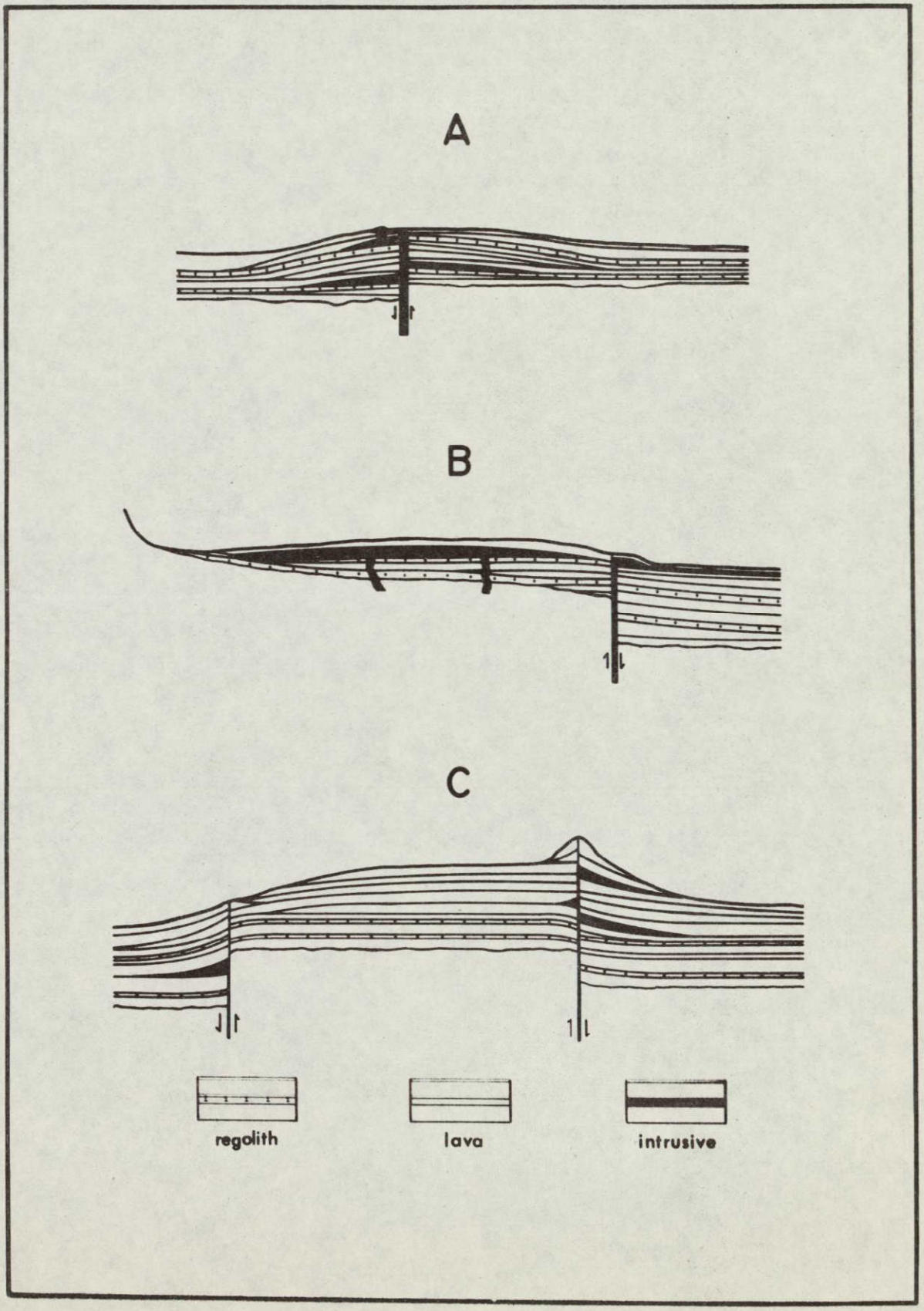

FIGURE 39

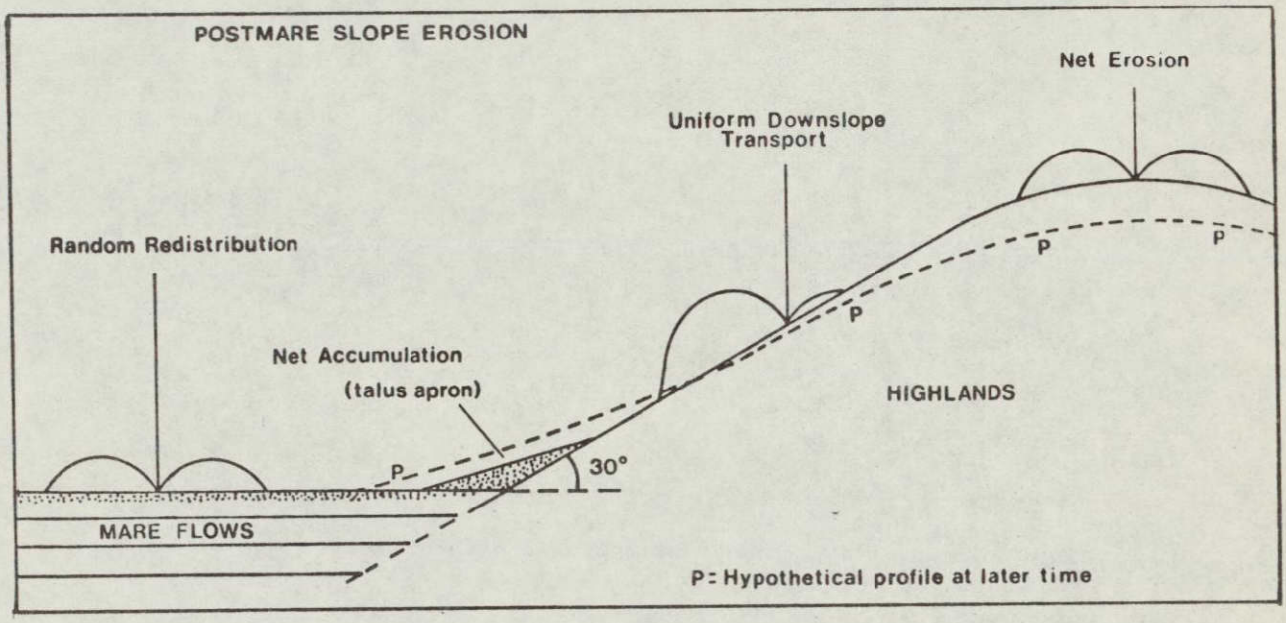

FIGURE 40A

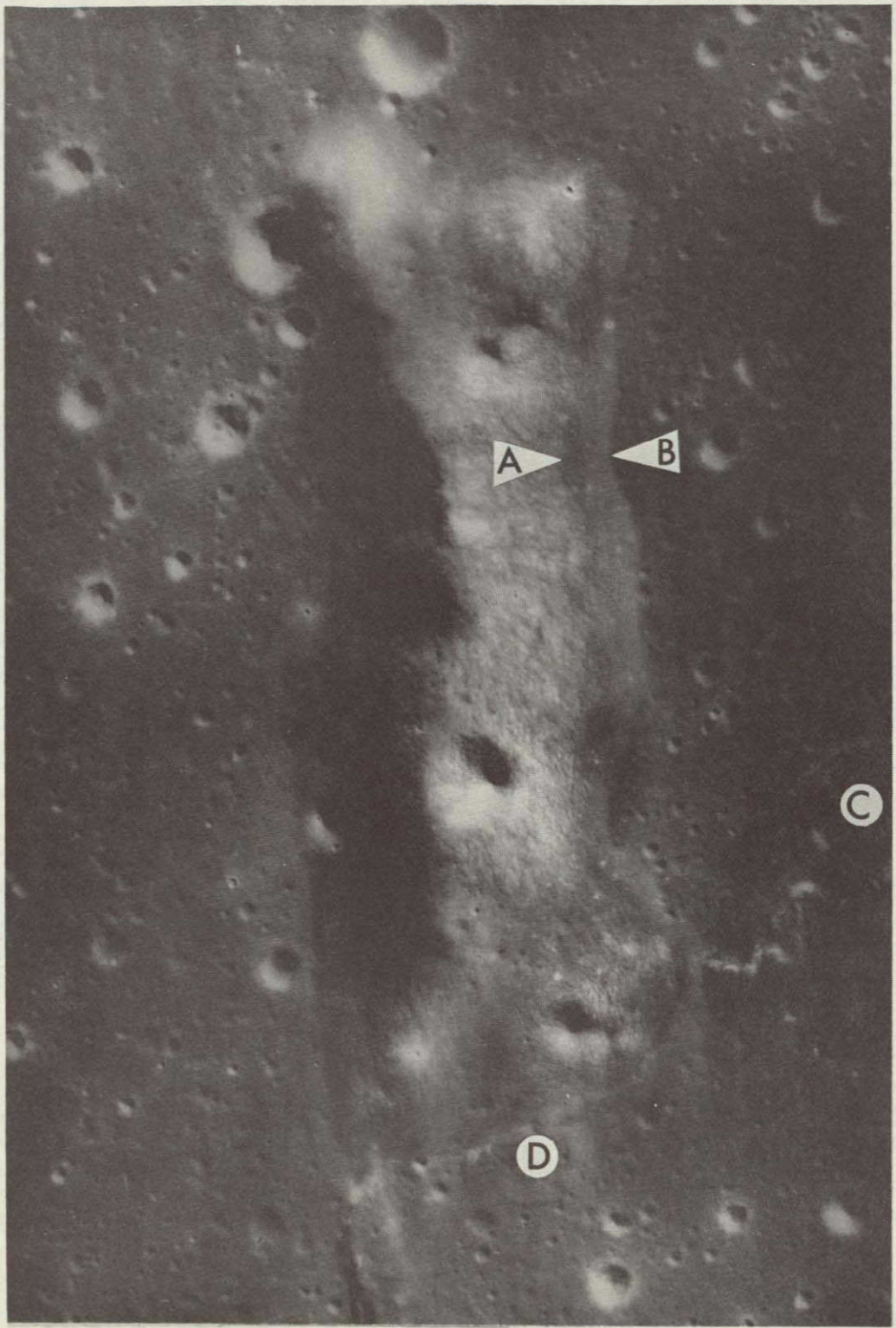

FIGURE 40 B

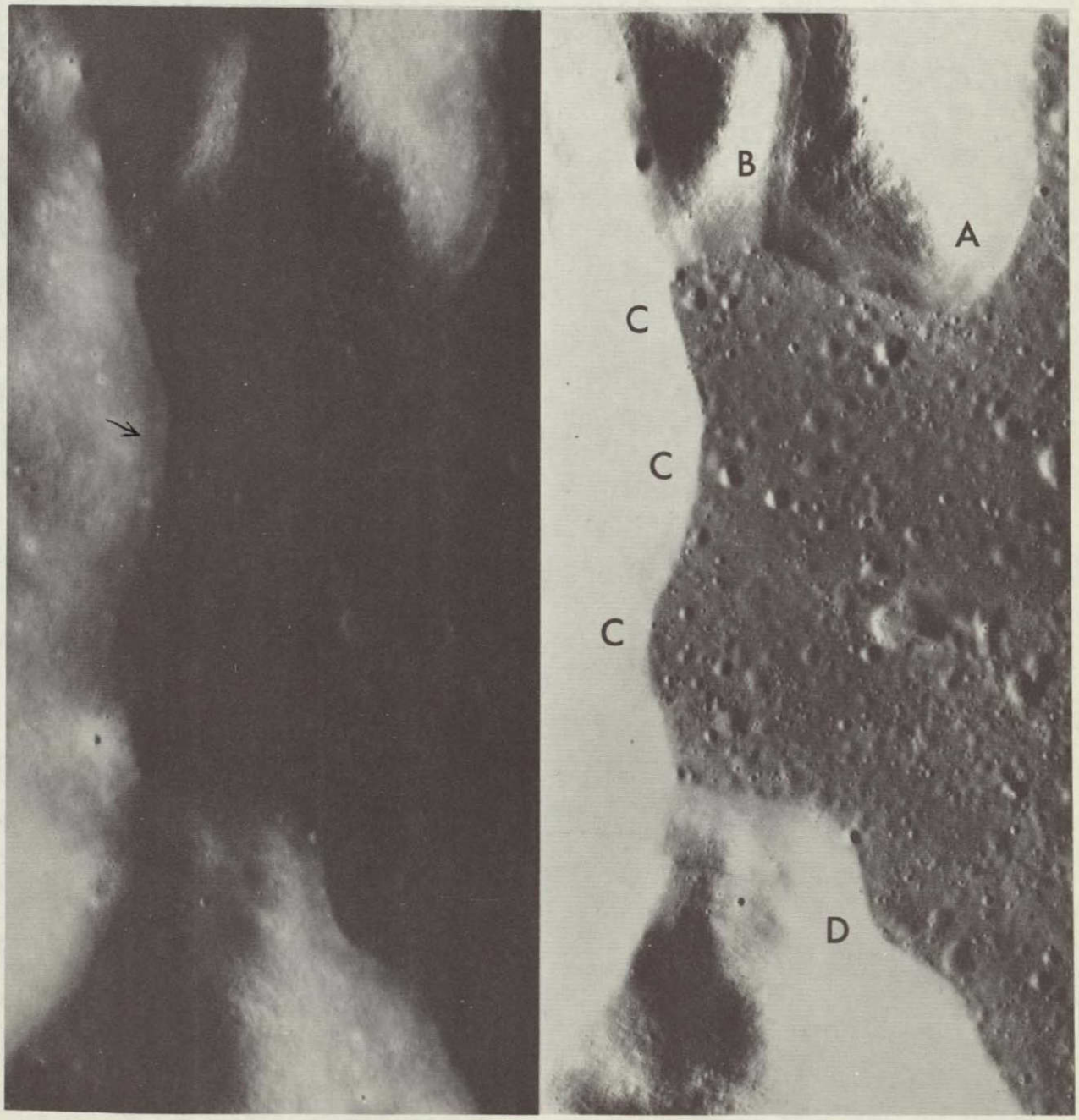

FIGURE 41

V. MODIFICATION OF PREMARE IMPACT CRATERS BY VOLCANISM AND TECTONISM

A. Introduction

Many lunar craters and ring structures exhibit morphological characteristics which cannot be explained solely by impact erosion models. Such craters are common along the edges of the maria and in other areas where volcanism has occurred, and this distribution has caused geologists to explain many of them as either entirely endogenic in origin (Morris and Wilhelms, 1967; Kosofsky and El-Baz, 1970; DeHon, 1971; Greene, 1971; Fielder, 1967; Smith, 1966; Strom, 1971; McCall, 1965, Cameron and Padgett, 1974), or the result of endogenic modification of impact craters (Baldwin, 1963; Pike, 1968; Pike, 1971; Young et al., 1973b; Brennan et al., 1974; Schultz, 1974).

Morphological studies of and comparisons with possible terrestrial analogs reveal that many lunar craters and ring structures show some resemblance to calderas or resurgence cauldrons of the Valles type (Smith, 1966; DeHon, 1971). Tectonism in the form of uplift of lunar crater floors along ring fractures and faults which transect craters is clearly evident in many of the examples described (DeHon, 1971; Strom, 1971; Fielder, 1967; Kosofsky and El-Baz, 1970).

Analysis of Apollo metric and panoramic photography as well as Lunar Orbiter photography indicates that many such craters and ring structures in the maria are impact craters that have been modified by endogenic processes including partial or complete inundation by mare lavas, plutonism, fissure volcanism, and tectonism (Cruikshank et al., 1973; Young et al., 1973b; Brennan et al., 1974; Schultz, 1974). The purpose of this paper is to propose origins for several of the wide variety of such features found in and adjacent to the maria, and to relate their development to the complex processes of mare filling.

B. General Characteristics of Modified Craters

Most modified craters discussed in this paper are located near the margins of the circular maria where the lava fill is, presumably, relatively thin, and they exhibit the following generalized characteristics:

1. uplifted centers of crater floors bounded by steep, outward facing scarps concentric with the crater rims (most common in craters greater than 25 km in diameter).
2. lava filled interiors (complete filling most common in craters smaller than 25 km in diameter) or partial filling to form a moat around uplifted centers (most common in craters greater than 25 km in diameter).

3. partial or complete secondary rims which result from volcanism along ring fractures.
4. sinuous rilles which lie within or extend across crater rims.
5. circularity indices (Ronca and Salisbury, 1966) greater than those of most terrestrial calderas.
6. fractured crater floors (most common in craters greater than 25 km in diameter).
7. low interior relief as compared to fresh impact craters.
8. central peaks resembling those of impact origin (most common in craters greater than 25 km in diameter).
9. presence of apparent pyroclastic cones on crater floors (uncommon).

C. The Caldera Analogy

Terrestrial calderas, which are in some respects similar to modified lunar craters, fall into one of the following categories:

1. Kilauean calderas
2. Krakatoan calderas
3. resurgence cauldrons of the Valles type

These calderas exhibit some morphologic characteristics that are found in modified lunar craters, particularly fissure flows and fractured floors; however, the differences are more numerous than the similarities.

Kilauean calderas are rarely greater than 10 km in diameter (Smith, 1966) and are typically found at the summits of large shield volcanoes whose diameters are several times as large as those of the associated calderas. In contrast, the lunar craters with which these calderas are compared have diameters as large as several hundred km and their rim crest diameters are much greater than half as large as their outer rim slope diameters.

The Krakatoan calderas are usually found at the summits of large composite volcanoes and generally are less than 15 km in diameter (Smith, 1966), far less than the diameters of the volcanoes. In some cases larger Krakatoan calderas are found in association with groups of volcanic cones (Smith, 1966). None of these relationships are observed in lunar craters. Ash-flows, which are commonly deposited around Krakatoan calderas have not been documented on the Moon.

Resurgence cauldrons of the Valles type resemble modified lunar craters more closely than any other possible terrestrial analogs. They are characterized by uplift of their interior portions along ring fractures as well as intra-caldera graben and volcanism. Several lunar craters which resemble resurgence cauldrons, for example Ritter and Sabine, have smooth rims which have been interpreted as being of volcanic orgin (DeHon, 1971;

Morris and Wilhelms, 1967; Kosofsky and El-Baz, 1970).

Detailed comparisons of the morphologies of modified craters and resurgence cauldrons reveal that important differences with genetic significance exist. The central portions of resurgence cauldrons are usually domical in structure, whereas the uplifted floors of modified craters are nearly always in the form of a concave plateau. The rings of lava cones or domes which surround the central uplifts in resurgence cauldrons have not been observed in modified lunar craters. In fact, volcanic cones are not common in modified lunar craters. The rims of most modified craters, including Ritter and Sabine but excluding the most highly modified varieties, are much more uniform than those of resurgence cauldrons and they are like the debris rings deposited around explosion and impact craters (Smith, 1966). The smooth rims of craters like Ritter and Sabine may be due to impact erosion (they are both of Imbrian age according to Wilhelms and MacCauley, 1971) and a predominance of fine grained fragments in the rim material. In addition, the lavas associated with resurgent cauldrons are silicic and include welded tuffs (Smith and Bailey, 1968; Branch, 1966), neither of which has been identified on the moon.

Cameron and Padgett (1974) have suggested that many lunar craters may have origins similar to those of terrestrial ring structures. However, the common association of rhyolitic welded tuffs as well as granitic ring dikes in terrestrial ring structures seem unlikely occurrances in the basaltic maria. In addition, Smith (1966) has pointed out that many terrestrial ring structures may be the eroded roofs of resurgent cauldrons. But no known surficial processes (i.e. impact or mass wasting) on the lunar surface appear capable of the denudation necessary to expose plutons emplaced beneath the surfaces of the maria.

Several lunar ring structures, including the Flamsteed P ring (Fielder, 1967; Strom, 1971), have discontinuous chains of hills which lie along circular arcs. The hills have higher albedo than the surrounding mare material and resemble highland material (Strom, 1971). Strom (1971) has suggested that these hills may be of volcanic origin and possibly are composed of viscous extrusive or pyroclastic materials; however, it is equally likely that these hills are merely remnants of a former ejecta rim.

Terrestrial calderas, including ring structures, are significantly different in shape from modified craters. Circularity indices (Ronca and Salisbury, 1966) for fresh lunar craters examined in this study average 0.89 (see Table 4) and those of modified craters average 0.87 (see Table 5). Although many terrestrial calderas have vaguely circular or elliptical shape, many others are completely noncircular.

During the course of this study published descriptions of several terrestrial ring structures and calderas were analyzed.

In addition, brief field examinations were made of the Ossipee Cauldron and the Valles, Lake City, Creede, Platoro, and Northumberland Calderas. The circularity indices of a number of similar terrestrial structures are listed in Table 6. The average circularity index is 0.70. As a group, these features exhibit a wider variation in circularity than either fresh or modified lunar craters (Murray and Guest, 1970); this is particularly true of the largest ring structures and calderas. Comparison of circularities of Martian craters with those of both terrestrial impact craters and calderas (Oberbeck et al., 1972) indicates that significant differences exist between the circularities of volcanic and impact craters. A full appreciation of these differences is best obtained by a visual comparison between photographs of modified lunar craters and geologic maps of terrestrial calderas and ring dikes, such as those published by Jacobson (1958), Branch (1966), Turner (1963) or Bailey and Maufe (1960). On careful inspection it can be seen that the comparisons between the morphologies of terrestrial calderas and modified lunar craters are not convincing.

D. Modification of Impact Craters

The formation of meteorite impact craters results in a surface configuration that is gravitationally unstable, brecciation and fracturing of near surface rocks, and in some cases production of an impact melt. In many terrestrial impact craters, especially those 30 km or larger in diameter, a large volume of impact-generated melt fills the center of the crater and is both overlain and underlain by brecciated country rock (Dence, 1964; 1968; 1971). Gravity investigations indicate that low density rock other than sedimentary fill underlies the basins. Drilling of terrestrial impact craters has shown that this is due to porosity produced by brecciation (Innes, 1964). The low density rock undoubtedly contributes to the gravitational imbalance associated with lunar craters.

Subsequent mobilization of the lunar crust during episodes of magmatic activity frequently results in the uplift of crater floors along circular faults. On the Moon this has occurred primarily in and adjacent to the maria. In most cases lava flooding of the crater floors also occurs and this sometimes causes the surface evidence of faults to be obscured. Figure 42A illustrates the crater Gaudibert which is located in a highland area adjacent to the Oceanus Procellarum. Due to its high elevation, Gaudibert has not been flooded by lavas; however, mobilization of the crust which probably occurred during nearby volcanism has resulted in uplift of the crater floor along a well defined circular fault. A graben (arrow) extends across the crater interior and is terminated at both ends by the circular fault.

It is apparent that the floor of Gaudibert has moved essentially as a single block during uplift. This is probably the result of motion taking place along circular fractures produced during the impact process, but it is not known to what degree a layer of solidified impact-melted rock, which certainly must exist in a crater of this size range, contributes to the

single block behavior of the crater floor.

E. Modified Craters 25 km and Larger in Diameter

The craters Taruntius (Figure 42,B), Haldane (Figure42,C), and Posidonius (Figure42,D) all exhibit central uplifts bounded by scarps. In addition, the floors of Posidonius and Haldane have been flooded by lavas. This explains why several sets of arcuate fractures are observable on the floor of Taruntius, whereas in Haldane and Posidonius evidence of only those fractures along which motion has occurred since flooding is visible.

The flooding of Posidonius has apparently occurred in at least two episodes. The older flow(s) having preceded the central uplift and the younger flow(s) having filled most of the low area between the rim and central uplift, forming a moat. A sinuous rille extends nearly throughout the extent of the younger lava. The northwestern portion of the rim of Haldane has been breached, and flooding of the lowest portion of the moat has occurred. The absence of mare lavas within Taruntius may be due to its location on a small highland area between Mare Fecundatatis and Mare Tranquillitatis.

The crater Doyle (Figure 43,B) exhibits both a central uplift with a prominent outward facing escarpment (arrows) and fracturing of parts of its floor. There is also evidence of lava flooding which has apparently occurred after the uplifting of the crater floor. The floor of Dalton (Figure 43,A) contains a well developed system of concentric fractures similar to those of Taruntius.

Taruntius, Haldane, Posidonius, Doyle, and Dalton have central peaks which resemble those of other lunar impact craters of comparable size which have not been modified by volcanism or tectonism. Similar central peaks have been observed in terrestrial explosion craters (Roddy, 1968; Wilshire et al., 1972) and in terrestrial meteorite craters (Dence, 1964), 1968; Roddy; 1968). A large central peak can be seen in Gaudibert. The degree to which these central peaks are preserved appears to be related to crater flooding with preservation being best in unflooded craters like Taruntius and Gaudibert. This may result both from partial burial by the lavas which flood craters and the erosive effects of the flooding process. The existance of such central peaks which do not closely resemble any known terrestrial volcanic landforms suggests an impact origin for the craters in which they are observed.

Several modified craters with completely flooded interiors and extensively breached rims are illustrated in Figure 44. The unnamed crater with a breached rim in Figure 44A is composed of material that resembles the rims of impact craters as well as the small isolated remnants of terra material which are adjacent to it. The mare lavas which fill the interior are continuous with the lavas which completely surround it. The large gap in

the southwestern portion is occupied by a mare ridge which meets the ends of both large rim segments "end to end", and lies just inside the former position of the once continuous rim. These spatial relationships suggest that the volcanism and plutonism which contributed to the ridge formation (Young et al., 1973b)occurred along fractures formed at the time of the impact which formed the crater. Additional evidence of volcanism can be seen to the southwest where a sinuous rille crosses the crest of a similar mare ridge segment and extends into the interior of the crater. The portion of the sinuous rille which is at the crest of the ridge has been filled by extrusion of lava from the fracture vents under the ridge crest following the emplacement of the uppermost lava flow which contains the sinuous rille. It seems likely that breaching of the rim could have resulted primarily from the erosive action of flowing lava. Absence of a central peak might be readily explained by the same process.

Lambert R (Figure 44,B) has formed in a similar manner, but has been more extensively modified. The interior is both completely filled and completely surrounded by mare lavas. Complete inundation of portions of the rim by lavas is indicated by the sinuous rille which crosses the northwestern portion of the rim.

Most of the rim resembles the basaltic mare lavas and/or mare ridges and appears to be a secondary rim of volcanic origin. Some volcanism has occurred along the northwestern portion of the rim since the last episode of flooding and has filled the sinuous rille at its crest. This relationship is best viewed in stereo on higher sun angle photos such as Apollo 17 metric camera fram AS17-2286. Only a small portion of the rim along the southwestern edge of the crater appears to be of impact origin, and it is identical in both surface texture and albedo to the rim in Figure 44,A.

The varying extent to which individual impact craters have been modified can be readily explained as resulting from processes which are known to occur within the maria. Lambert R is located approximately halfway between the rim and center of Mare Imbrium, an area where a thick lava fill is highly probable. The crater illustrated in Figure44,A is located just to the north of the mare ridge system where the Herigonius rilles begin. This area is probably a major source of eruption of lavas in the surrounding portions of the Oceanus Procellarum. Evidence of out flow of lavas is indicated by the Herigonius rilles which extend to the south and the smaller rille which extends to the north and into the crater (Young et al., 1973a and b). The slope of the surface as illustrated on Lunar Topographic Orthophotomaps LTO75C-1 and LTO75C-2 extends down from the Herigonius Rille and ridge vent area to the northeast and through the two gaps in this crater rim. The eruption of a large volume of lava near an impact crater would likely result in extensive erosion of the crater rim and, if breaching

of the rim occurred, "rapid" flooding of its interior. The lunar surface upon which the mare lavas were extruded, both here and elsewhere, was composed of highly fragmented regolith formed by the premare meteorite flux. The erosive action of thick tongues of molten lava on such material would undoubtedly have been far more effective than flowing water in a terrestrial stream because of the higher density of the lava (comparable to that of the material over which it flowed) and the correspondingly greater bouyant force on individual fragments at the surface. Several similar examples of erosion by lavas have been cited by Cruikshank et al. (1973), and Young et al. (1973b). In many cases this mechanism might result in the complete obliteration of surface evidence of craters except where remnants of impact rims protruded out of the lava fill or where volcanism along arcuate fractures formed during the impact event resulted in secondary rims. An additional result of the rapid flooding of the interior of an impact crater is the alteration of the surface to a gravitationally more stable configuration. This explains why uplifted centers are not observed in craters modified by flooding in the manner of those illustrated in Figure 44.

In contrast, craters located along the margins of the maria or immediately adjacent in the highlands (see Posidonius, Figure 42D) usually do not exhibit evidence of extensive rim destruction or lava flooding of sufficient thickness to retard the formation of central uplifts. This seems to be a logical consequence of their locations in areas where lava flooding is either relatively thin or not present.

F. Modified Craters Less Than 25 km in Diameter

Figure 45 illustrates several additional examples of modified craters in the 10-25 km diameter range. The crater Swasey (Figure45,A) in Mare Smythii is one of a very few craters that exhibit convincing evidence of pyroclastic eruptions. A chain of craters lies along a fracture in the floor which extends from near the center and terminates at the rim. It is composed of material that appears to be dark mantle material much like that found along the margin of Mare Serenitatis and elsewhere in southern Mare Smythii, including the craters, Kiess, Widmannstätten, Kao, and Helmert. A volcanic origin has also been suggested for some dark-haloed craters found elsewhere on the Moon (Salisbury et al., 1968).

The small crater in Figure45,B consists of a discontinuous ring of high albedo hills that are remnants of an impact rim and a flooded interior with a central uplift. As in Posidonius, the flooding of the crater interior has included at least two episodes of volcanism, one prior to the formation of the central uplift and one which occurred later. A hypothetical cross-section of this mode of modification is illustrated in Figure 45,C. The crater is located in northeastern Mare Crisium immediately adjacent to the highlands and well outside of the

concentric mare ridge system in Mare Crisium. The lava fill in this area is presumably thinner than in the center of Mare Crisium.

The circular features illustrated in Figure 45,D and 45,E are representative of many others in the maria. The most consistantly observed physical characteristics include circular outline, lack of any observable difference between the surface of the interior and the surrounding mare surface, and outer slopes which are commonly steeper than inner slopes. It has been suggested (Cruikshank et al., 1973) that some such features are "ghost rings" formed by complete inundation of small impact craters by mare lavas followed by draping of the cooling lava crust over the buried crater rim. Although the evidence for inundation by mare lavas is quite convincing, it does not appear to be the sole process involved. The inverted topography configuration seems unlikely to be the result of a simple draping mechanism. Many such features are located near mare ridges and, as in Figure 45,D, have small ridge-like forms of probable volcanic origin which extend from their rims. These small ridge-like forms are also found at the crests of mare ridges (Figure 45D) and resemble terrestrial "squeeze ups". It seems reasonable that emplacement of small plutons in or above the brecciated rock beneath the floors of inundated craters as illustrated in Figure45,F would result in the inverted topography which is observed.

G. Relief-Diameter Relationships of Lunar Craters

Pike (1968, 1974b)has shown that a simple relationship exists between the interior relief (R_i) and rim crest diameter (D_r) for fresh lunar craters (Figure 46, curve A). Analysis of Apollo metric photographs, Lunar Topographic Orthophotomaps, and data tabulated by Pike (1968) indicate that a similar relationship exists for modified craters which lie along the margins of the maria (Figure 46, curve B). The curves for both fresh and modified craters have similar slopes but differ in that the interior relief of modified craters is less than that of fresh craters by approximately one order of magnitude. This reduction in interior relief is due primarily to lava flooding and uplifting of crater floors. Although, in some instances the erosive effects of flowing lava, mass wasting, and subsequent meteorite erosion have also contributed by reducing the height of the impact rims. Curve B (Figure 46) represents an approximation of the reduction of lunar crater relief by modification. Many craters which have been less extensively modified exhibit a lesser degree of relief reduction. The values of D_r and R_i for such craters generally lie between curves A and B (Figure46). The separation between the two curves then represents an approximation of the effect on one aspect of crater morphology due to volcanism and tectonism. The overall results of modification, as indicated by the relationship between interior relief and rim crest diameter, is to alter the morphology of impact craters to a more stable gravitational configuration.

H. Circularity of Lunar Craters

Most fresh impact craters have circular rim crests with high circularity indices (ratio of area bounded by rim crest/area of minimum circumscribed circle). The average circularity index for the fresh craters examined in this study (curve C, Figure 46) is 0.89, and the average circularity index of the modified craters (curve B, Figure 46) is 0.87. These values indicate that modification of craters by volcanism and tectonism does not cause significant changes in crater circularity. Pike (1968) compared the circularity indices of impact craters of widely varying ages, excluding flooded craters in the maria, and found no correlation between crater circularity and crater age, indicating that degradation of craters by mass wasting and meteorite impact does not significantly change crater circularity. In contrast, Adler and Salisbury (1969) measured circularity indices of 487 lunar craters and concluded that two populations of lunar craters exist and that the circularity indices of both decrease with increasing age. They hypothesized that one of the two populations consist of impact craters and the other of impact craters in the maria that were initially circular and later distorted by faulting along concentric and radial fractures. However, they did not present supporting evidence other than the circularity measurements. The results of the present study are clearly in agreement with the observations reported by Pike (1968) and differ completely from those of Adler and Salisbury (1969). With few exceptions (one of which is the crater Goclenius) little evidence of distortion of crater rims by faulting were observed in the craters studied for this report.

Pike (1974a)has presented strong evidence, using multivariate analysis of seven dimensionless topographic variables measured on twenty-two different categories of terrestrial and extraterrestrial craters, that individual impact craters and volcanoes are not readily distinguished with confidence on the basis of single topographic variables, including circularity index. However, he concludes that single topographic variables can distinguish volcanic craters as a class from impact craters as a class. In addition Pike considered several categories of volcanic craters (tuff rings, maars, cindercones, small lava shields, small lava domes and oceanic islands) which bear little resemblance to the lunar craters examined in the present study. For these reasons his most recent analysis neither contradicts nor strongly supports the evidence considered here.

The close agreement between circularity indices and the interior relief versus rim crest diameter relationships of fresh and highly modified lunar craters support the argument that a genetic relationship exists between both groups of craters, and these observations are compatible with the crater modification model described.

I. Conclusions

The modified craters described in this report are impact craters that have been modified by endogenic processes and are not primary endogenic features. They have been modified during episodes of basaltic volcanism and plutonism, isostatic adjustment, and meteorite erosion in and adjacent to the maria. As such they are the result of processes (impact, basaltic volcanism) that are known to have occurred widely on the moon and not the result of processes (ring dike implacement, cauldron resurgence, or caldera collapse) which have been observed on Earth but for which there is little evidence of widespread occurrance on the moon. It appears that the relative importance, sequence, and volume of volcanism, plutonism, and faulting in the modification of individual impact craters is the primary reason for most observed variations in morphology among these features. In some cases variations may be due, in part, to whether the craters from which these features have developed were formed prior to, early, or late in the history of mare filling.

VI. SMALL SCALE VOLCANIC FEATURES

A variety of small volcanic features, which in most cases have terrestrial analogues, are present in the lunar maria. One type of feature consists of rimless, non-circular craters, that appear to have formed by collapse of lava crusts over vents during the waning stages of volcanism. Several are shown at S and S' on Figure 23. The example at C (Figure 25) is 4 km in diameter and 200 m deep. Many such craters are located near mare ridges as the example, Lorca, which is at one end of Dorsum Owen (LTO map 42A4). Lorca is a maximum 8 km in diameter and 400 m deep. Several much smaller examples are located at the summits of mare ridges (Figure 22, F and H, Figure 29, V) and in addition, may have sinuous rilles extending from them (Figure 22, Figure 21, G, B, E). All of these spatial relationships support the interpretation that some rimless craters were volcanic vents, or that they collapsed into cavities as a result of drainage of lava beneath a surface crust.

Volcanic cones are uncommon on the Moon in contrast to their wide distribution on the Earth. Two examples of volcanic cones can be observed in southeastern Mare Serenitatis. Isis (LTO map 42C3S1) is apparently the source of a small rille, while Osiris (LTO map 42C3S2) is located at the end of a fracture. Both Isis and Osiris are less than 100 m in height.

Wilhelms (1973) has described some possible cinder cones associated with dark mantle materials in Mare Crisium and pyroclastic chain craters have been observed in Mare Smythii (Brennan, 1975a; Section V of this report) and elsewhere (Heiken and McKay, 1974).

Figure 47 illustrates a small lava flow (M-M') adjacent to the base of the rim of a fresh impact crater. Parts of the rim above the lava flow appear to have been scoured. The slope of the lava tongue and the freshness of the crater both suggest that the source of the lava was impact melt either ejected from the crater, or erupted from its flank. The occurrence of similar impact melt has been documented in terrestrial impact craters (Dence, 1964, 1968, 1971) and adjacent to King Crater on the lunar farside.

Similar small volcanic features undoubtedly formed between and following all episodes of mare flooding and during some impact events. They have been largely destroyed by subsequent lava flooding and impact erosion.

Captions: Figures 42-47

Figure 42. (A) Gaudibert AS16 metric frame 0144 (D_r=33.8 km); (B) Taruntius AS15 metric frame 2210 (D_r=54.6 km); (C) Haldane AS17 metric frame 2641 (D_r=40.2 km); (D) Posidonius Lunar Orbiter IV frame 79 (D_r=100.5 km); D_r=rim crest diam.

Figure 43. (A) Dalton Lunar Orbiter IV frame 182 (D_r=64 km); (B) Doyle Lunar Orbiter I frame 8 (D_r=30.7 km); D_r=rim crest diam.

Figure 44. (A) Ring north of the Herigonius Rille AS16 metric frame 2836 (D_r=67.0 km); (B) Lambert R AS15 metric frame 1011 (D_r=56.9 km); D_r=rim crest diam.

Figure 45. (A) Swasey AS17 metric frame 2635 (D_r=20.9 km); (B) Crater in northern Mare Crisium AS17 metric frame 0281 (D_r=12.5 km); (C) Hypothetical cross section of crater illustrated in part (B); (D) Crater in Mare Tranquillitatis AS17 metric frame 0307 (D_r=18.9 km); (E) Crater in Mare Fecundatatis AS16 metric frame 0135 (D_r=20.0 km); (F) Hypothetical cross section of crater illustrated in part (E); D_r=rim crest diam.

Figure 46. Relationship between rim crest diam.(D_r) and interior relief (R_i) of lunar craters; A=fresh-craters reported by Pike (1974b); B=Modified craters examined in this study; C=Fresh craters examined in this study.

Figure 47. Enlarged view of 1.5 km crater from Figure 21 (M) showing small lava(?) flow (M-M') extending radially from rim. Flow may be impact melt from crater F ejected across rim (scoured at M) or injected laterally through side of rim ejecta. Apollo panoramic frame 16-5474. No LTO map.

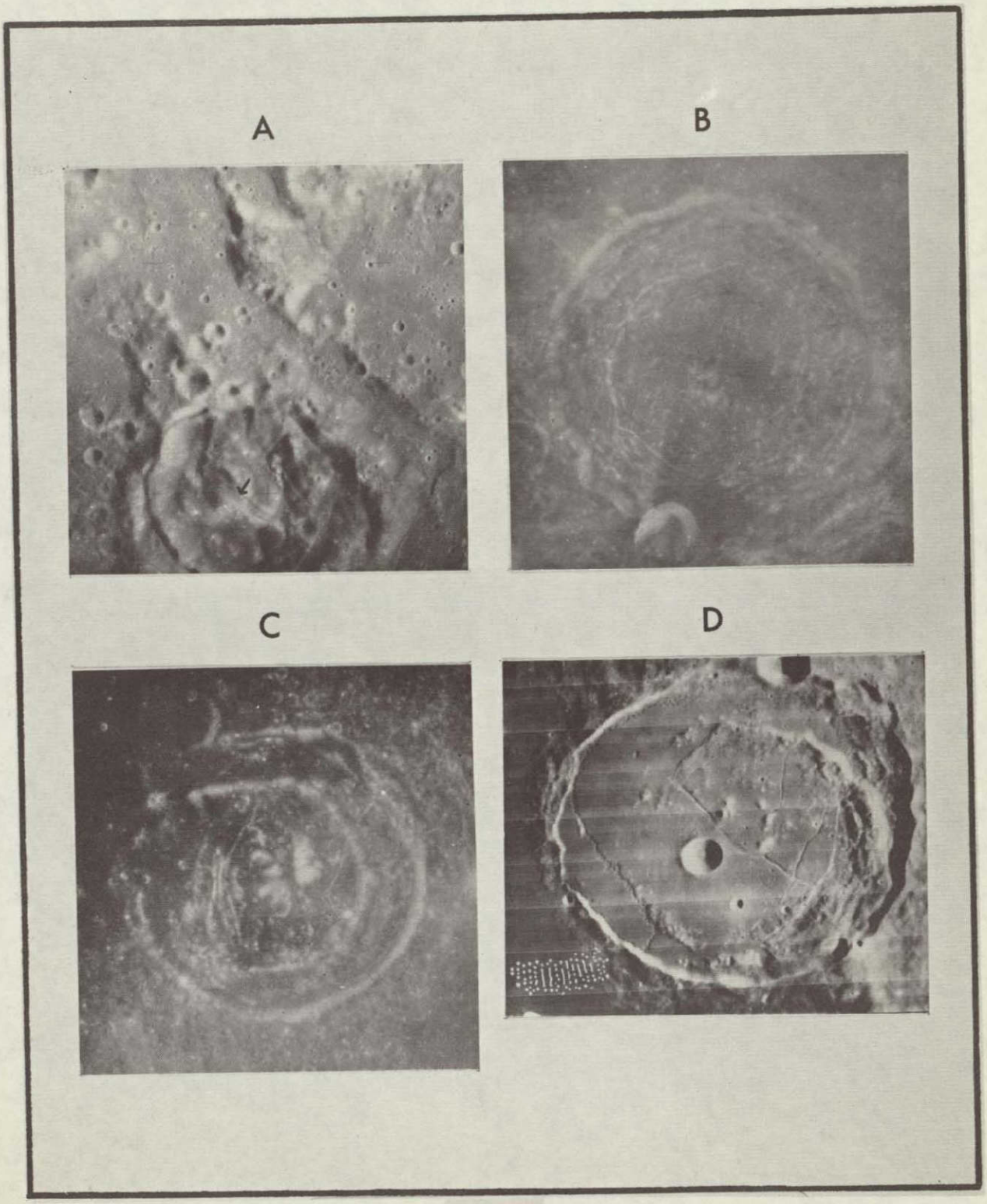

FIGURE 42

FIGURE 43

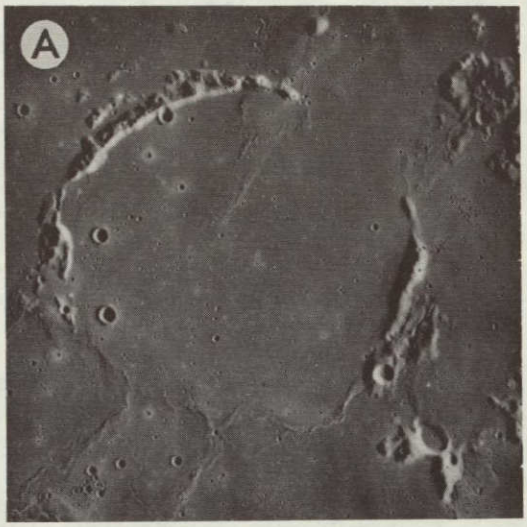

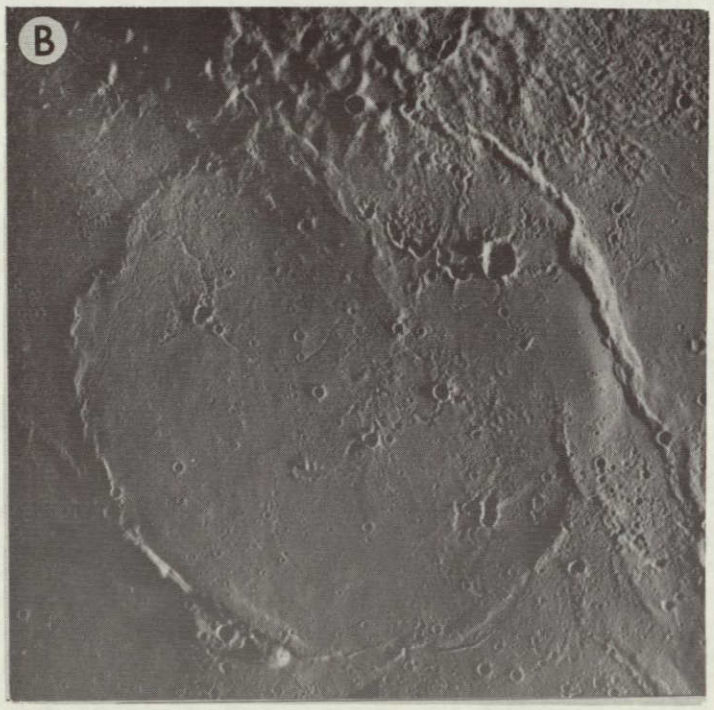

FIGURE 44

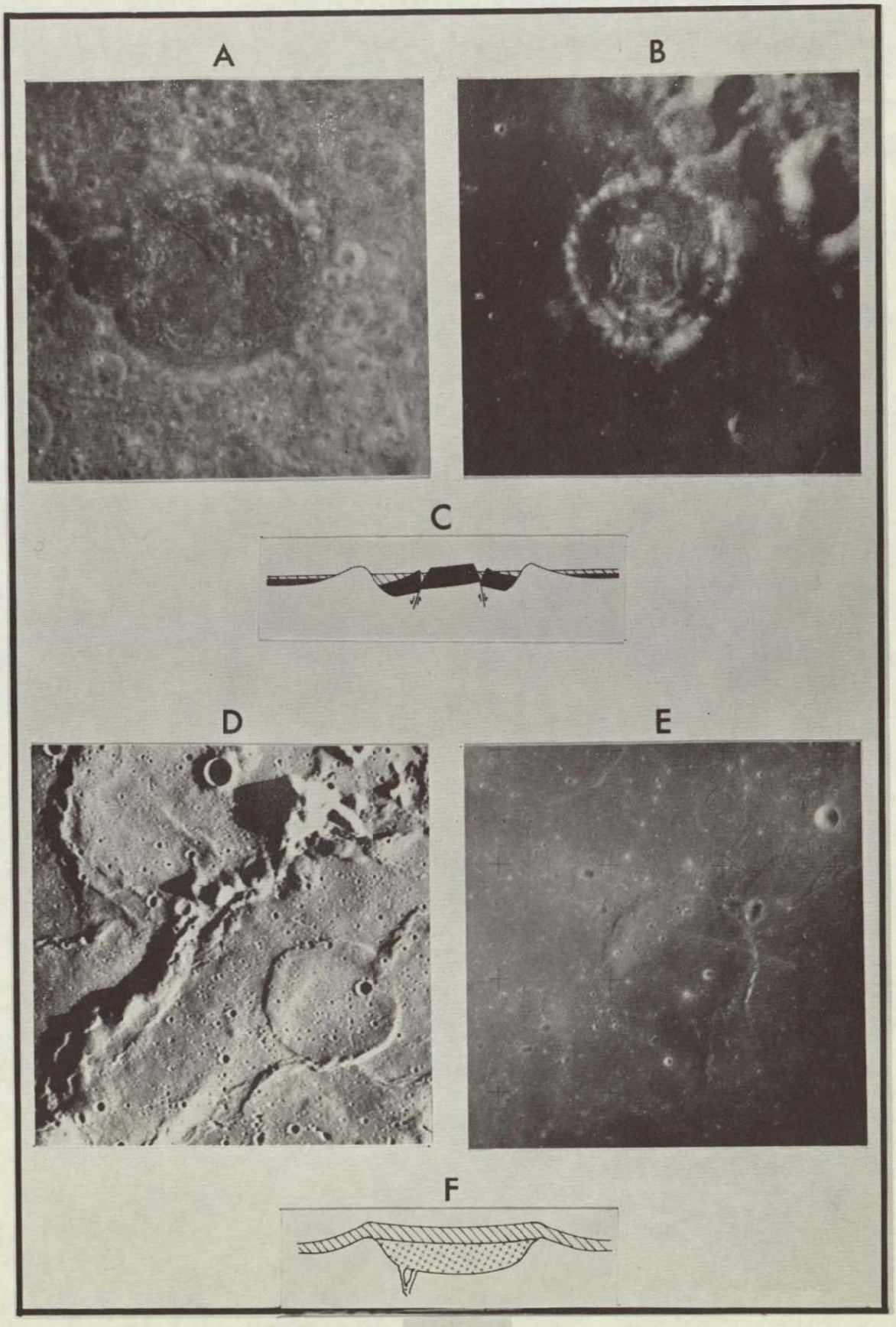

FIGURE 45

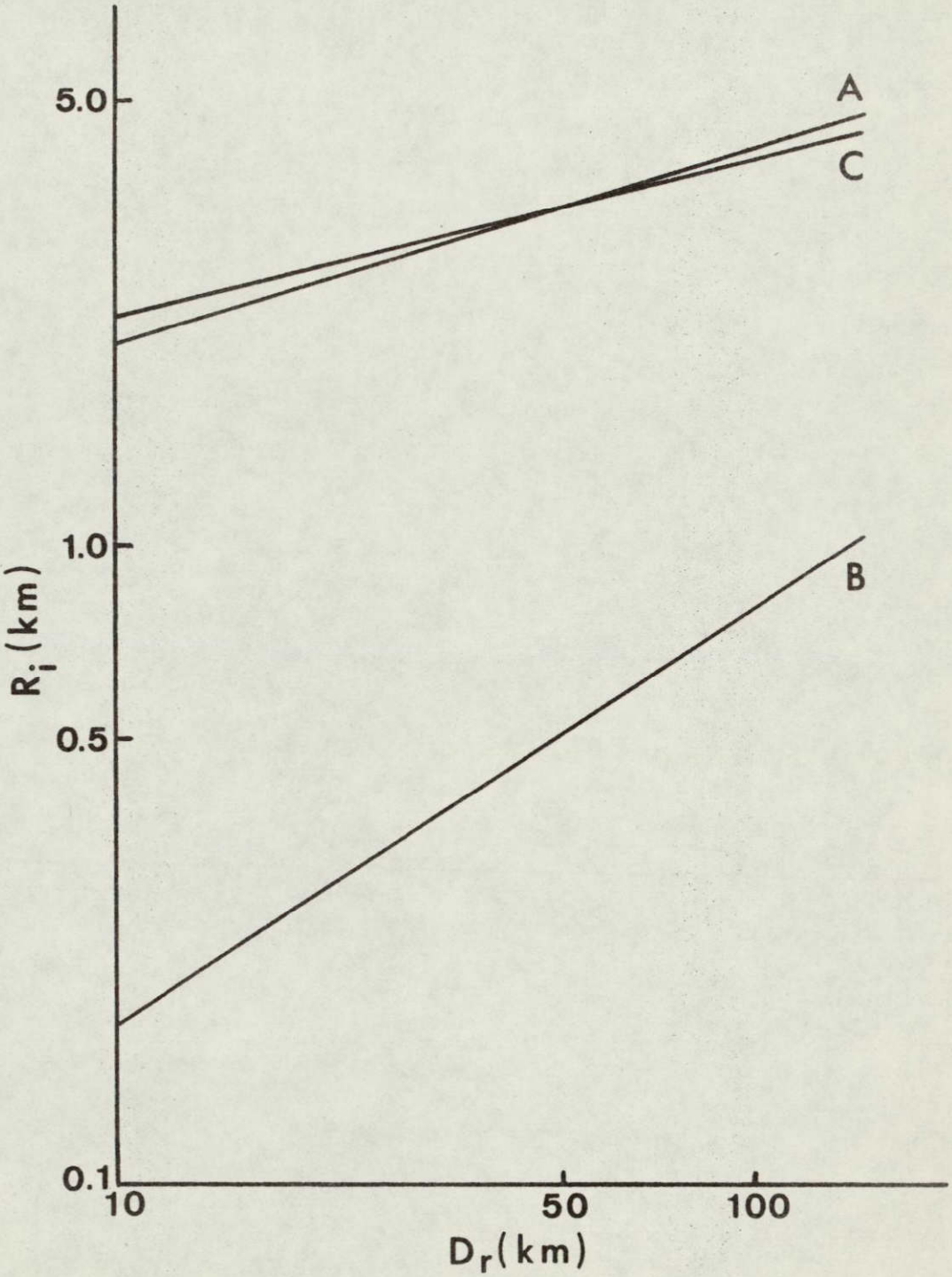

FIGURE 46

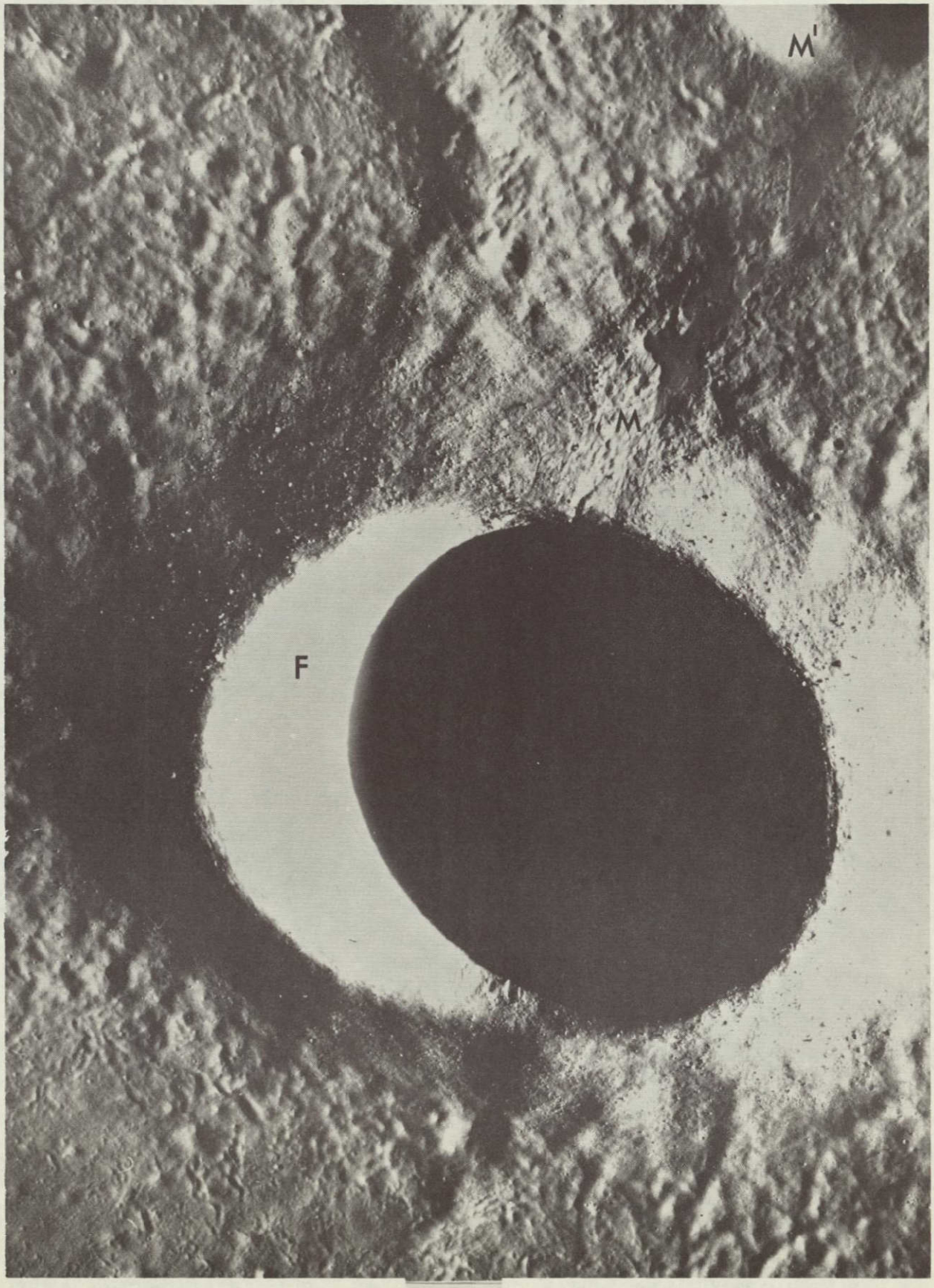

FIGURE 47

VII. MULTIPLE RING STRUCTURES AND THE PROBLEM OF CORRELATION BETWEEN LUNAR BASINS

A. Introduction

Multi-ringed basin structures on the lunar surface have been observed and described for many years (Gilbert, 1893; Baldwin, 1949; Baldwin, 1963). More recently, Hartmann and Kuiper (1962), Hartmann and Wood (1971), and Wilhelms and McCauley (1971), have attempted to define and tabulate recognizable rings for a large number of basins ranging in size from Mare Imbrium down to Antoniadi. In general, the outermost rings resemble fault scarps with steeper inner slopes and gentler outer slopes, while the innermost rings are commonly expressed as isolated peaks, mare ridges, or rilles (Hartmann and Wood, 1971). Similar multi-ringed basin structures have been observed on Mercury (Trask and Guest, 1975; Gault et al., 1975; Strom et al., 1975).

Several different theories of origin have been suggested. Some attribute ring formation to frozen tsunami-like waves (Baldwin, 1949, 1963, 1972; VanDorn, 1968,1969), others call on interference between shear and compressional waves (Johnson et al., 1964), or standing waves (Chadderton et al., 1969). In all of the preceding explanations the waves are envisioned to be generated by meteorite impact. Most other investigators have attributed the rings to faulting at the time of impact or during subsequent tectonism along fractures formed by impact (Hartmann and Kuiper, 1962; Mackin, 1969; Hartmann and Wood, 1971; Howard et al., 1974; Fielder, 1963; McCauley, 1968; Head, 1974b).

Study of ring structures inevitably has lead to comparisons between the ringed basins. Since Mare Orientale is the youngest, freshest basin, it has usually been used as the standard for comparison (Hartmann and Wood, 1971; Howard et al., 1974; Moore et al., 1974; Reed and Wolfe, 1975).

The purposes of this report are to identify concentric elements which can be unequivocally correlated between individual basins, determine if a simple relationship exists between the diameters of the concentric elements, and to make comparisons between the multi-ringed basins, including Mare Orientale.

B. Methods

Most circular mare basins that are relatively fresh, and not structurally complicated by multiple impacts, exhibit prominant rims with steep, scarp-like inner slopes. In basins where subsequent lava flooding has occurred, the lava surface extends up to the base of the prominent rim and contains a well developed concentric system of mare ridges. Mare Crisium (Figure 48) is a typical example.

In the younger basins rim crests and concentric ridge systems can be identified unambiguously and their diameters can be measured. In addition, the rim crests are usually the most prominent of the rings (Hartmann and Wood, 1971). For these reasons it is concluded that the two ring types are fundamental characteristics of typical flooded basins.

The multi-ringed basins described above have rim crest diameters that range from just over 100 kilometers (Letronne) to more than 1300 km (Mare Imbrium). Unfortunately, a relatively small number are amenable to metric analysis. Many other mare basins are known, but are complicated by overlap with adjacent basins (Mare Tranquillitatis, Mare Fecundatatis, Mare Nectaris, Mare Vaporum, Sinus Aestuum), great age (Mare Smythii), or incomplete lava flooding (Mare Orientale).

The examples chosen for this study include Letronne, Mare Imbrium, Mare Crisium and Mare Serenitatis, which are covered, at least in part, by Apollo generation photography and LTO maps, Mare Humorum and Mare Orientale. Values of rim crest diameter (D_b) and concentric ridge system diameter (D_{cr}) are tabulated below.

Basin	D_{cr}(km)	D_b(km)
Letronne	80	113
Mare Humorum	278	376
Mare Crisium	386	484
Mare Serenetatis	412	606
Mare Imbrium	626	1336

The Flamsteed Ring structure in the Oceanus Procellarum (Lunar Orbiter IV photograph 143 H) consists of a circular ring of terra-like peaks protruding above the mare surface and an inner concentric system of mare ridges. It resembles the other circular mare basins in most respects except that it has been nearly completely buried by mare lavas. This is apparently the result of its small size and location in the interior portion of Oceanus Procellarum. The values of D_b(123 km) and D_{cr}(93 km) are very close to those of Letronne; however, the Letronne values were used in this analysis because they were made on recently published LTO maps. The relationship between rim crest diameter and concentric ridge system diameter is:

$$D_{cr}=506.7 \log D_b-983.5 \qquad (1)$$

correlation coefficient = .989

The values of ring diameter listed above agree within ten percent of values published by Hartmann and Wood (1971) and Reed and Wolfe (1974). The single exception is the value of 606 km for D_b* for Mare Serenitatis. Reed and Wolfe (1975) conclude that the Taurus-Littrow massifs are part of the ejecta rim around the Serenitatis basin (a view that is not questioned here) and

that the Littrow Ring (750 km diameter) locates the position of the rim crest. The value of D_b reported here was measured on LTO maps from the center of the Serenitatis basin into the highlands along the margin. The adjacent highlands no longer exhibit the typical continuous rim crest with steeper inner slope and gentler outer slope, and appear to have been altered tectonically along much of the southern margin. This may be due to the close proximity of the Tranquillitatis and Imbrium basins. For these reasons the measurement is somewhat subjective and may be an underestimate of the original rim crest diameter; however, the diameter of the Littrow Ring, which lies a considerable distance into the highlands, may be an overestimate. In either case the relationship given by equation (1) would not be substantially changed (Figure 49).

C. Recognition and Spacing of Rings

Hartmann and Kuiper (1962) and Hartmann and Wood (1971) have reported that successive ring diameters for many basins exhibit a spacing in which their diameters differ by a factor equal to $\sqrt{2}$. They assign unit diameter to the most prominent ring in each basin and then determine ratios between diameters of the remaining rings. Howard et al. (1974, Figure 6) have reported similar measurements and conclude that the rings are spaced at intervals crudely approximating ratios of $\sqrt{2}$. In both reports, the morphology and origin of the various types of rings (peak rings, ridge systems, rim crests) are not considered. Equation 1 suggests that the $\sqrt{2}$ relationship does not hold for concentric ridge systems and basin rim crests.

The deviation from a $\sqrt{2}$ spacing ratio of basin rims and concentric ridges is most evident in Mare Imbrium. The rims and ridges in the other basins used in this analysis are not as conspicuously different. This suggests the alternatives that Mare Imbrium is either fundamentally different from the other ringed basins or that ring spacing for very large basins differs from that of smaller basins much like the differences in interior relief of large and small impact craters described by Pike (1974). The latter possibility cannot be verified or disproved on the Moon because of the small number of basins with rim diameters greater than 1000 km. It has been assumed in this analysis that Mare Imbrium is not fundamentally different from the other ringed basins.

Another aspect of ring identification and analysis that is unclear concerns the criteria used to locate individual rings. Both concentric and radial fabric are clearly evident within and around mare basins, but it is not always obvious why rings are located at specific radial distances from basin centers. One case in point is the second ring of Mare Imbrium given by Wilhelms and McCauley (1971). This ring lies approximately halfway between the rim crest and concentric ridge system and passes through material that is composed largely of ejecta around craters (Sinus Iridum, Plato, Aristillus, Archimedes) as well as

mare lavas. Wilhelms and McCauley do not locate rings in similar positions in Mare Crisium, Mare Humorum or Mare Serenitatis. This suggests the possibilities that the ring may be either a fundamental element of only the largest basins, or that it is merely located in an area where concentric fabric is recognizable. The latter seems the more realistic possibility in view of the origin of much of the material along the ring.

Another example is given by the second ring in Mare Serenitatis delineated by Reed and Wolfe (1974), who have modified the ring structure of Wilhelms and McCauley. They locate the second ring in the arc of the Montes Haemus but do not extend it to coincide with any other topographic features within the basin, a serious deficiency for a fundamental structural element. For this reason and because their estimate of the rim crest diameter (750 km diameter Littrow Ring) seems improbably large, the ring structure originally proposed by Wilhelms and McCauley seems to be more realistic.

Examination of the outermost rings proposed for the mare basins reveals additional inconsistancies. Wilhelms and McCauley (1971) identify only one ring outside of the rim crest of Mare Imbrium (Montes Appeninus), but identify two exterior to the rim of Mare Serenitatis and three exterior to the rim of Mare Crisium, despite the greater age of the latter two basins. Similarly, Hartmann and Wood (1971) identify two rings exterior to the rims of Mare Crisium and Mare Humorum and none exterior to the rim of the younger Mare Imbrium. Such inconsistancies suggest either that rings have no meaningful spacing and number or that the delineation of many rings may be the result of subjective choices. It seems many rings may have been located in areas of concentric fabric whose radial distances from basin centers are not in any way unique or consistent.

D. Mare Orientale

Mare Orientale (Figure 50) is the youngest (Stuart-Alexander and Howard, 1970) and freshest of the multi-ringed mare basins. Inevitably, when circular basins are discussed they are compared with the Orientale basin (Howard et al., 1974; Moore et al., 1974; Reed and Wolfe, 1975; Head, 1974b). Five rings have been delineated in the Orientale basin (Hartmann and Wood, 1971) but the outermost ring, 1300 km in diameter, is poorly defined--if it exists at all (Moore et al., 1974; Howard et al., 1974). This result is significant in that Wilhelms and McCauley (1971) have delineated five rings for Mare Crisium, and four rings each for both Mare Humorum and Mare Serenitatis in spite of their greater age. Lava flooding is incomplete by comparison with other mare basins, and, although some mare ridges are present in the interior, a system of concentric ridges has not developed.

Most who have studied Mare Orientale believe that either the outer Rook Ring (Figure 50, A) or the Cordillera Ring (Figure 50, B) is equivalent to the rims of the flooded mare basins

(Reed and Wolfe, 1975; Moore et al., 1974; Head, 1974b). In either case, using the relationship illustrated in Figure 49, it is possible to estimate the position where a concentric ridge system might have formed had lava flooding of Mare Orientale been as extensive as in other mare basins. The estimates are given below:

Basin Rim	D_{cr}(km)	D_b(km)
Outer Rook Ring	425	600
Cordillera Ring	515	900

In either case the predicted diameter for the crest of the concentric ridge system is smaller than that of the outer Rook Ring and does not coincide with the inner Rook Ring (diameter 480 km) of Hartmann and Wood (1971).

Figure 51 is a sketch map of the eastern two-thirds of the inner portion of the Orientale basin. The map shows fractures and ridges in the basin interior and was constructed from a mosaic of Orbiter IV photographs. For this reason the figure is somewhat distorted and the accompanying scale should be considered approximate. The fractures are widely, but not uniformly, distributed with a dominant concentric fabric and a secondary but clearly recognizable, radial component.

A comparison of Figures 50 and 51 reveals that most of the continuous portion of the lava fill lies within the concentric band of fractures with only isolated areas of lava located outside. The Lacus Veris and several other small areas of lava lie at the base of the outer Rook Ring (Figure 50, A) and extend along an arc of approximately 90 degrees from east to north. In a few restricted areas the lavas appear to fill lows in the outer Rook Ring and to extend completely across it. The possibility that erosion by flowing lava, which has been described elsewhere on the Moon (Cruickshank et al., 1973; Young et al., 1973b, Brennan, 1974), is responsible for the breaching of the outer Rook Ring is strongly suggested by the distribution of the lava. Several other small areas of lava, including the Lacus Autumni, are located at the base of the Cordillera (Figure 50,B) in the northeastern part of the basin. Neither area is continuous with the central lava filled portion, which indicates that lavas have been erupted from a number of widely separated source vents.

Howard et al. (1974) and Moore et al. (1975) have suggested that the lavas in the interior may be impact melted material. This interpretation is extended to include the knobby basin material between the Rook and Cordillera by Moore et al. In contrast, McCauley (1968) has suggested that the knobby basin material as fall-back material from a base surge column or material slumped from the Cordillera rim. The existence of mare ridges in the western interior part of the basin (Head,

1974b) indicates that multiple episodes of volcanism have occurred (see Section III of this report), and argues against production of lava in a single catatrophic event.

It is not immediately obvious from the distribution of fractures in Mare Orientale, where a concentric ridge system might have been most likely to form if complete flooding had occurred. Prominent concentric fractures are located over a wide range of radial distances from the basin center, and all appear to be likely conduits for fissure volcanism. It may very well be that basin impacts produce a homogeneous system of fractures in concentric and radial pattern (Hartmann and Wood, 1971) which are selectively activated by subsequent tectonism. This leads directly to the suggestion that basin floor topography may ultimately control the locations of the fractures activated, and therefore, also the location of the concentric mare ridge systems. Presumably the lowest areas would be flooded, and thereby acquire supracrustal loads, earliest. This would possibly result in down faulting of the basin centers, a phenomenon which has apparently occurred in Mare Crisium, Mare Serenitatis and Mare Imbrium. Topographic profiles E through H on Figure 26 (Section III of this report) illustrate that the central portion of Mare Crisium is lower than the marginal areas and that the change occurs abruptly on the inner slopes of the concentric ridges.

The present distribution of lava suggests that continued volcanism would have flooded the entire area within the Cordillera. Since the outer Rook Ring shows evidence of already having been partially breached by lavas, the implication is that a more extensive episode of volcanism might have substantially destroyed larger portions if not most of it by lava erosion and foundering. In addition the knobby basin material which lies outside the Rook does not resemble the ejecta outside the rim of Mare Crisium as described by Wilhelms (1973) or the radial pattern on the outer slopes of the Montes Appenninus as reported by Mutch (1970). For these reasons it is tentatively concluded that the Cordillera rather than the outer Rook Ring is the rim of the Orientale basin (Moore et al., 1974; Head, 1974b) and that the most probable location for development of a concentric ridge system, given complete lava flooding, is along a circular arc of just over 500 km diameter and positioned inside the base of the Rook Mountains.

Since some disagreement exists as to whether the outer Rook Ring or Cordillera is equivalent to the rims of the other mare basins, it is necessary to consider the implications for interbasin ring correlations for both interpretations. If the outer Rook Ring is the rim of Mare Orientale, then there is only one other clearly identifiable ring outside, the Cordillera. This implies that the rings outside of basin rims which Wilhelms and McCauley (1971) have proposed for Mare Humorum (2), Mare Crisium (3), and Mare Serenitatis (2), are more numerous than those identifiable at Orientale. If the Cordillera is the true rim of

the Orientale basin, then, since there are no other clearly identifiable rings outside, none of the outer rings described around the Crisium, Humorum and Serenitatis basins can be correlated with those around Mare Orientale. In either case it is clear that a simple one to one correspondence of the outermost rings between Mare Orientale and several other basins does not exist.

It is possible that the outermost rings formed around the basins are easily destroyed by subsequent meteorite bombardment or endogenic processes, and that their preservation may depend on a fortuitous combination of circumstances. However, this explanation seems inadequate in view of the fact that the two youngest basins, Imbrium and Orientale, have the fewest rings outside their rims. It seems more likely that the delineation of the outermost rings has been a rather subjective process, and that many rings may simply have been located in areas where a concentric fabric is recognizable. A third possibility that must be considered is that a homogeneous system of concentric and radial fractures produced by impact may extend well beyong the basin rims and may be subsequently activated by tectonism. Therefore many outer rings may reflect impact induced anisotropy in the lunar crust, and their locations are then determined by endogenic processes. All three possible explanations imply that the correlation of rings, and particularly the outermost rings, between mare basins may be difficult at best, and that caution is necessary.

E. Conclusions

The results of this analysis suggest that:

1. The $\sqrt{2}$ spacing relationship does not correctly describe the spacing of concentric ridge systems and rim crests in multi-ringed lunar basins.

2. Delineation and correlation of the outermost rings around multi-ringed lunar basins is questionable.

3. It is concluded that the Cordillera is the rim of the Orientale basin (not the transient crater produced at the time of impact) and is therefore equivalent to the Montes Appeninus around Mare Imbrium, the second basin rings of Mare Crisium, Mare Serenitatis and Mare Humorum, as defined by Wilhelms and McCauley (1971), the rim of Letronne, and the ring of terra-like summits of the Flamsteed ring.

VIII. EVOLUTION OF MARE SMYTHII

A. Introduction

Mare Smythii is one of the oldest of the lunar mare basins. Stuart-Alexander and Howard (1970), as a result of a comparative study of mare basins, place it in their oldest category (Class 1). Although Mare Smythii is similar in many respects to other mare basins, it also exhibits a number of distinctive characteristics. The contact between the mare surface and adjacent highlands is generally quite irregular and is probably the result of the great age of the basin (Brennan, 1975a). In contrast to most other maria, Mare Smythii does not have a system of concentric mare ridges in its interior. Partly for this reason, it does not exhibit the multi-ringed character of most other similar basins. Hartmann and Wood (1971) list only one ring, the rim, which can be identified with certainty. The mare surface varies from smooth and planar, much like the surfaces of other maria, to gently rolling and hummocky. The interior of Mare Smythii contains a large number of craters which show evidence of volcanic and tectonic modification (Brennan, 1975b). In contrast to the other mare basins, modified craters in Mare Smythii are anomalously abundant and are not restricted to the marginal portions of the mare surface.

The purposes of this study are to identify the major structural and stratigraphic units of Mare Smythii, determine its history, and to relate its evolution to the other circular maria.

B. Physiography

The irregular surfaces of Mare Smythii and the adjacent highlands reflect the intense cratering which occurred between the formation and filling of the basin. In order to characterize the shape of the basin and remove the topographic effects of individual large craters, elevations were averaged over 1° by 1° spherical rectangles on 1/250,000 scale Lunar Topographic Orthophotomaps with a contour interval of 100 m. The resultant averaged elevations were then contoured. Figure 52 is a topographic map of those "smoothed" elevations.

The western portion of the Smythii basin is nearly circular, but the eastern half has a polygonal configuration. This is due to the existence of several large impact craters in the southeastern (Hirayama) and northeastern (Babcock and Mcadie) parts. The surface of Mare Smythii is asymmetrical, with the lowest areas displaced to the northeast of the geometrical center of the basin.

The southwestern third of the surface is 100-200 m higher than the average elevation of approximately 3800 m.

C. Stratigraphy

Three major stratigraphic units can be recognized in Mare Smythii (Figure 53). Smooth, planar mare material occupies a large continuous area in the northeastern portion and several smaller areas, including the interiors of several large craters in the western, central, and eastern portions of the basin. This material has low albedo and resembles the basaltic lava surfaces found in the other maria. Mare ridge structures occur only in areas of smooth, planar mare material.

Most of the rest of the surface is composed of hummocky and undulatory mare material, which has a higher albedo than the planar material. The darker planar material fills embayments in the hummocky and undulatory surface, contains far fewer large craters, and appears to be noticeably less battered. All of these relationships suggest a younger age for the planar material. The surface of the undulatory and hummocky material is heterogeneous in that it resembles the low relief "planar and undulatory terra" and "rounded terra hills" observed in some parts of the highlands (Wilhelms, 1973) as well as the plains material described by Oberbeck et al. (1974). This material was emplaced during the interval between basin formation and the volcanism which formed the smooth planar areas, and probably originated as ejecta from the many large craters and secondaries which impacted in and near the Smythii basin prior to the onset of volcanism. Because of the small scale of Figure 53, crater rim, slope and floor materials and some small terra hills within Mare Smythii have not been delineated.

Several craters in southern Mare Smythii contain large exposures of a very low albedo material that strongly resembles the dark mantle observed at the Apollo 17 landing site (Heiken and McKay, 1974). Its surface varies from smooth to irregular and it appears, locally, to mantle parts of the hummocky and undulatory surface. The crater Swasey contains an elongate deposit of this material along a fracture. In Swasey the dark mantle exhibits the form of a pyroclastic deposit in that it comprises steep slopes which extend away from both sides of the central fracture. Most of the floors of the other flooded and modified craters in the hummocky and undulatory surface contain similar, smaller exposures of this material.

Since both the dark mantle and the lava flows in northeastern Mare Smythii are fresh looking and both are younger than the hummocky portion of the surface it seems likely that they were formed during the same general episode of volcanism. In the crater Kao the dark material mantles a smooth surface much like the interior portion of the flooded craters elsewhere in the basin. Crater density measurements made on this area (see

Section I of this report) indicate that its age is nearly the same as the mare surface at the Apollo 15 landing site in Mare Imbrium. The Apollo 15 Site is of the same age as many other areas in the lunar maria (Boyce and Dial, 1975). For this reason it is probable that the dark mantle material and associated lava flows which may locally underlie it are of Imbrian age. The most probable reason that the volcanism resulted in widespread lavas in the northeastern portion of the basin and scattered occurrences of pyroclastic material (and possibly lava) in the southwestern area is that the magma rose hydrostatically (Solomon, 1975) and its areal distribution was influenced by the topography of the surface above.

Many of the abundant craters with modified floors (Doyle, Camoëns, Kiess, Widmanstätten, Kao) and battered rims (Brennan, 1975b), which are superimposed on the undulatory and hummocky surface contain lava and/or dark mantle on their floors. These superposition relationships support the relative ages described above.

D. Surface Composition

The X-ray fluorescence spectrometer carried by Apollos 15 and 16 recorded measurements along ten ground tracks across Mare Smythii (Adler et al., 1973). In general, high Al/Si ratios measured in the highland areas are similar to those from anorthositic rocks collected on the Apollo 11, 12, and 15 missions, and the low Al/Si and high Mg/Si ratios measured across the maria are similar to those of basaltic rocks collected at the mare landing sites (Adler et al., 1973).

It is important to note that the X-ray fluorescence experiment is a measurement of surface composition and provides no information on subsurface composition below depths of approximately 0.1 mm (Adler et al., 1972). Another limitation inherent in the X-ray fluorescence measurements is the resolution. The field of view of the instrument is 60° (Adler et al., 1972) which indicates that at orbital altitudes radiation from an area of approximately 100 km by 100 km would be measured. Adler et al. (1974) point out that approximately 68 percent of the total radiation comes from an area 70 km by 70 km. Thus it is unlikely that resolution of individual areas less than approximately 100 km diameter is possible. Adler et al. (1974) have delineated several anomalous areas in Mare Tranquillitatis by separating residuals from trend surfaces. In most cases the anomalous areas have dimensions that range from 70 km to well over 100 km.

Stewart et al. (1975) have contoured Al/Si ratio data (Figure 3) and Mg/Si ratio data (Figure 4) obtained from the Smythii basin by Adler et al. (1973). Both of their figures, when compared to Figure 52 of this report, are seen to exhibit areal trends for averaged composition ratios similar to those of the averaged topographic elevations. These rather striking

similarities suggest that a direct relationship exists between the origin, composition, distribution, and structural history of the basin filling materials.

The low values of the Al/Si ratio and high values of the Mg/Si ratio which were measured across the northern portion of Mare Smythii (Adler et al., 1973) support the conclusion, based on photogeologic evidence, that the planar mare material there is basaltic lava. The values of both ratios measured in the southwestern hummocky portion of the basin are intermediate between the observed values for highland (anorthositic) and mare (basaltic) areas, and indicate an intermediate surface composition for these materials. Although the hummocky material has been derived primarily from the adjacent highlands by impact, it is mantled in a large number of small areas by both mare lava and dark mantle, many of which are too small to be delineated on Figure 53 (especially the dark mantle areas). Thus the composition of the surface is seen to be a weighted average of the various lithologies which occur on the surface rather than a measure of the composition of the debris that comprises most of the volume of the fill. It is assumed that the dark mantle material has the same basaltic composition as the mare lavas (Heiken and McKay, 1974).

E. Smythii Mascon

Figure 54 was reproduced in part and slightly modified from data published by Sjogren et al. (1974a, Figure 4). It represents the fit of mass point values to Doppler residual gravity data. Mass units are 10^{-6} times the mass of the Moon. The mascon indicated by Figure 54 is displaced to the northeast from the center of the basin and appears to be centered on the largest area of planar mare material. This indicates that a substantial density contrast exists between the planar and hummocky mare material with the former being more dense. Like the X-ray fluorescence data, the gravity data exhibits trends that are present in the smoothed topography illustrated in Figure 52.

The mass distribution reproduced in Figure 54 suggests that the lavas which occur in the area of planar mare in western Mare Smythii (centered at 1°S 83°E) as well as in the northeastern portion of the basin, are relatively thick whereas those in the flooded craters in the southern part are relatively thin. Gravity data published by Sjogren (1974b, Plate 1) indicate that the gravity anomaly associated with Mare Smythii is smaller than that observed in Mare Crisium, a more completely flooded basin of similar size. This suggests that the average density of the fill in Mare Smythii is lower than that of Mare Crisium (assuming that the densities of basin floor and rim material are the same for both), an observation that is compatible with the origins of basin fill proposed in this report.

Stewart et al. (1975b, Figure 6) have used buried craters to estimate thickness of basin fill in Mare Smythii. Since many of

the craters which they used were formed during a period of high impact flux and may have been subjected to significant erosion of the rims, they conclude that the thickness estimates are minimum values. Evidence considered in this report (Brennan, 1975b) suggests that many of the craters used by Stewart et al. (1975b) have formed over the considerable interval of time between basin formation and the onset of volcanism and tectonism which has modified several of the craters. Thus the increment of fill which has accumulated since the formation of individual craters is unknown. In addition the effects of crater modification on rim height are not completely known. This is particularly true of the estimates for the southern and southwestern portions of the basin where modified craters are most abundant. As a result the thickness estimates may be unrealistically low.

Stewart et al. (1975a) explain the high elevation and thin fill of southwestern Mare Smythii by upwarping of that portion of the basin floor. The upwarping presumably took place prior to the onset of mare volcanism and thus explains the absence of mare lavas in that area. They do not explain the causes of the tectonism which resulted in upwarping. In most circular basins, tectonism activitates basin fractures and produces a multi-ringed configuration (see Section VII of this report) which is not observed in southwestern Mare Smythii. Several of the large modified craters in Mare Smythii including Haldane (2°S 84°E), Kiess, and Widmanstätten (7°S 85°E) exhibit similar concentric fractures, both within and outside of their rims (Figure 53), which have been activated during tectonism. It is not clear how a large scale uplift could have occurred in the Smythii basin without being strongly influenced by the impact-produced anisotropy in the basin floor. For these reasons it is concluded that the thickness estimates of Stewart et al. (1975b) are both unrealistically low and are not supported by other independent evidence. The gravity differences between the northeastern and southwestern areas are attributed to differences in the average density of the fill in both areas, rather than substantial differences in the thickness of the fill.

Lava thickness in northeastern Mare Smythii has been estimated from the crater Pirandello at 450-475 m (Stewart et al., 1975b). Unfortuantely, Pirandello is located at the Summit of the mare ridge system and is unlikely to have persisted through the entire interval of volcanism, including ridge formation, thus this thickness estimate is almost certainly a rather conservative lower bound.

F. Basin Structure

Typical interior basin structure is well developed in only the large areas of dark planar mare in the Smythii basin where crudely concentric and radial ridge segments have developed. The absence of similar radial and concentric structural elements elsewhere in the basin suggests that by Imbrian time much of the basin interior was in isostatic equilibrium so that tectonism

strongly affected only those areas that were not at equilibrium. The areas affected include the large impact craters that exhibit extensive modification (Brennan, 1975b) as well as the large areas of planar mare.

Since all fresh craters and impact basins have surface configurations that are gravitationally unstable (Brennan, 1975b) it is evident that the surface configuration of parts of Mare Smythii were substantially altered prior to Imbrian volcanism and tectonism. It appears that these changes were the result of the emplacement of a thick fill of debris from impacts adjacent to the basin, particularly near the southwestern portion. The ejecta would presumably have had a similar density to the material that comprises the adjacent highlands from which it was derived, and would therefore have simply filled in parts of the Smythii basin without resulting in the development of a supracrustal load due to the high density mass excess normally produced by lavas.

The ejecta fill in the Smythii basin was apparently not completely uniform in thickness. The irregularities of the eastern part of the basin rim suggest that the distribution of the ejecta fill was probably nonuniform and was influenced by a small number of medium sized (Hirayama and smaller) impacts within the basin and in close proximity to the basin rim. The present topography of the entire mare surface suggests that the relief on the surface of the ejecta fill might have been at least 1 km. Subsequently, impacts formed craters such as Haldane, Widmanstätten, Milton, and others which resulted in additional localized areas of isostatic imbalance to which later tectonism was restricted. Because the filling of northeastern Mare Smythii with ejecta was not as complete as elsewhere, the resulting surface elevations were low enough for extensive lava flooding to occur. Mare ridges developed there much as they have elsewhere in the flooded portions of the circular maria.

G. Evolution of Mare Smythii

The evolution of Mare Smythii began with the formation of the basin by a large impact event followed by a long interval of intense meteorite bombardment which caused the irregularities in its rim and formed the many large craters adjacent to it. Much of the ejecta from these subsequent impacts was emplaced in the basin to partially fill it with material whose density is lower than that of basaltic lava and comparable to that of the basin rim and floor. The surface of the fill resembles that of plains material as well as planar and undulatory terra found elsewhere on the Moon.

Volcanism in the basin resulted in the filling of only the lowest areas with successive lava flows and the simultaneous formation of mare ridges. In the southern portion of the basin, volcanism occurred in the form of thin lava flows and discontinuous blankets of pyroclastic material. Mobilization of the crust during volcanism caused the modification of large impact craters within the older ejecta fill in the southwestern part

of the basin (see Section VII).

The evolution of Mare Smythii has resulted from the same processes which have affected the other circular maria. The differences between it and the other circular maria can be readily accounted for by its great age and the intense meteorite flux between the formation of the basin and the onset of Moon-wide volcanism that resulted in the flooding of the maria.

Captions: Figures 48-54

Figure 48. Geologic sketch map of Mare Crisium showing only major structural elements and stratigraphic units. Unshaded area consists of planar mare material that is interpreted to be basaltic lava; cross-hatched area is composed of dark mantle. Solid lines with double barbs represent ridge crests. Solid lines with single barbs represent escarpments along which the barb points down slope. Solid lines without barbs represent other lineaments on the mare surface.

Figure 49. Relationship between diameter of concentric ridge crests (D_{cr}) and basin rim diameter (D_b) for multi-ringed basins: Mare Imbrium (I), Mare Serenitatis (S), Mare Crisium (C), Mare Humorum (H), and Letronne (L).

Figure 50. Photograph of Mare Orientale showing the crests of the outer Rook (A) and Cordillera (B) rings. Lunar Orbiter IV photograph M 187.

Figure 51. Sketch map of the eastern two-thirds of the interior of the Orientale basin. Solid lines are prominent fractures in the basin floor. Solid lines with double barbs represent ridge crests.

Figure 52. Smoothed topographic map of Mare Smythii. Elevation contours are in meters and are based on mean elevations of 1° by 1° spherical rectangles.

Figure 53. Geologic sketch map of Mare Smythii showing only major structural elements and stratigraphic units. Lined area consists of planar mare material that is interpreted to be basaltic lava; unlined area consists of undulatory and hummocky mare material; cross-hatched area is composed of dark mantle. Solid lines with double barbs represent ridge crests. Solid lines with single barbs represent escarpments along which the barb points down slope. Solid lines without barbs represent fractures. Crests of crater rims and rim remnants are represented by circular arcs.

Figure 54. Surface mass point distribution for Mare Smythii and surrounding area. Mass units are 10-6 times the mass of the Moon. Reproduced from Sjogren, et al. (1974, Figure 4).

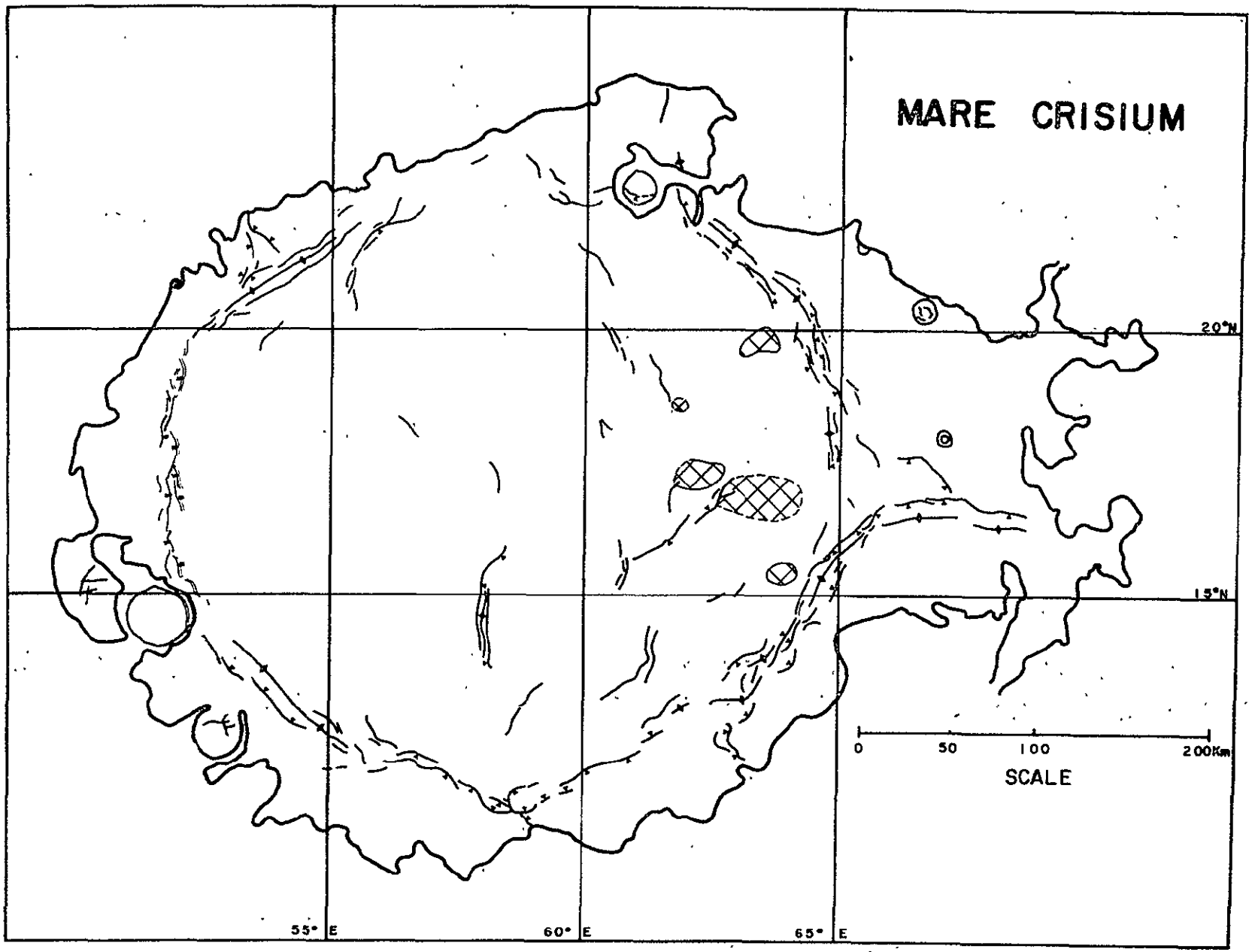

FIGURE 48

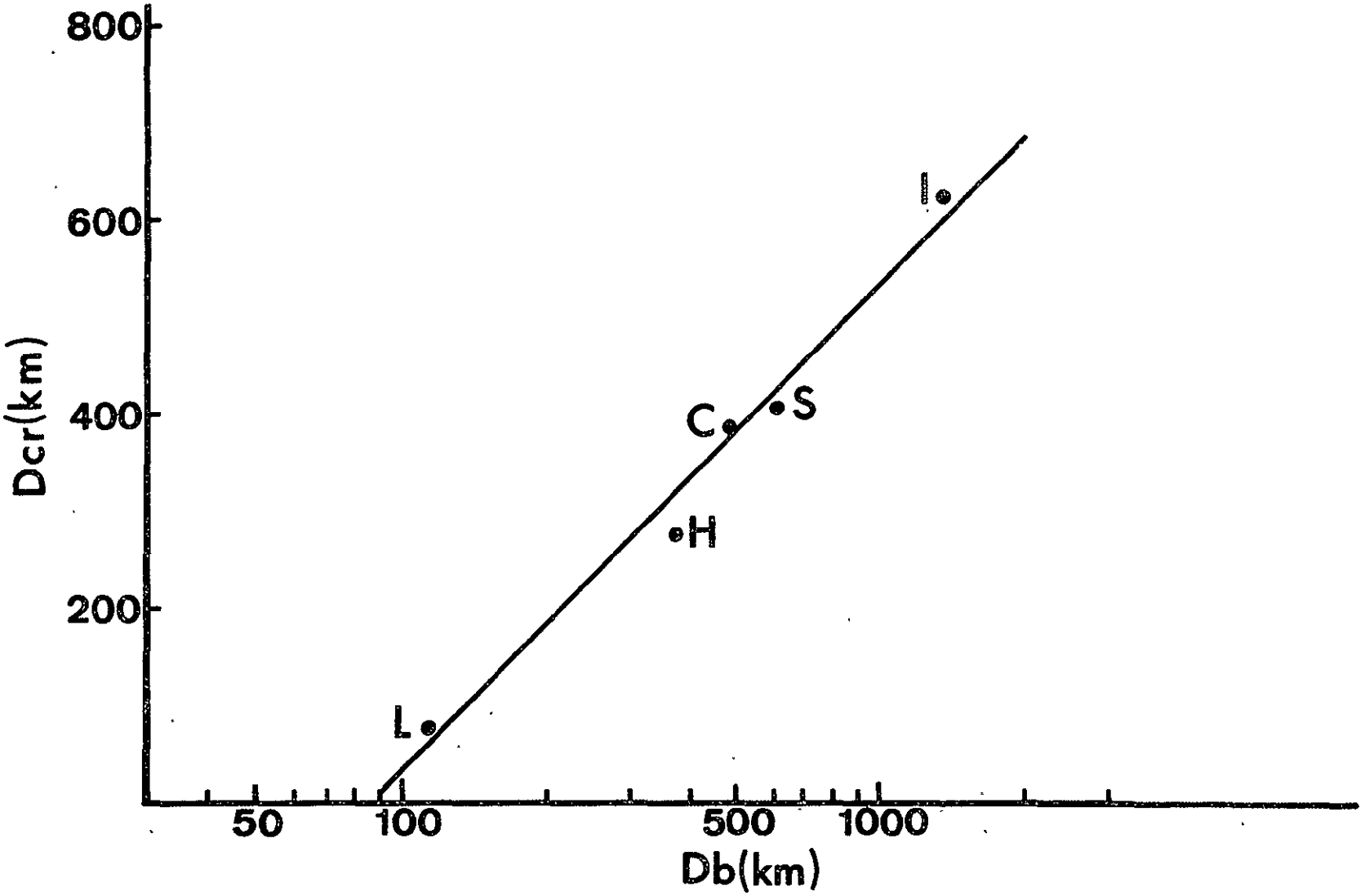

FIGURE 49

FIGURE 50

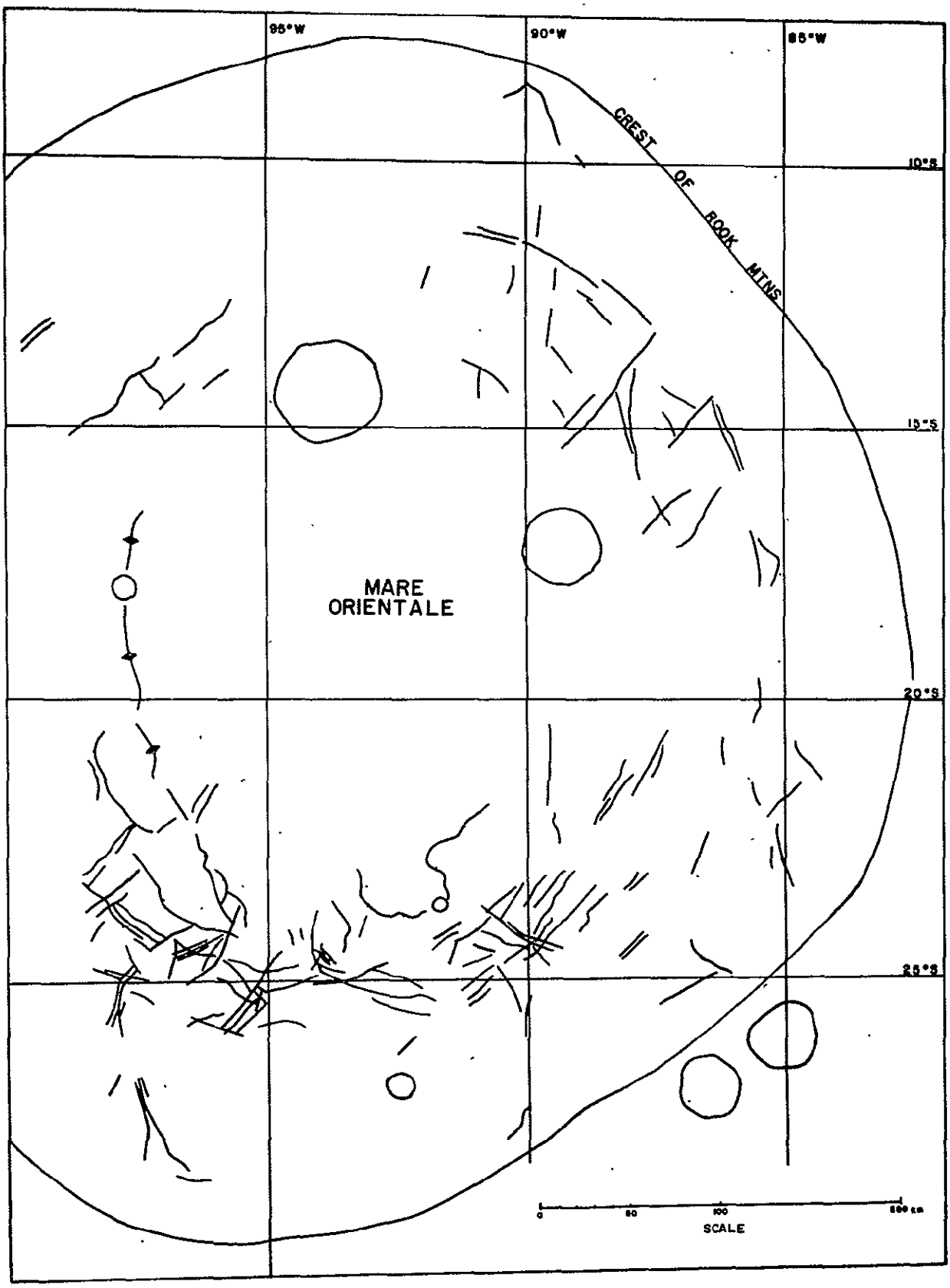
95°W
90°W
85°W
CREST OF BOOK MTNS.
10°S
15°S
MARE
ORIENTALE
20°S
25°S
0
50
100
SCALE

FIGURE 51

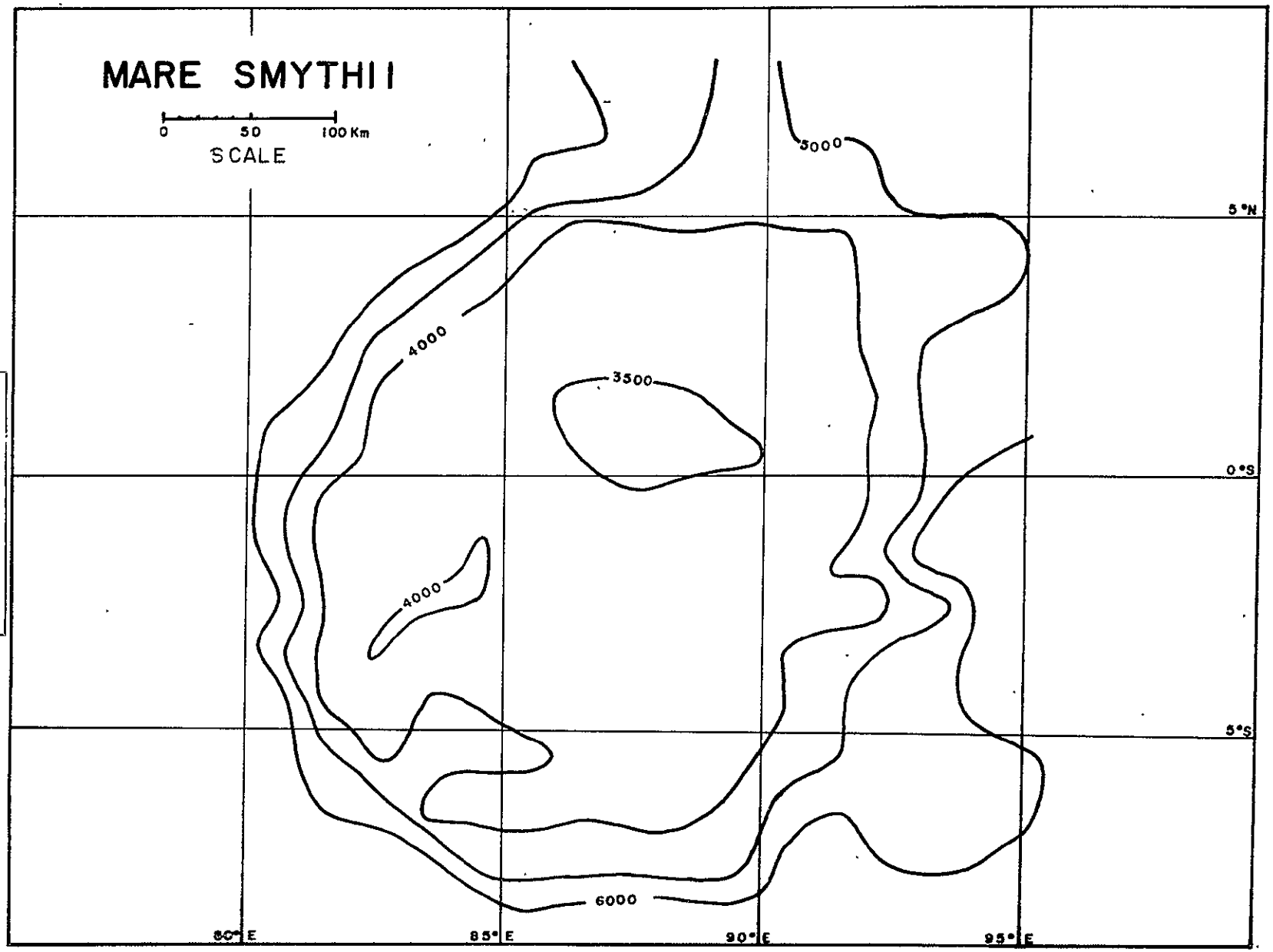
MARE SMYTHII
0
50
100 Km
SCALE
5000
4000
3500
4000
6000
5°N
0°S
5°S
80° E
85° E
90° E
95° E

FIGURE 52

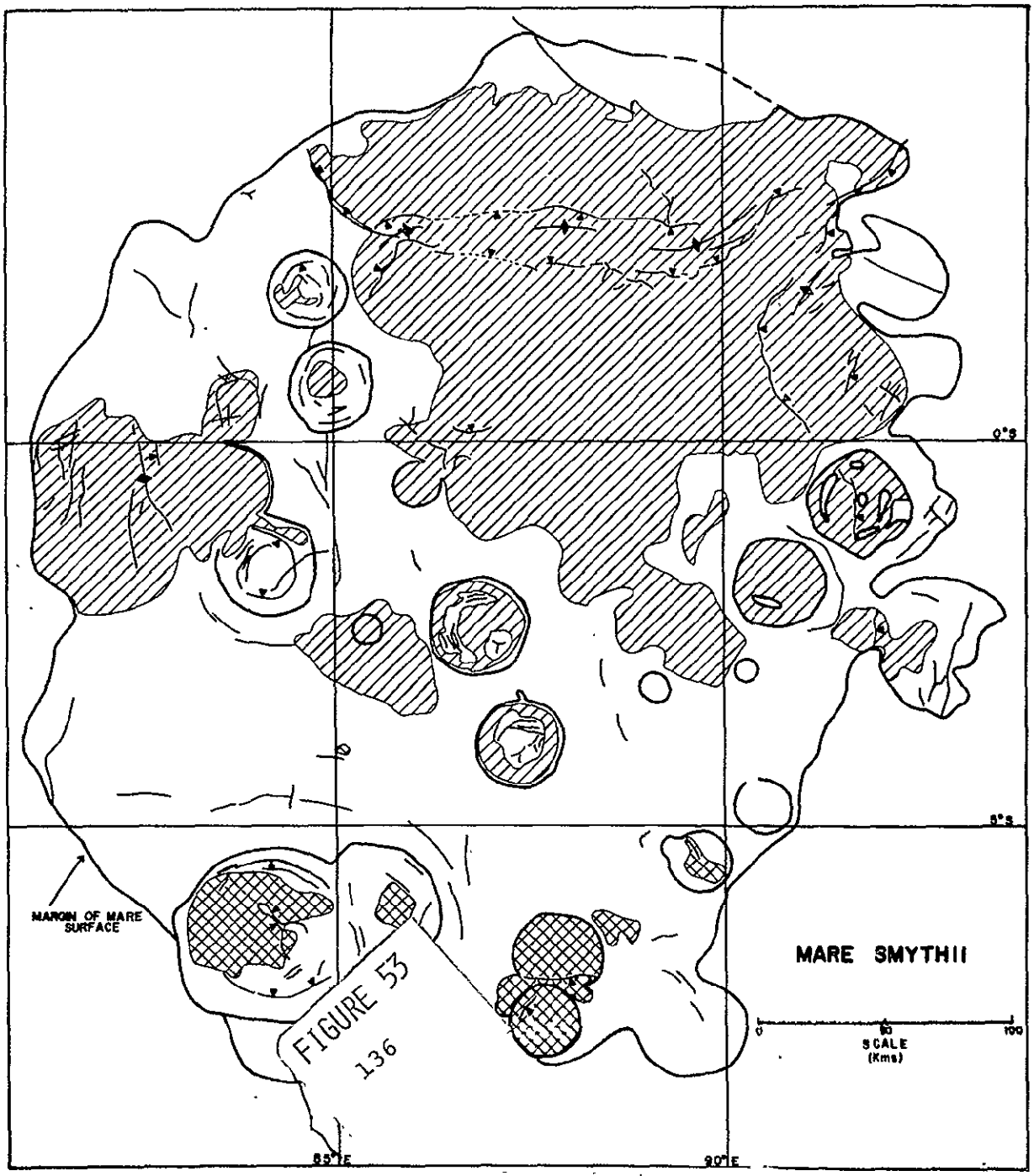
0°S
5°S
MARGIN OF MARE SURFACE
MARE SMYTHII
0
50
100
SCALE (Kms)
FIGURE 53
136
85°E
90°E

FIGURE 52

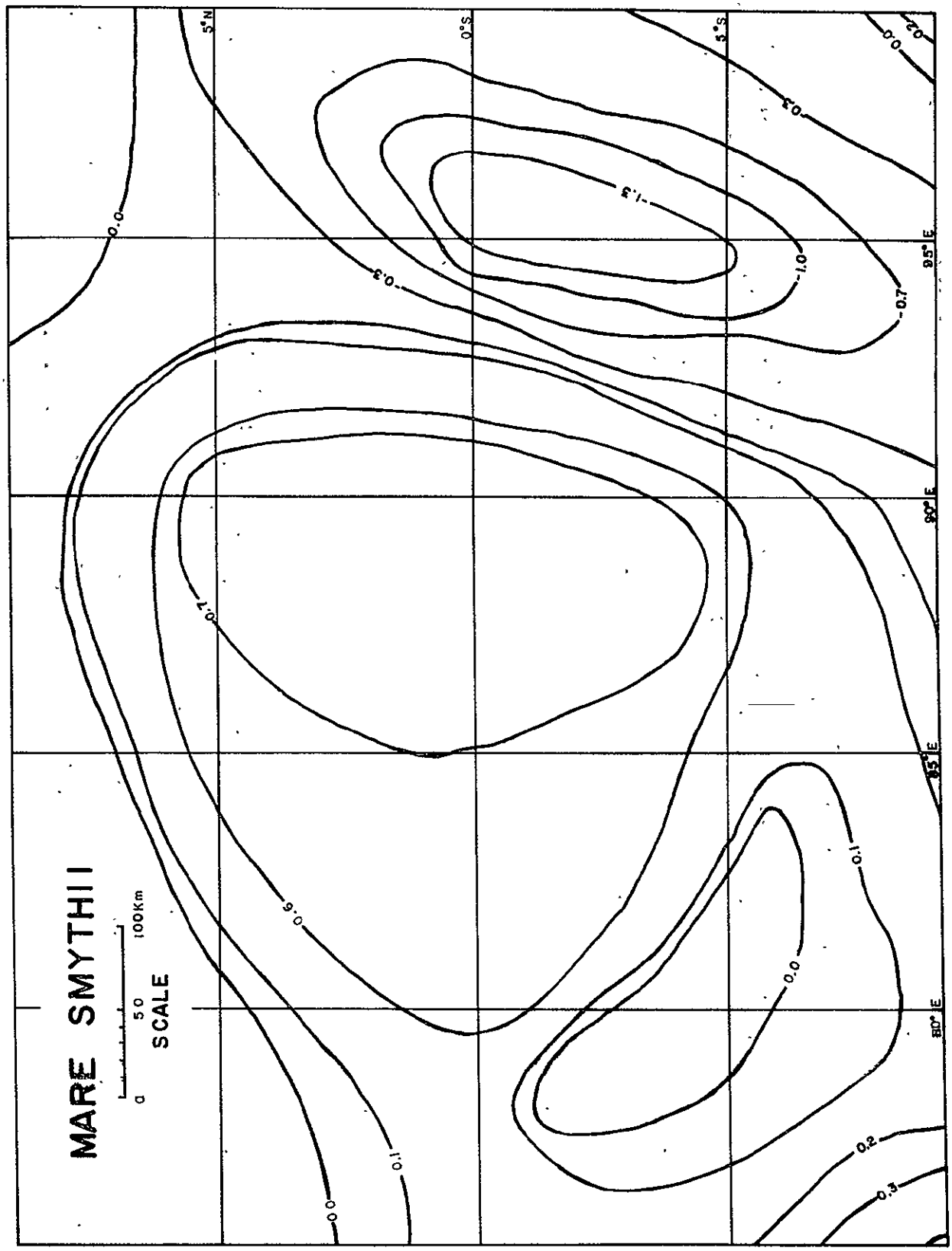
MARE SMYTHII
SCALE
0
50
100Km
5°N
0°S
5°S
95° E
90° E
85° E
80° E
0.0
0.3
1.3
1.0
0.7
0.6
0.1
0.2

FIGURE 54

GENERAL CONCLUSIONS AND RECOMMENDATIONS

The geology of the lunar maria has undoubtedly been strongly controlled by the early tectonic history of individual mare basins. The evolution of specific features within the maria depends largely upon their spacial relationships to basin ring structures and related fracture systems. The relief and detail now preserved on many mare rilles, ridges, modified craters and faults is dependent both upon their positions with respect to the major sources of volcanic activity as well as the depths to which different parts of individual basins were filled with volcanics. It is probably correct to assume that the portions of the individual maria which now preserve the greatest diversity of volcanic and structural features are the regions which underwent volcanism and tectonism for the longest time because of their coincidental (favorable) position with regard to the structural fabric of the region as a whole and their relation to subsurface magma sources.

The second most important factor influencing the degree to which details of the surface geology in individual basins can be understood is the thickness of the regolith covering the surface, which is directly related to the age (cumulative meteorite flux) of each region. Equilibrium cratering is capable of destroying all surface details having dimensions of tens of meters in the older maria. However, the effects of equilibrium cratering (regolith thickening) change with increasing age so as to produce surfaces on which progressively fewer small craters (<200 m) are preserved. In the diameter range below 500 m it is necessary to carefully determine the relative proportions of different size craters over an interval (100-500 m) in order to fully examine the potential influence of several factors on apparent surface age. Although rapid techniques for relative surface age determinations are very useful, it appears equally important to interpret other related aspects of surface and subsurface geology by means of complete analysis of crater size-frequency distributions.

Because impact erosion and impact gardening processes distribute energy relatively uniformly over equal cross sectional areas of the moon, our understanding of mixing and transport (erosion) conditions on the lunar slopes must be modified from ingrained concepts we might subconsciously apply from experience with terrestrial geology. Because postmare lunar slope erosion has apparently been relatively slow, some quantitative estimates can be made, using appropriate models, concerning relative or comparative slope ages to compliment crater frequency distributionages on mare surfaces. This kind of slope erosion analysis might be applied to the analysis of relative ages of some of the younger highland craters or scarps which up to the present have only been compared as to gross similarities.

To obtain further detailed and meaningful information concerning these specifics of lunar geology it will be necessary to combine detailed topographic mapping (1:50,000 and 1:10,000)

with remote sensing data (such as infrared reflectance spectroscopy) and detailed crater size-frequency analyses. This will produce some further understanding of the surface and shallow subsurface structure of the maria and the highlands.

A more quantitative understanding of lunar equilibrium cratering and slope erosion may allow a more complete analysis of apparent meteorite flux variations with time and could be applied to remote sensing studies of some other planets.

Careful delineation of crater frequency distributions in key mare regions could allow more quantitative comparisons of time stratigraphic horizons and better regional correlations between mare basins, as well as information on any relative variations in the meteorite flux with time.

Detailed low sun elevation (10-35°) photography of a greater portion of the younger lunar maria would be very useful for continuing such studies. Some of the most detailed surface geology can be seen in the Oceanus Procellarum Area which was very incompletely covered by Apollo missions.

Appendix I - Crater Size Frequency Data

Area 1 5° (104 m/mm, 18.72 m)*		Area 2 4° (104 m/mm, 18.72 m)		Area 3 5° (104 m/mm, 18.72 m)	
m	craters	m	craters	m	craters
109	340	109	341	109	554
128	251	128	308	128	404
147	162	147	235	147	236
165	110	165	190	165	168
184	70	184	113	184	85
203	48	203	86	203	42
222	37	222	66	222	41
240	26	240	53	240	35
259	20	259	37	259	21
278	15	278	22	278	14
296	10	296	15	296	9
315	8.0	315	15	315	7
334	6.5	334	8.5	334	8
353	6.0	353	12	353	3
371	7.0	371	7.0	371	2
390	4.5	390	7.0	390	4
409	4.0	409	4.5	409	5
427	2.0	427	8.0	427	2
446	4.0	446	3.5	446	2
465	1.5	465	1.5	465	2
484	1.5	484	2.0	484	2
502	2.0	502	3.0	502	2
521	2.0	521	2.5	521	2
540	1.5	540	1.5	540	3
558	1.0	558	1.0	558	1
	(2)		(2)		(1)

* First number is scale of photo used; second is crater diameter interval. All data plotted at center of intervals. Sun elevation in degrees.

Number in parantheses is the number of individuals who counted area.

Appendix I - Crater Size Frequency Data

Area 4 4° (104 m/mm, 18.72 m)		Area 5 4° (104 m/mm, 18.72 m)		Area 6 7° (107.5 m/mm, 19.35 m)	
m	craters	m	craters	m	craters
109	287	109	534	112	589
128	263	128	389	132	412
147	195	147	261	151	232
165	138	165	182	170	160
184	104	184	124	190	81
203	75	203	74	209	58
222	55	222	62	228	35
240	37	240	49	248	27
259	30	259	33	267	20
278	21	278	24	286	14
296	19	296	21	306	10
315	14	315	14	325	4.3
334	10	334	14	345	6.3
353	5.5	353	10	364	2.7
371	10	371	7.5	383	4.0
390	5.0	390	7.5	403	2.3
409	4.5	409	4.5	422	2.0
427	4.0	427	3.0	441	2.0
446	6.0	446	3.5	461	2.0
465	3.0	465	3.5	480	2.7
484	2.0	484	3.0	499	1.7
502	2.0	502	1.5	518	1.0
521	1.0	521	2.0		
		540	2.0		
		558	1.0		
(2)		(2)		(3)	

Appendix I - Crater Size Frequency Data

Area 7 7° (107.5 m/mm, 19.35 m)		Area 8 11° (103.3 m/mm, 18.59 m)		Area 9 14° (101 m/mm, 18.18 m)	
m	craters	m	craters	m	craters
112	537	108	559	106	536
132	295	127	406	124	349
151	170	146	244	142	194
170	111	164	168	161	121
190	46	183	93	179	68
209	33	201	63	197	48
228	23	220	47	215	26
248	18	239	28	233	26
267	11	257	21	251	17
286	7.0	276	19	270	8.3
306	3.0	294	11	288	5.7
325	2.3	313	7.6	306	4.7
345	2.0	332	6.0	324	6.7
364	2.0	350	6.3	342	2.7
383	1.3	369	7.3	361	5.0
403	1.0	387	1.3	379	3.7
422	1	406	3.6	397	2.0
441	1.3	425	1.3	415	3.7
461	1	443	1.3	433	1.3
		462	1.6	451	1
		480	1.3	469	1
		498	1.3		
		518	1		
(3)		(3)		(3)	

Appendix I - Crater Size-Frequency Data

Area 10 35° (100.6 m/mm, 18.12 m)		Area 11 17° (103.6 m/mm, 18.65 m)		Area 12 19° (103 m/mm, 18.54 m)	
m	craters	m	craters	m	craters
106	758	109	564	108	436
124	413	127	341	127	358
142	206	146	215	145	253
160	112	165	153	164	160
178	66	183	64	182	116
196	46	202	53	201	78
215	27	221	31	219	60
233	19	239	21	237	36
251	16	258	18	256	28
269	9.7	277	10	275	18
287	7.3	295	10	293	9.0
305	6.3	314	5.7	312	9.5
323	5.0	333	5.3	330	10
341	2.3	351	4.0	349	6.0
360	1.3	370	1.7	368	3.5
378	1.3	389	5.3	386	3.0
396	2.0	407	3.0	405	3.0
414	2.7	426	1	423	4.5
432	1.3	444	1	442	1.5
450	1.3			460	1.0
468	1				
	(3)		(3)		(2)

Appendix I - Crater Size Frequency Data

Area 13 19° (103 m/mm, 18.54 m)		Area 14 19° (103 m/mm, 18.54 m)		Area 15 24° (103.3 m/mm, 18.59 m)	
m	craters	m	craters	m	craters
108	585	108	684	108	355
127	416	127	424	127	258
145	249	145	241	146	152
164	141	164	147	164	108
182	103	182	99	183	65
201	66	201	68	201	48
219	42	219	51	220	42
237	33	237	34	239	29
256	32	256	28	257	26
275	25	275	24	276	16
293	12	293	13	294	17
312	8.0	312	9.7	313	11
330	5.7	330	7.3	332	6.6
349	4.3	349	7.0	350	6.0
368	3.7	368	4.0	369	8.0
386	6.0	386	4.3	387	6.3
405	5.3	405	2.0	406	4.3
423	3.0	423	3.3	425	4.0
442	2.3	442	1.0	443	3.3
460	2.0	460	1.7	462	2.6
479	1.0	479	1.0	480	1.6
				499	1
(3)		(3)		(3)	

Appendix I - Crater Size Frequency Data

Area 16a 52° (104 m/mm, 18.72 m)		Area 16b 4° (89.8 m/mm, 16.16 m)		Area 16c 34° (104 m/mm, 18.72 m)	
m	craters	m	craters	m	craters
109	547	94	734	109	566
128	383	110	651	128	389
146	287	127	477	146	275
165	195	143	348	165	193
184	152	159	239	184	132
203	115	175	188	203	96
221	74	191	135	221	79
240	67	207	119	240	63
259	47	224	91	259	54
277	32	240	74	277	42
296	26	256	59	296	29
315	18	272	46	315	25
334	11	288	32	334	17
352	10	304	33	352	11
371	6.8	321	24	371	11
390	5.3	337	15	390	6.0
409	3.8	353	13	409	6.0
427	3.0	369	12	427	3.0
446	4.5	385	8.3	446	5.3
464	1.5	401	12	464	5.3
483	2.3	418	9.1	483	5.3
501	1.0	433	4.8	501	3.8
521	1.0	450	5.5	521	3.8
		466	5.0	539	3.8
		482	5.3	558	1.5
		498	4.5	577	1.5
		515	3.6	595	1.0
		531	4.3		
		547	1.3		
		563	2.0		
		579	2.0		
		595	2.0		
		612	2.3		
		628	2.3		
		644	1.0		
		660	2.0		
		676	1.0		
(3)		(3)		(3)	

Appendix I - Crater Size-Frequency Data

Area 17a 52° (104 m/mm, 18.72 m)		Area 17b 4° (89.8 m/mm, 16.16 m)		Area 17c 34° (104 m/mm, 18.72 m)	
m	craters	m	craters	m	craters
109	210	94	546	109	310
128	147	110	457	128	210
146	117	127	376	146	162
165	101	143	299	165	128
184	86	159	225	184	104
203	69	175	173	203	86
221	51	191	132	221	75
240	54	207	110	240	62
259	56	224	99	259	64
277	42	240	78	277	39
296	25	256	56	296	33
315	24	272	43	315	24
334	12	288	41	334	15
352	13	304	36	352	12
371	12	321	31	371	12
390	8.2	337	30	390	9.3
409	4.1	353	16	409	7.0
427	7.2	369	18	427	7.3
446	5.1	385	18	446	6.0
464	4.1	401	12	464	4.0
483	3.0	418	6.1	583	5.0
501	4.1	433	7.2	501	4.7
521	4.1	450	6.1	521	3.3
539	2.0	466	9.2	539	2.7
558	2.0	482	6.1	558	3.3
577	2.7	498	6.1	577	3.0
595	2.6	515	6.1	595	2.0
614	2.3	531	5.1	614	2.0
623	1.0	547	2.0	633	1.0
		563	5.1		
		579	1.7		
		595	1.7		
		612	2.3		
		628	1.0		
(3)		(3)		(3)	

Appendix I - Crater Size-Frequency Data

Area 18 21° (91.88 m/mm, 16.54 m)		Area 19 21° (94 m/mm, 16.9 m)		Area 20 24° (95.25 m/mm, 17.12 m)	
m	craters	m	craters	m	craters
96	576	99	547	100	712
113	397	116	469	117	479
130	286	133	306	134	350
146	207	150	215	151	221
163	140	167	131	168	138
179	118	184	89	186	100
196	85	201	61	203	56
212	66	217	53	220	49
229	60	234	37	237	38
245	44	251	26	254	33
262	35	268	14	271	18
278	24	285	12	288	14
295	27	302	9.4	305	12
311	20	319	8.6	323	10
328	15	336	4.4	340	7.1
345	12	353	5.0	357	6.2
361	10	370	2.6	374	5.4
378	8.3	387	3.6	391	2.7
394	9.7	404	2.2	408	3.6
411	4.7	420	1.6	425	1.8
427	7.3	437	1.0	442	2.7
444	5.0			459	1.8
460	4.7			476	1.0
477	4.7				
493	2.3				
509	2.7				
526	3.0				
543	1.0				
	(3)		(5)		(3)

Appendix I - Crater Size-Frequency Data

Area 21 29° (94.8 m/mm, 17.06 m)		Area 22 33° (94.5 m/mm, 17.01 m)		Area 23 21° (100.8 m/mm, 18.14 m)	
m	craters	m	craters	m	craters
99.5	476	99	534	106	131
117	420	116	351	124	129
134	270	133	232	142	121
151	195	150	163	160	128
168	138	167	108	178	79
185	94	184	80	197	79
202	60	201	59	215	64
219	43	218	43	233	66
236	39	235	46	251	61
253	34	252	35	269	45
270	23	269	21	287	38
287	20	286	21	305	29
304	13	303	17	324	21
321	11	320	12	342	18
338	10	337	10	360	12
355	8.4	354	4.3	378	18
373	6.5	371	5.0	396	11
390	4.7	388	7.3	414	11
407	6.3	405	4.3	432	11
424	2.8	422	3.3	451	7.6
441	3.7	439	1.3	469	4.7
458	3.7	456	1.0	487	5.3
475	2.8			505	4.0
492	1.0			523	3.0
509	0			541	4.3
				559	1.7
				577	4.7
				595	1.0
(2)		(3)		(3)	

Appendix I - Crater Size-Frequency Data

Area 24 46° (93.6 m/mm, 16.84 m)		Area 25 . 23° (104 m/mm, 18.72 m)		Area 26 38° (92.6 m/mm, 16.67 m)	
m	craters	m	craters	m	craters
98	62	109	272	97	364
115	45	128	231	114	267
132	40	146	176	131	199
149	41	165	142	147	155
166	41	184	85	164	107
182	38	203	65	181	78
199	41	221	51	197	60
216	37	240	36	214	45
233	31	259	36	231	34
250	27	277	25	247	25
267	16	296	18	264	15
284	18	315	12	281	16
300	16	334	10	297	6.3
317	16	352	8	313	5.0
334	9.0	371	8.6	331	6.0
351	9.5	390	5.3	347	3.6
368	11	409	4.3	363	3.0
385	9.0	427	3.3	381	2.3
401	11	446	4.3	397	3.0
418	5.0	464	2.3	414	1.6
435	7.5	483	4.3	431	1.6
452	2.0	502	1	447	1.6
469	5.0	521	2	467	1.0
485	2.0	540	2.4		
502	3.0	558	2.4		
519	1.0	577	1		
536	4.0	596	1		
553	2.0				
570	2.0				
586	1.0				
	(2)		(3)		(3)

Appendix I - Crater Size-Frequency Data

Area 27 37° (108.5 m/mm, 19.53 m)		Area 28 58° (110 m/mm, 19.8 m)		Area 29 17° (107.30 m/mm, 19.31	
m	craters	m	craters	m	craters
114	383	116	375	113	545
133	330	135	326	132	377
153	261	155	237	151	216
172	191	175	166	171	153
192	141	195	120	190	81
212	102	215	80	209	60
231	72	234	56	229	46
251	59	254	50	248	35
270	42	274	35	267	26
290	32	294	31	286	21
309	21	314	19	306	11
329	14	333	15	325	10
348	10	353	9.0	344	9.3
368	8.0	373	6.3	364	7.7
387	7.0	393	8.0	383	7.0
407	4.0	413	6.3	402	8.0
426	3.0	432	5.0	422	4.3
446	4.0	452	3.7	441	2.3
465	4.0	472	4.0	460	3.0
485	2.3	492	1.7	480	2.0
505	2.3	512	3.3	499	1.0
524	2.0	532	1.3	518	1.7
544	1.0	552	1.0	538	1.3
				557	1.0
(3)		(3)		(3)	

Appendix I - Crater Size-Frequency Data

Area 30 4° (93.2 m/mm, 16.78 m)		Area 31 9° (94.118 m/mm, 16.94 m)		Area 32 14° (95.59 m/mm, 16.39 m)	
m	craters	m	craters	m	craters
99	1376	99	713	96	608
115	1244	116	536	112	465
131	808	133	316	129	294
148	514	150	207	145	218
165	326	167	100	162	106
182	222	184	79	178	86
199	140	200	67	194	56
215	106	217	43	211	40
232	95	234	32	227	36
249	54	251	22	243	17
266	38	268	17	260	22
282	21	285	14	276	16
299	19	302	7.5	293	13
316	13	319	6.3	309	11
333	14	336	4.3	325	5.3
350	13	353	5.0	342	4.3
366	14	370	2.3	358	2.3
383	7.2	387	2.6	375	3.6
400	5.4	404	3.3	391	2.0
417	3.6	421	1.0	407	3.3
433	2.7	438	3.0	424	1.6
450	2.7	455	1.0	440	2.0
467	2.7			457	1.3
484	1.8			473	1.6
500	1.0			489	2.3
				506	1.0
(2)		(3)		(3)	

Appendix I - Crater Size-Frequency Data

Area 33a 34° (111 m/mm, 19.9 m)		Area 33b 10° (103 m/mm, 18.5 m)		Area 34 35° 108.6 m/mm, 19.55 m)	
m	craters	m	craters	m	craters
117	359	108	274	114	590
137	164	127	229	134	513
158	127	145	214	153	347
179	113	164	157	173	244
200	68	182	123	192	170
221	75	201	92	212	113
242	44	219	70	231	67
263	34	238	52	251	47
284	32	256	46	270	46
305	20	275	32	290	35
326	20	293	22	309	32
347	13	312	18	329	16
368	9.5	330	16	349	15
389	9.5	349	11	368	13.5
410	6.6	367	8.5	388	4.5
431	4.7	386	7.6	407	7.0
452	3.8	404	6.6	427	4.0
473	3.8	423	8.5	446	4.5
494	5.7	441	4.7	466	4.5
515	2.8	460	4.7	485	4.5
536	1.9	478	2.8	504	2.0
557	1.0	497	1.9	525	4.5
		515	2.8	544	1.5
		534	2.8	564	1.5
		552	1.9	584	1.0
		571	1.0		
(3)		(3)		(2)	

CRATER COUNT AREAS - TABLE 1

NO*	PAN ** FRAME	LAT	LONG	SUN	LTO MAP	MARE REGION
1	17-3133S	21N	38.5W	5°	_____	Imbrium, Brayley
2	17-3131S	20.5N	37.8W	4°	_____	Imbrium, Brayley
3	17-3133N	23.5N	38.5W	5°	_____	Imbrium, Brayley
4	17-3131C	23.4N	37.9W	4°	_____	Imbrium, Brayley
5	17-3131N	24.5N	37.9W	4°	_____	Imbrium, Brayley
6	17-3127	22.6N	36.4W	7°	_____	Imbrium, Brayley
7	17-3126	22.6N	36.2W	7°	_____	Imbrium, Brayley
8	17-3113	25.5N	32W	11°	39 B3	Imbrium, Diophantus-Euler
9	17-3104	25.5N	29.5W	14°	40 A4	Imbrium, N of Euler
10	15-0272	27N	28.3W	35°	40 A4	Imbrium, N of Euler
11	17-3094	23N	25.5W	17°	_____	Imbrium, E of Euler
12	17-3090	23.6N	24.3W	19°	_____	Imbrium, E of Euler
13	17-3088N	25.6N	23.5W	19°	40 A3	Imbrium, W of Lambert
14	17-3088S	25N	23.3W	19°	40 A3	Imbrium, W of Lambert
15	17-3076	25.7N	18.5W	24°	40 B4	Imbrium, E of Lambert
16a	15-0214	23.5N	352E	52°	41 D1	Imbrium, N of Wallace
16a	15-0216	23.5N	352E	52°	41 D1	Imbrium, N of Wallace
16b	15-9411	23.5N	352E	4°	41 D1	Imbrium, N of Wallace
16c	17-3039	23.5N	352E	34°	41 D1	Imbrium, N of Wallace
17a	15-0219	23.5N	352.5E	52°	41 D1	Imbrium, N of Wallace
17b	15-9404	23.5N	352.5E	4°	41 D1	Imbrium, N of Wallace
17c	17-3044	23.5N	352.5E	34°	41 D1	Imbrium, N of Wallace
18	15-9433	25.5N	1.4E	21°	41 B4	Imbrium, W of Hadley Rille
19	15-9348	24.5N	11.5E	21°	42 A4	Serenitatis, E of Lorca
20	15-9341	24N	16E	24°	42 A3	Serenitatis, NW of Bessel
21	15-9329	25N	20E	29°	42 A3	Serenitatis, NE of Bessel
22	15-9310	25N	25E	33°	42 B2	Serenitatis, S of Very
23	17-2296	20.5N	37.4E	21°	43 D2	Tranquillitatis, Sinus Amoris
24	15-9270	21.5N	38.3E	46°	43 D2	Tranquillitatis, Sinus Amoris
25	17-2292	21N	39E	23°	43 D2	Tranquillitatis, Sinus Amoris
26	17-2245	18N	55E	38°	44 D4	Crisium, NE of Swift
27	17-2252	20N	54.5E	37°	44 D4	Crisium, E of Peirce
28	15-9729	6.5S	87.6E	58°	81 B3	Smythii, Kao
29	17-2774	19.3S	129.5E	17°	101 B2	Tsiolkovsky, NE
30	15-0366	24N	62.7W	4°	_____	O.Procellarum, Schiaparelli C
31	15-0356	28.5N	58.5W	9°	_____	O.Procellarum, Lichtenberg A
32	16-5460	11S	328.3E	14°	75 C2	O.Procellarum, NW of Norman
33a	16-5404	8S	348.5E	34°	76 C2	Nubium, N of Kundt
33b	16-4684	8S	348.5E	10°	76 C2	Nubium, N of Kundt
34	16-5402	10S	349.5E	35°	76 C2	Nubium, NE of Kundt

* As appears on Figures in text. ($\sim$350 km^2)

** Letters indicate North, South or Center if more than one area.

Table 1A

Relative Ages of Mare Surfaces Listed in Table 1*

	Location	Areas
Youngest	Eratosthenian (Phase III) Equivalents	9,10,31
	Eratosthenian (Phase I) Equivalents	1-7,11(?), 12,13,14, 15,30,32
	Central Serenitatis Equivalents	19,20,21,22
	Apollo 15 Site Area Equivalents	18,26(?),27, 28,29,33(?), 34
	Imbrium near Crater Wallace	16,17
Oldest	Tranquillitatis (Sinus Amoris)	23,24,25

* Regions grouped together are approximately equivalent in age with uncertainties indicated by (?).

Table 2
Example of Individual Variations
For Crater Counts of Three Individuals (O,L,F)

Crater Dia. in m (center of 17 m interval)	Individual Counts (373 km^2) O	L	F	Average	Max. Deviation From Mean (Nearest %)
99	862	656	766	761	14
116	648	472	596	572	17
133	355	302	353	337	10
150	235	190	237	221	14
167	98	113	111	107	8
184	100	73	79	84	19
200	73	65	79	72	10
217	54	39	46	46	17
234	34	30	37	34	12
251	25	23	21	23	9
268	20	16	17	18	11
285	18	15	13	15	20
302	12	5	6	7.6	58
319	3	12	4	6.3	90
336	4	2	7	4.3	63
353	8	5	2	5.0	60
370	2	0	5	2.3	117
387	1	4	3	2.6	54
404	2	4	4	3.3	39
421	1	0	1	0.66	100
438	6	2	1	3.0	100
455	3	0	1	1.3	100
472	0	1	1	0.66	100
489	1	2	3	2.0	50
506	3	1	0	1.3	130
523	3	0	1	1.3	130
540	1	0	1	0.66	100
557	0	2	0	0.66	212

Raw data for Area 31, not normalized to 350 km^2

Table 3
Hypothetical Crater Size-Frequency Distributions for Selected Regions to Accompany Figure 10

I_e		S		I_W		T	
D*	C**	D	C	D	C	D	C
108	450	100	600	109	360	108	232
127	270	117	410	128	280	126	190
146	160	134	280	146	220	144	151
164	100	151	195	165	173	163	123
183	62	168	135	184	137	181	100
201	39	185	94	203	108	200	82
220	42	202	65	221	86	218	67
239	29	219	46	240	67	237	54
257	19	236	42	259	52	255	44
276	15	253	27	277	42	273	36
294	12	270	21	296	33	294	28
313	9.0	287	17	315	26	310	24
332	6.8	304	13	334	27	329	19
350	5.4	321	10.5	352	15	347	16
369	4.2	338	8.4	371	13	365	12
387	3.2	355	6.5	390	11	393	9.3
406	2.5	372	5.1	409	9.0	412	7.5
425	1.9	389	4.1	427	7.7	430	7.1
443	1.5	406	3.2	446	6.3	449	6.0
462	1.1	423	2.5	464	5.5	467	5.2
		440	2.0	483	4.5	485	4.5
		457	1.6	501	3.9	504	3.8
		474	1.2	521	3.2	522	3.3
		491	1.0	539	2.7	540	2.8
				558	2.3	558	2.4
				577	1.9	577	2.1
				595	1.6	596	1.7
				614	1.3	614	1.5
				633	1.1	632	1.3
				652	1.0	650	1.1

* Diameters plotted at center of interval.

** Craters in 350 km^2 area.

Table 4
Fresh Lunar Impact Craters

Crater	Rim Crest Diameter D_r (km)	Interior Relief R_i (km)	Circularity Index C.I.	Source
Timocharis	33.79	3.20	.90	LT040B3
93.3E, 7.0S	17.25	2.37	.92	LT082A4
Theophilus	100.8	4.10	.85	LT078C2
Proclus	27.5	3.90	.80	LT043C3
Picard	23.5	2.28	.94	LT062A1
Peirce	18.6	2.11	.90	LT044D4
Lambert	29.96	2.51	.93	LT040A3
King	76.4	4.00	.87	LT065C1
Hill	16.0	3.84	.93	LT043C1
Geissler	17.6	2.96	.86	LT081A2
Diophantus	18.13	2.86	.91	LT039B3
Delisle	25.29	2.43	.88	LT039B1-B2
Dawes	17.4	2.38	.86	LT042C3
Carmichael	19.9	3.68	.90	LT043C4
Black	19.13	3.16	.98	LT081C1
Bessel	15.30	2.01	.90	LT042D2
Antolycus	39.20	3.15	.88	Pike, 1968
Tycho	84.7	4.60	.88	Pike, 1968
Aristarchus	40.0	3.15	.88	Pike, 1968
Aristillus	55.3	3.30	.91	Pike, 1968
Copernicus	93.0	3.80	.88	Pike, 1968
Eudoxus	67.1	3.20	.89	Pike, 1968
Langrenus	132.0	4.35	.84	Pike, 1968
Stevinus	74.5	3.70	.82	Pike, 1968

.89 = average C.I.

LTO - Lunar Topographic Orthophotomap

$R_i = 1.34\ D_r^{.239}$

correlation coefficient = .696

Table 5
Modified Lunar Impact Craters

Crater	Rim Crest Diameter D_r (km)	Interior Relief R_i (km)	Circularity Index C.I.	Source
Lambert R	98.0	0.40	.92	LTO40A3-B4
10S 35W	67.0	0.25	.85	LTO75C1-C2
Taruntius	56.0	0.85	.92	LTO61-C2
Herigonius Nu	18.0	0.27	.91	LTO75-C2
Lick	31.7	0.75	.92	LTO62A1
15N 32E	18.6	0.04	.81	LTO61A1
Jansen R	23.3	0.30	.88	LTO60B2
Briggs	28.5	1.15	.91	LTO38A4
Warner	33.3	0.26	.86	LTO81B3-B2
Haldane	40.2	0.39	.91	LTO81B2
Lebesque	12.2	0.32	.81	LTO81B3
Swasey	20.9	0.36	.88	LTO82A4-81B3
Milton	35.1	0.28	.86	LTO82A1
Widmanstätten	47.8	0.38	.78	LTO81B4-B3
Helmert	28.0	0.75	.73	LTO81-B3
Talbot	13.0	0.26	.83	LTO81B2
Camoens	34.6	0.26	.86	LTO63C3-C4
0°30'S 86°E	18.3	0.11	.83	LTO81B2
Kiess	70.0	0.96	.89	LTO81B3-B4
Doyle	30.7	0.42	.98	LTO63C3-C4
Hume	44.1	0.25	.96	LTO82A4
Runge	38.6	0.28	.84	LTO81B2
Kao	39.5	0.17	.87	LTO81B3
Tasso	39.8	0.49	.77	LTO82A1
Posiodonis	100.5	1.85	.80	Pike, 1968
Lubiniezky	44.0	0.50	.94	Pike, 1968
Kies	44.1	0.55	.84	Pike, 1968
Puiseau	25.0	0.40	.95	Pike, 1968
Ritter	30.9	1.10	.96	Pike, 1968
Sabine	30.3	1.30	.93	Pike, 1968
Encke	29.4	0.65	.87	Pike, 1968
Egede	37.1	0.10	.85	Pike, 1968
Cassini	56.5	1.00	.89	Pike, 1968

0.87 = average C.I.

LTO - Lunar Topographic Orthophotomap

$R_i = 0.41\ D_r^{.647}$

correlation coefficient = .403

Table 6
Terrestrial Calderas and Related Structures

	Circularity Index C.I.
Timber Mtn. Caldera	0.78
Creede Caldera	0.75
Valles Caldera	0.76
Lake City Caldera	0.68
Silverton Caldera	0.79
Black Mtn. Caldera	0.66
Toba Cauldron	0.34
Long Valley	0.59
Rotorua Caldera	0.66
Virgina Dale ring complex	0.81
Ossipee Cauldron	0.80
Alnsjö Cauldron	0.78
Sande Cauldron	0.70
Liruei Cauldron	0.73
Glen Coe ring complex	0.51
Amo ring complex	0.76
Buji ring complex	0.72
Kudaru ring complex	0.62
Kofayi ring complex	0.42
Jos Bukuru ring complex	0.63
Featherbed ring complex	0.83
Bagstowe ring complex	0.73
Lochaber ring complex	0.72
Kallon ring complex	0.78
Cumberland Range ring complex	0.83
Warby ring complex	0.67
Claret Creek ring complex	0.85
Mokai ring complex	0.84
Okatina ring complex	0.78
Trou Au Natron	0.72
Kikai	0.66
Suswa Caldera	0.70
Crater Lake	0.80
Aso Caldera	0.66
Abrym Caldera	0.78
Kilombe Caldera	0.55
Rabaul Caldera	0.61
	0.70 = average C.I.

REFERENCES AND BIBLIOGRAPHY

Adams,J.B. and McCord,T.B. (1972) Electronic spectra of pyroxenes and interpretation of telescopic spectral reflectivity curves of the moon. Proc. Third Lunar Sci. Conf., Geochim. Cosmochim. Acta, Suppl. 3, Vol. 3, pp. 3021-3034. MIT Press.

Adams,J.B., Pieters,C., and McCord,T.B. (1974) Orange glass: evidence for regional deposits of pyroclastic origin on the moon. Proc. Lunar Sci. Conf. 5th, pp. 171-186.

Adler,I., Trombka, J., Gerard,J., Schmadebeck,R., Lowman,P., Blodgett,H., Yin,L., Eller,E., Lamothe,R., Gorenstein,P., Bjorkholm,P., Harris,B., and Gursky,H. (1972) X-ray fluorescence experiment. Apollo 15 Prelim. Sci. Rpt., NASA SP-289, pp. 17-1 - 17-7.

Adler, I., Trombka, J., Gerard, J., Lowman, P., Schmadebeck, R., Bodget, H., Eller, E., Yin, L., Lamothe, R., Oswald, G., Gorgenstein, P., Bjorkholm, P., Gursky, H., Harris,B., Golub, L., and Harnden, F.R. (1973a) X-ray fluorscence experiment. In Apollo 16 Prelim. Sci. Rpt., NASA SP-315, 14 pp.

Adler, I., Trombka, J.I., Schmadebeck, R., Lowman, P., Blodgett, H., Yin, L., Eller, E., Podwysocki, M., Weidner, J.R., Bickel, A.L., Lum, R.K.L., Gerard, J., Gorenstein, P., Bjorkholm, P., and Harris, B. (1973b) Results of the Apollo 15 and 16 X-ray experiment. Proc. 4th Lunar Sci. Conf., Suppl. 4, Geochim. Cosmochim. Acta, V. 3, pp. 2783-2791, Pergamon Press.

Adler, J.E.M. and Salisbury, J.W. (1969) Circularity of lunar craters. Icarus, V. 10, pp. 37-52.

Apollo Lunar Sounder Experiment Team (1974) Apollo 17 Preliminary Science Report. NASA SP-300, pp. 22-1 - 22-26.

Arvidson, R., Drodz, R.J., Hohenberg, C.M., Morgan, D.J., and Popeau, G. (1975) Horizontal transport of the regolith, modification of features, and erosion rates on the lunar surface. The Moon, pp. 1367 - 1379.

Bailey, E.B. and Maufe, H.B., (1916) The geology of Ben Nevis and Glencoe and the surrounding country. Scotland Geological Survey Memoir, No. 53 (1960, 2nd revised ed.).

Baldwin, R.B. (1949) The face of the moon. Univ. of Chicago Press, Chicago.

Baldwin, R.B. (1963) The measure of the moon. Univ. of Chicago Press, Chicago, 488 pp.

Baldwin, R.B. (1972) The Tsunami model of the origin of ring structures concentric with large lunar craters. Phys. Earth Planet, Interiors 6, pp. 327-339.

Bjork, R.L. (1961) Analysis of the formation of Meteor Crater. Arizona: A preliminary report. J. Geophysical Res. 66, pp. 3379-3387.

Boyce, J.M., Dial, A.L. (1975) Relative ages of flow units in Mare Imbrium and Sinus Iridum. Proc. Lunar Sci. Conf. 6th, pp. 2585-2597.

Boyce, J.M., Dial, A.L., and Soderblom, L.A. (1974) Ages of the lunar nearside light plains and maria. Proc. Lunar Sci. Conf. 5th, pp. 11-23.

Branch, C.D. (1966) Volcanic cauldrons, ring complexes, and associated granites of the Georgetown Inlier, Queensland. Department of Natural Development, Bureau of Mineral Resources, Geology and Geophysics Bulletin #76.

*Brennan, W.J. (1975a) Modification of premare impact craters by volcanism and tectonism. The Moon 12, pp. 449-461.

*Brennan, W.J. (1975b) Evolution of Mare Smythii (abstract). In Lunar Science VI, pp. 86-88. The Lunar Science Institute, Houston.

*Brennan, W.J. (1976) Multiple ring structures and the problem of correlation between lunar basins (abstract). In Lunar Science VII, The Lunar Science Institute, Houston (in press).

Bryan, W.B. (1973) Wrinkle-ridges as deformed surface crust on ponded mare lava. Lunar Sci. Conf. 45h, pp. 93-106.

Bryan, W.B., Jezek, P.A., and Adams, M.L. (1975) Volcanic and tectonic evolution of crater Goclenius, western Mare Fecunditatis. Proc. Lunar Sci. Conf. 6th, pp. 2563-2571.

Cameron, W.S., and Padgett, J.L. (1974) Possible lunar ring dikes. The Moon, V. 9, pp. 249-294.

Carr, M.H. (1965) Geologic map of the Timocharus region of the Moon. U.S.G.S.

Chadderton, L., Krajenbrink, F., Katz, R., and Poveda, A. (1969) Standing waves on the Moon. Nature 223, 259.

Chapman, C.R., Mosher, J.A., and Simmons, G. (1970) Lunar cratering and erosion from Orbiter 5 photographs. Journal of Geophys. Res., 75, pp. 1445-1466.

Choate, R. (1966) Lunar slope angles and surface roughness from Ranger photographs. Jet Propul. Lab. Tech. Rep. 32-994.

Colton, G.W., Howard, K.A., and Moore, H.J. (1972) Mare ridges and arches in southern Oceanus Procellarum. Apollo 16 Preliminary Science Report, NASA SP-315, pp. 90-93.

Cruikshank, D.P., Hartmann, W.D., and Wood, C.A. (1973) Moon: 'ghost' craters formed during mare filling. The Moon, V. 7, pp. 440-452.

Cruikshank, D.P. and Wood, C.A. (1972) Lunar rilles and Hawaiian volcanic features: possible analogues. The Moon 3, pp. 412-447.

DeHon, R.A. (1971) Cauldron subsidence in lunar craters. Journal of Geophysical Research, V. 76, No. 33, pp. 5712-5718.

Dence, M.R. (1964) A comparative structural and petrographic study of probable Canadian meteorite craters. Meteoritics, V. 2, pp. 249-270.

Dence, M.R. (1968) Shock zoning at Canadian craters: petrography and structural implications. In French, B.M. and Short, N.M. eds., Shock metamorphism of natural materials. Proceedings of the First Conference held at NASA, Goddard Space Flight Center, Greenbelt, Maryland, pp. 169-184.

Dence, M.R. (1971) Impact melts. Journal of Geophysical Research, V. 76, No. 23, pp. 5552-5565.

Eggleton, R.E., Schaber, G.G., and Pike, R.J. (1974) Photogeologic detection of surfaces buried by mare basalts (abstract). In Lunar Science--V, pp. 200-201. The Lunar Science Institute, Houston.

El-Baz, F., Worden, A.M., and Brand, V.D. (1972) Astronaut observations from lunar orbit and their geologic significance. Proc. Third Lunar Sci. Conf., Geochim. Cosmochim. Acta, Suppl. 3, V. 1, pp. 85-104. MIT Press.

Fielder, G. (1963) Nature of the lunar maria. Nature 198, 1256.

Fielder, G. (1967) Volcanic rings on the moon. Nature 213, pp. 333-336.

Gault, D.E. (1970) Saturation and equilibrium conditions for impact cratering on the lunar surface: criteria and implications. Radio Science, 5, pp. 273-291.

Gault, D.E., Quaide, W.L., and Oberbeck, V.R. (1968) Impact cratering mechanics and structures. In Shock metamorphism of natural materials (Eds. French, B.M. and Short, N.M.), pp. 87-99. Mono Book Corp., Baltimore, Md.

Gault, D.E., Guest, J.E., Murrary, J.B., Dzurisin, D., and Malin, M.C. (1975) Some comparisons of impact ctaters on Mercury and the Moon. Jour. Geophys. Res., V. 80, No. 17, pp. 2444-2460.

Gilbert, G.K. (1893) The moons face, a study of the origin of its features. Philosophical Soc. of Washington, Bull. XII, pp. 241-292.

Greeley R. (1971) Lunar Hadley Rille: considerations of its origin. Science 172, pp. 722-725.

Greeley R. (1972) Additional observations of actively forming lava tubes and associated structures. Hawaii, Modern Geology 3, 157-160.

Greeley R. and Gault D.E. (1970) Precision size-frequency distributions of craters for 12 selected areas of the lunar surface. Moon, 2, pp. 10-77.

Greeley R. and Hyde J.H. (1972) Lava tubes of the cave basalt, Mount St. Helens, Washington. Geol. Soc. America Bull. 83, pp. 2397-2418.

Green, J. (1971) Copernicus as a lunar caldera. Journal of Geophysical Research, V. 76, No. 23, pp. 5719-5731.

Green, J. and Short N.M., Eds. (1971) Volcanic landforms and surface features: a photographic atlas and glossary. Springer-Verlag.

Hackmann, R.J. (1966) Geologic map of the Montes Appeninys region of the moon. U.S. Geol. Surv., Map I-463.

Hartmann, W.K. (1973) Ancient lunar mega-regolith and subsurface structure. Icarus 18, pp. 634-636.

Hartmann, W.K. and Kuiper, G.P. (1962) Concentric structures surrounding lunar basins. Comm. Lunar Planetary Lab 1, 51.

Hartmann, W.K. and Wood C.A. (1971) Moon: origin and evolution of multi-ring basins. The Moon 3, pp. 3-78.

Head, J.W. (1974a)Lunar dark mantle deposits: possible clues to the distribution of early mare deposits. Proc. Lunar Sci. Conf. 5th, pp. 207-222.

Head, J.W. (1974b)Orientale multi-ringed basin interior and implications for the petrogenesis of lunar highland samples. The Moon, 11, pp. 327-356.

Heiken, G. and McKay, G.S. (1974) Petrography of Apollo 17 Soils: in Lunar Science V, The Lunar Science Institute, Houston, pp. 319-321.

Hess, W.N. and Nordyke, M.D. (1961) Throwout calculations for explosion craters. J. Geophys. Res. 66, pp. 3405-3412.

Hodges, C.A. (1973) Mare ridges and lava lakes. Apollo 17 Prel. Science Report, pp. 31-12 - 31-21.

Howard, K.A., Carr, M.H., and Muehlberger, W.R. (1974) Basalt stratigraphy of southern Mare Serenitatis. In Apollo 17 Prel. Science Report, NASA SP-300, Section 29, Part A, 1-12.

Howard, K.A., and Muehlberger, W.R. (1973) Lunar thrust faults in the Taurus-Littrow region. Apollo 17 Prel. Sci. Report, pp. 31-22 - 31-25.

Howard K.A., Head, J.W., and Swann, G.A. (1972) Geology of Hadley Rille. Proc. Third Lunar Sci. Conf., Geochim. Cosmochim. Acta, Suppl. 3, V. 1, pp. 1-14. MIT Press.

Howard, K.A., Wilhelms, D.E., and Scott, D.H. (1974) Lunar basin formation and highland stratigraphy. Rev. Geophys. Space Phys. V. 12, No. 3, pp. 309-327.

Innes, M.J.S. (1964) Recent advances in meteorite crater research at the Dominion Observatory, Ottawa, Canada. Meteoritics, V. 2, pp. 219-241.

Jacobson, R.R.E., Macleod, W.N., and Black, R. (1958) Ring-complexes in the younger granite province of Northern Nigeria. Geological Society of London Memoir 1, 72 pp.

Johnson, G.G., Vand, V., and Dachille, F. (1964) Additional rims around Ries Kessel Meteorite Crater. Nature 201, 592.

Johnson, T.V., Matson, D.L., Phillips, R.J., and Saunders, R.S. (1975) Vidicon spectral imaging: color enhancement and digital maps. Proc. Lunar Sci. Conf. 6th, pp. 2677-2688.

Kosofsky, L.J., and El-Baz, F. (1970) The moon as viewed by Lunar Orbiter. 152 pp., NASA SP-200.

Lucchitta, B.K. and Sanchez, A.C. (1975) Crater studies in the Apollo 17 region. Proc. Lunar Sci. Conf. 6th, pp. 2427-2443.

Lucchitta, B.K. and Schmitt, H.H. (1974) Orange material in the Sulpicius Gallus Formation at the southwestern edge of Mare Serenitatis. Proc. Lunar. Sci. Conf. 5th, pp. 223-234.

Leonardi, P. (1972) Winding and meandering furrows on the lunar surface. Modern Geology 3, pp. 151-156.

Mackin, J.H. (1969) Origin of lunar maria. Bull. Geol. Soc. Am. V. 80, No. 5, pp. 735-748.

McCall, G.J.H. (1965) The Caldera analogy in selenology. Annals of the New York Academy of Science, V. 122, pp. 843-875.

McCauley, J.F. (1968) Preliminary photogeologic map of the Orientale basin region. In G.E. Ulrich, Advanced systems traverse research project report. U.S. Geol. Survey Interagency Rept., Astrogeology 7, pp. 32-33.

McCord, T.B., Charette, M.P., Johnson,T.V., Lebofsky, L.A., and Pieters, C. (1972) Lunar spectral types. J. Geophys. Res. 77, pp. 1349-1359.

McGill, G.E. (1971) Attitude of fractures bounding straight and arcuate lunar rilles. Icarus 14, pp. 53-58.

McGill, G.E. (1974) Morphology of lunar craters: a test of lunar erosional models. Icarus, 21, pp. 437-447.

Moore, H.J. (1967) Seleucus Quadrangle: geologic map No. I-527, U.S.G.S.

Moore, H.J., Hodges, C.A. and Scott, D.H. (1974) Multi-ringed basins--illustrated by Orientale and associated features. Proceedings of the Fifth Lunar Science Conference, Suppl. 5, Geochim. et Cosmochim. Acta, V. 1, pp. 71-100.

Moore, H.J. and Schaber, G.G. (1974) An estimate of the yield strength of Imbrium lava flows. In Lunar Science VI, The Lunar Science Institute, pp. 572-574.

Morris, E.C. and Wilhelms, D.E. (1967) Geologic map of the Julius Ceasar Quadrangle of the Moon. U.S. Geol. Surv., Map I-510.

Muehlberger, W.R. (1974) Structural history of southeastern Mare Serenitatis and adjacent highlands. Proc. Lunar. Sci. Conf. 5th, pp. 101-110.

Murase T. and McBirney A.R. (1970) Viscosity of lunar lavas. Science 167, 1491-1493.

Murphey, B.F. and Vortman, L.J. (1961) High-explosive craters in desert alluvium, tuff and basalt. J. Geophys. Res., 66, pp. 3389-3404.

Murrary, J.B. and Guest, J.E. (1970) Circularities of craters and related structures on earth and moon. Modern Geology, V. 1, pp. 149-159.

Mutch, T.A. (1970) Geology of the Moon. Princeton University Press, Princeton, 324 pp.

*Nichols, D.J., Young, R.A., and Brennan, W.J. (1974) Lunar kipukas as evidence for an extended tectonic and volcanic history of the maria (abstract). In Lunar Science--V, pp. 550-552. The Lunar Science Institute, Houston.

Nordyke, M.D. (1961) Nuclear craters and preliminary theory of the mechanics of explosive crater formation. J. Geophys. Res. 66, pp. 3439-3459.

Nugent, R.C. (1967) Jointing in a quaternary basalt, Buckboard Mesa, Nevada, and its effect on cratering experiments. Ph.D. dissertation, Northwestern University, pp. 1-237.

Oberbeck, V.R. (1971) Laboratory simulation of impact cratering with high explosives. J. Geophys. Res., 76, pp. 5732-5749.

Oberbeck, V.R., Aoyagi, M., Greeley, R., and Lovas, M. (1972) Planimetric shapes of lunar rilles. Apollo 16 Preliminary Science Report, NASA SP-315, Section 29, Part Q.

Oberbeck, V.R., Aoyagi, M., and Murray, J.B. (1972) Circularity of Martian Craters. Modern Geology, V. 3, pp. 195-199.

Oberbeck, V.R., Morrison, R.H., Hörz, F., Quaide, W.L., and Gault, D.E. (1974) Smooth plains and continuous deposits of craters and basins. Proc. Lunar. Sci. Conf. 5th, pp. 111-136.

Offield, T.W. and Pohn, H.A. (1970) Lunar crater morphology and relative-age determination of lunar geologic units--Part 2. Applications. U.S. Geol. Survey Prof. Paper 700-C, C163-C169.

Olson, A.B. and Wilhelms, D.E. (1974) Geologic map of the Mare Undarum Quadrangle, U.S.G.S.

Phillips, R.J., Adams, G.F., Brown, W.E., Jr., Eggleton, R.E., Jackson, P., Jordan, R., Peeples, W.J., Porcello, L.J., Ryu, J., Schaber, G., Sill, W.R., Thompson, T.W., Ward, S.H., and Zelenka, J.S. (1973) The Apollo 17 Lunar Sounder. Proc. Fourth Lunar Sci. Conf., Geochim. Cosmochim. Acta, Suppl. 4, V. 3, pp. 2821-2831, Pergamon.

Phillips, R.J. and Saunders, R.S. (1974) Interpretation of gravity, anomalies in the irregular maria (abstract). In Lunar Science--V, pp. 596-597. The Lunar Science Institute, Houston.

Pike, R.J. (1968) Meteoritic origin and consequent endogenic modification of large lunar craters--a study in analytical geomorphology. Ph.D. Thesis, The University of Michigan, 404 pp.

Pike, R.J. (1971) Genetic implications of the shapes of Martian and lunar craters. Icarus, 15, pp. 384-395.

Pike, R.J. (1974a)Craters on Earth, Moon, and Mars: multivariate classification and mode of origin. Earth and Planetary Science Letters, 22, pp. 245-255.

Pike, R.J. (1974b)Depth/diameter relations of fresh lunar craters: revision from spacecraft data. Geophysical Letters, V. 1, No. 7, pp. 291-294.

Podwysocki, M.H., Weidner, J.R., Andre, C.G., Bickel, A.L., Lum, R.S., Adler, I., and Trombka, J. (1974) An analysis of the Apollo 15 x-ray fluorescence experiment for detailed lunar morphological and geochemical parameters (abstract). In Lunar Science--V, pp. 611-612. The Lunar Science Institute, Houston.

Porcello, L.J., Ryu, J., Schaber, G., Sill, W.R., Thompson, T.W., Ward, S.H., and Zelenka, J.S. (1973) The Apollo 17 Lunar Sounder. Proc. Fourth Lunar Sci. Conf., Geochim. Cosmochim. Acta, Suppl. 4, V. 3, pp. 2821-2831, Pergamon.

Quaide, W.L. (1965) Rilles, ridges, and domes-clues to maria history. Icarus, 4, pp. 374-389.

Quaide, W.L., and Oberbeck, V.R. (1968) Thickness determinations of the lunar surface layer from lunar impact craters. J. Geophys. Res., 73, pp. 5247-5270.

Reed, V.S. and Wolfe, E.W. (1975) Origin of the Taurus-Littrow massifs. Proceedings of the Sixth Lunar Science Conference, Suppl. 6, Geochim. et Cosmochim. Acta, V. 1, pp. 2443-2461.

Roddy, D.J., Boyce, J.M., Colton, G.W., and Dial, A.L. (1975) Meteor Crater, Arizona, rim drilling with thickness, structural uplift, diameter, depth, volume, and mass-balance calculations. Prod. Lunar Sci. Conf. 6th, pp. 2621-2645.

Roddy, D.J. (1968) The Flynn Creek Crater, Tennessee. In French, B.M. and Short, N.M., eds., Shock metamorphism of natural materials. Proceedings of the First Conference held at NASA, Goddard Space Flight Center, Greenbelt, Maryland, pp. 291-322.

Ronca, L.B. (1973) The filling of the lunar mare basins. The Moon 7, 239-248.

Ronca, L.B. and Green, R.R. (1970) Statistical geomorphology of the lunar surface. Geol. Soc. Amer. Bull. 81, pp. 337-352.

Ronca, L.B. and Salisbury, J.W. (1966) Lunar history as suggested by the circularity index of lunar craters. Icarus, V. 5, pp. 130-138.

Salisbury, J.W., Adler, J.E.M., and Smalley, V.G. (1968) Dark-haloed craters on the Moon. Mon. Not. R. Astr. Soc., 138, pp. 245-249.

Schaber, G.G. (1973) Lava flows on Mare Imbrium: geologic evaluation from Apollo orbital photography. Proc. Lunar Sci. Conf. 4th, pp. 73-92.

Schaber, G.G., Thompson, T.W., Eggleton, R.E., and Zisk, S.H. (1974) Lava flows in Mare Imbrium, Part II: evaluation of anomalously low earth-based radar reflectivity (abstract). In Lunar Science--V, pp. 660-662. The Lunar Science Inst., Houston.

Schaber, G.G., Thompson, T.W., and Zisk, S.H. (1975) Lava flows in Mare Imbrium: an evaluation of anomalously low earth-based radar reflectivity. U.S. Geol. Survey Inter-agency Report No. 64 (submitted to The Moon).

Schubert, G., Lingenfelter, R.E., and Peale, S.J. (1970) The morphology, distribution, and origin of lunar sinuous rilles. Reviews of Geophysics and Space Physics 8, pp. 199-225.

Schubert G., Schwartz, K., Sonett, C.P., Smith, B.F., and Colburn, D.S. (1974) Mare Imbrium: a regional site of anomalous electrical conductivity (abstract). In Lunar Science--V, pp. 678-679. The Lunar Science Institute, Houston.

Schultz, P.H. (1974) Lunar Science V, The Lunar Science Inst., Houston, pp. 681-683.

Schultz, P.H. and Gault, D.E. (1975) Seismically induced modification of lunar surface features. In Lunar Science-VI, pp. 724-726, The Lunar Science Institute, Houston.

Schumm, S.A. (1970) Experimental studies on the formation of lunar surface features of fluidization. Geol. Soc. Am. Bull. 81, pp. 2539-2552.

Scott, D.H., Diaz, J.M., and Watkins, J.A. (1975) The geologic evaluation and regional synthesis of metric and panoramic photographs. Proc. Lunar Sci. Conf. 6th, pp. 2531-2541.

Scott, D.H. (1973) Small structures of the Taurus-Littrow region. Apollo 17 Prel. Sci. Rept. pp. 31-25 - 31-29.

Shoemaker, E.M., Batson, R.M., Holt, H.E., Morris, F.C., Rennilson, J.J., and Whitaker, E.A. (1969) Observations of the lunar regolith and the Earth from the television camera on Surveyor 7. J. Geophys. Res., 74, pp. 6081-6095.

Sjogren, W.L. (1973) Lunar orbital data map--Plate IV. Proceedings of the Fourth Lunar Science Conference, Geochimica. et Cosmochimica. Acta, Suppl. 4, V. 1. p. iii.

Sjogren, W.L. (1974) Plate 1. Lunar gravity at 100 km altitude. Proceedings of the Fifth Lunar Science Conference; Geochim. et Cosmochim. Acta, Suppl. 5, V. 1, Plate 1.

Sjogren, W.L. and Wollenhaupt, W.R. and Wimberly, R.N. (1974a) Lunar gravity via Apollo 15 and 16 Subsatellite. Moon 9, pp. 115-128.

Smith, R.L. (1966) In Hess, W.N., Menzel, D.H., and O'Keefe, J.A., eds., The nature of the lunar surface. Proceedings of the 1965 IAU-NASA Symposium: Baltimore, Maryland, Johns Hopkins, pp. 241-257.

Smith, R.L., and Bailey, R.A. (1968) Resurgent cauldrons. In Coats, R.R., Hay, R.L., and Anderson, C.A., eds., Studies in volcanology. Geol. Soc. America Memoir 116, pp. 613-662.

Smith, R.L. (1966) Terrestrial calderas, associated pyroclastic deposits, and possible lunar applications in the nature of the lunar surface. In Hess, W.N., Menzel, D.H., and O'Keefe, J.A., eds., The nature of the lunar surface. Proceedings of the 1965 IAU-NASA Symposium: Baltimore, Maryland, Johns Hopkins, pp. 241-258.

Soderblom, L.A. (1970) A model for small-impact erosion applied to the lunar surface. J. Geophys. Res., 75, pp. 2655-2661.

Soderblom, L.A. (1972) The process of crater removal in the lunar maria. Apollo 15 Prel. Sci. Rept., NASA SP-289, pp. 25-87 - 25-91.

Soderblom, L.A. and Lebofsky, L.A. (1972) Technique for rapid determination of relative ages of lunar areas from orbital photography. J. Geophys. Res., 77, pp. 279-296.

Solomon, S.C. (1975) Mare volcanism and lunar crustal structure. Proceedings of the Sixth Lunar Science Conference, Geochim. et Cosmochim. Acta, Suppl. 6, V. 1, pp. 1021-1042.

Stewart, H.E., Waskom, J.D., and DeHon, R.A. (1975a) Photogeology and basin configuration of Mare Smythii (abstract). In Lunar Science VI, pp. 777-779, The Lunar Science Inst., Houston.

Stewart, H.E., Waskom, J.D., and DeHon, R.A. (1975b)Photogeology and basin configuration of Mare Smythii. Proc. Lunar Sci. Conf. 6th, pp. 2541-2553.

Stöffler, D., Dence, M.R., Graup, G. and Abadian, M. (1974) Interpretation of ejecta formations at the Apolly 14 and 16 sites by a comparative analysis of experimental, terrestrial and lunar craters. Proc. Lunar Sci. Conf. 5th, pp. 137-150.

Strom, R.G. (1971) Lunar mare ridges, rings, and volcanic ring complexes. Modern Geology, V. 3, pp. 133-157.

Strom, R.G. and Trask, N.J. and Guest, J.E. (1975) Tectonism and volcanism on Mercury. J. Geophys. Res., V. 80, No. 17, pp. 2478-2508.

Stuart-Alexander, D. and Howard, K. (1970) Lunar maria and circular basins--a review. Icarus 12, 440.

Swann, G.A. (1974) A scheme for estimating the ages of small Copernican craters (abstract). In Lunar Science--V, pp. 761-763. The Lunar Science Institute, Houston.

Thompson, T.W., Howard, K.A., Shorthill, R.W., Tyler, G.L., Zisk, S.H., Whitaker, E.A., Schaber, G.G., and Moore, H.J. (1973) Remote sensing of Mare Serenitatis. Apollo 17 Preliminary Science Report, NASA SP-300, pp. 33-3 - 33-9.

Thompson, T.W., Shorthill, R.W., Whitaker, E.A. and Zisk, S.H. (1973) Complex origin of Mare Serenitatis floor: synthesis of remote observations (abstract). In Lunar Science--IV, pp. 726-727. The Lunar Science Institute, Houston.

Tija, H.D. (1970) Lunar wrinkle ridges indicative of strike-slip faulting. Geol. Soc. Amer. Bulletin, V. 81, pp. 3095-3100.

Titley, S.R. (1967) Geologic map of the Mare Humorum region of the Moon. U.S. Geol. Surv., Map I-495.

Trask, N.J. and Guest, J.E. (1975) Preliminary geologic terrain map of Mercury. J. Geophys. Res., V. 80, No. 17, pp. 2461-2477.

Trask, N.J. and Titley, S.R. (1966) Geologic map of the Pitatus region of the Moon. U.S. Geol. Surv., Map I-485.

Turner, D.C. (1963) Ring-structures in the Sara-Fier younger granite complex, Northern Nigeria. Quarterly Journal of the Geological Society of London, V. 119, pp. 345-366.

VanDorn, W.G. (1968) Tsunamis on the Moon? Nature 220, p. 1102.

VanDorn, W.G. (1969) Lunar maria: structure and evolution. Science 165, p. 693.

Wilhelms, D.E. (1968) Geologic map of the Mare Vaporum region of the Moon. U.S. Geol. Surv., Map I-548.

Wilhelms, D.E. (1973) Geologic map of the Northern Crisium region. Apollo 17 Preliminary Science Report, NASA SP-330, pp. 29-29 - 29-35.

Wilshire, H.G., Offield, T.W., Howard, K.A., and Cummings, D., (1972) U.S. Geological Survey Professional Paper 599-H, 42 pp.

Wolfe, E.W., Lucchitta, B.K., Reed, V.S., Ulrich, G.E., and Sanchez, A.G. (1975) Geology of the Taurus-Littrow Valley floor. Proc. Lunar Sci. Conf. 6th, pp. 2463-2483.

*Young, R.A. (1975) Mare crater size-frequency distributions: implications for relative surface ages and regolith development. Proc. Lunar Sci. Conf. 6th, pp. 2645-2663.

*Young, R.A. (1976a) Evidence for a shallow regional subsurface discontinuity in southern Mare Serenitatis. In Lunar Sci. VII, The Lunar Science Institute (in press).

*Young, R.A. (1976b) The morphological evolution of mare-highland contacts: a potential measure of relative mare surface age. In Lunar Science VII, The Lunar Science Institute (in press).

*Young, R.A., Brennan, W.J., Wolfe, R.W., and Nichols, D.J., (1973a) Analyses of lunar mare geology from Apollo photography. Proceedings of the Fourth Lunar Sci. Conf., Geochimica et Cosmochimica Acta, Suppl. 4, V. 1, pp. 57-71.

*Young, R.A., Brennan, W.J., Wolfe, R.W., and Nichols, D.J. (1973b) Volcanism in the lunar maria. Apollo 17 Prel. Sci. Rept., NASA SP-330, pp. 31-1 - 31-11.

*Young, R.A., Brennan, W.J., and Nichols, D.J. (1974a) Stratigraphic variations beneath lunar mare surfaces as indicated by ejecta characteristics of 0.5 to 2 km craters. In Lunar Science V, The Lunar Science Institute, Houston, pp. 863-865.

*Young, R.A., Brennan, W.J., and Nichols, D.J. (1974b) Problems in the interpretation of lunar mare stratigraphy and relative ages indicated by ejecta from small impact craters. Proc. Lunar Sci. Conf. 5th, pp. 159-170.

* Asterisk indicates publications completed as part of this contract.